



QUANTUM CHROMODYNAMICS NEAR THE CONFINEMENT LIMIT

Chris Quigg
Fermi National Accelerator Laboratory*
Batavia, Illinois 60510 USA

ABSTRACT

These nine lectures deal at an elementary level with the strong interaction between quarks and its implications for the structure of hadrons. Quarkonium systems are studied as a means for measuring the interquark interaction. This is presumably (part of) the answer a solution to QCD must yield, if it is indeed the correct theory of the strong interactions. Some elements of QCD are reviewed, and metaphors for QCD as a confining theory are introduced. The $1/N$ expansion is summarized as a way of guessing the consequences of QCD for hadron physics. Lattice gauge theory is developed as a means for going beyond perturbation theory in the solution of QCD. The correspondence between statistical mechanics, quantum mechanics, and field theory is made, and simple spin systems are formulated on the lattice. The lattice analog of local gauge invariance is developed, and analytic methods for solving lattice gauge theory are considered. The strong-coupling expansion indicates the existence of a confining phase, and the renormalization group provides a means for recovering the consequences of continuum field theory. Finally, Monte Carlo simulations of lattice theories give evidence for the phase structure of gauge theories, yield an estimate for the string tension characterizing the interquark force, and provide an approximate description of the quarkonium potential in encouragingly good agreement with what is known from experiment.

LECTURE 1: A FIRST LOOK AT QUARKONIUM

The strongly interacting particles we study in the laboratory are composite systems of quarks bound together by the color force described by the gauge theory called quantum chromodynamics (QCD). In these lectures we shall look at some of the basic elements of QCD as it relates to the problem of hadron structure. Our concerns will be with general features: quark confinement and the properties of the force between quarks, rather than with the details of hadron spectroscopy and interactions. An introduction to the literature on hadron physics can be found in the Bibliography to these lecture notes.

Within the restricted scope of these lectures, we shall try to answer the two questions,

- What does experiment say about the interaction between quarks?
- What does QCD say about the interaction between quarks?

and to compare theoretical expectation with experimental observation. Two specific items to be established from experiment are the form of the interquark interaction and the flavor-independence of the force between quarks. The light hadrons (those composed of up, down, and strange quarks) give us information about the strong interaction at distances in excess of about 1 fm, where the strong interaction is indeed formidable. The region between 0.1 fm and 1 fm has been mapped in studies of the heavy quarkonium states, $c\bar{c}$ or $b\bar{b}$ bound states. In this intermediate regime, there is good evidence for the flavor-independence of the interaction. Distances shorter than 0.1 fm are for the present inaccessible to hadron spectroscopy. The next quarkonium family, the still unobserved $t\bar{t}$ bound states, will allow us to begin to probe this region in which, as we shall see, it should be possible to compute the interaction reliably using perturbative methods.

Properties [1] of the ψ and T states are summarized in Tables 1 and 2, and the level schemes are indicated in Figs. 1 and 2. Clearly these families of heavy mesons have the appearance of atomic spectra with, as we shall see, readily identified candidates for radial and orbital excitations. That the analogy with atomic physics could be pursued in detail was suggested before the mapping of the ψ spectrum by Appelquist and Politzer [2]. They argued that for bound states in a Coulomb potential

$$V(r) = -\alpha/r \quad (1.1)$$

the mean velocity of the constituents is

$$B \sim \alpha \quad (1.2)$$

According to asymptotic freedom [3], the strong coupling constant of QCD decreases as $Q^2 \rightarrow \infty$, or equivalently as $r \rightarrow 0$, as

$$\alpha_s(Q^2) = \frac{12\pi}{(33-2n_f)\log(Q^2/\Lambda^2)} \quad (1.3)$$

where n_f is the number of active quark flavors and Λ is the QCD scale parameter. The Fourier transform of $(4/3)(-4\pi\alpha_s(Q^2)/Q^2)$ yields an asymptotic form for the interquark potential of

$$V(r) \underset{r \rightarrow 0}{\sim} - \frac{12\pi}{(33-2n_f)\log(1/r^2\Lambda^2)} \cdot \frac{4}{3r} \quad (1.4)$$

In a Coulomb potential, the scale of r is proportional to $1/m$; hence the relevant value of α_s is measured by $\log(\Lambda^2/m^2)$. We can therefore anticipate that as $m \rightarrow \infty$, the

running coupling constant " $\alpha_s(r)$ " decreases, so that the mean velocity of the bound constituents decreases. This leads to the expectation that quarkonium becomes a nonrelativistic problem for sufficiently heavy quark masses.

Within the bound-state picture, it is straightforward to guess the rough order of levels. Suppose first that the constituents are scalar particles denoted σ , with quantum numbers $J^{PC} = 0^{++}$. For $(\sigma\sigma)$ composites with angular momentum L , the bound-state quantum numbers are

$$C = (-1)^L \quad , \quad P = (-1)^L \quad , \quad (1.5)$$

so the ground state is a single 0^{++} level. The expected spectrum of $(\sigma\sigma)$ bound states is shown schematically in Fig. 3. This is not what is observed for the ψ and T families.

If instead the heavy mesons are $(f\bar{f})$ composites of spin-1/2 constituents f , the quantum numbers of a bound-state with orbital angular momentum L and spin S are

$$C = (-1)^{L+S} \quad , \quad P = (-1)^{L+1} \quad . \quad (1.6)$$

The ground state is therefore a hyperfine doublet of a 1S_0 (0^{-+}) level and a 3S_1 (1^{--}) level. The expected level scheme shown in Fig. 4 reproduces what is seen in the ψ and T families.

Scaling the Schrödinger Equation. Having identified the ψ and T as quark-antiquark bound states and motivated the possibility that the nonrelativistic approximation may be a fruitful one, we now proceed to an analysis in the context of the Schrödinger equation. In three dimensions, the Schrödinger equation is

$$-\frac{\hbar^2}{2\mu} \nabla^2 \Psi(\mathbf{r}) + [V(\mathbf{r}) - E] \Psi(\mathbf{r}) = 0 \quad . \quad (1.7)$$

For the special case of a central potential, we may write the wave function as

$$\Psi(\mathbf{r}) = R(r) Y_{\ell m}(\theta, \psi) \quad , \quad (1.8)$$

whereupon the Schrödinger equation separates. The radial wave function satisfies

$$-\frac{\hbar^2}{2\mu} \left(\frac{d^2}{dr^2} + \frac{2}{r} \cdot \frac{d}{dr} \right) R(r) - \left[E - V(r) - \frac{\ell(\ell+1)\hbar^2}{2\mu r^2} \right] R(r) = 0 \quad . \quad (1.9)$$

This may be placed in correspondence with the one-dimensional Schrödinger equation if we define the reduced radial wavefunction

$$u(r) = rR(r) \quad , \quad (1.10)$$

so that

$$-u''(r) = \frac{2\mu}{\hbar^2} \left[E - V(r) - \frac{l(l+1)\hbar^2}{2\mu r^2} \right] u(r) \quad , \quad (1.11)$$

with

$$\left. \begin{aligned} u(0) &= 0 \\ u'(0) &= R(0) = \sqrt{4\pi} \Psi(0) \text{ for s-waves} \\ \int_0^\infty dr [u(r)]^2 &= 1 \quad . \end{aligned} \right\} \quad (1.12)$$

A number of relations will prove useful in general. First, for s-waves, we show that

$$|\Psi(0)|^2 = \frac{\mu}{2\pi\hbar^2} \left\langle \frac{dV}{dr} \right\rangle \quad . \quad (1.13)$$

To do so, we multiply the s-wave Schrödinger equation

$$-u''(r) = \frac{2\mu}{\hbar^2} [E - V(r)] u(r) \quad (1.14)$$

by $\int_0^\infty dr u'(r)$ and integrate by parts:

$$-[u'(r)]^2 \Big|_0^\infty = \frac{2\mu}{\hbar^2} [E - V(r)] [u(r)]^2 \Big|_0^\infty - \frac{2\mu}{\hbar^2} \int_0^\infty dr [u(r)]^2 \left(- \frac{dV}{dr} \right) \quad , \quad (1.15)$$

so that

$$4\pi |\Psi(0)|^2 = \frac{2\mu}{\hbar^2} \left\langle \frac{dV}{dr} \right\rangle \quad . \quad (1.16)$$

By similar arithmetic it is easy to prove the Virial Theorem

$$E - \langle V \rangle = \langle T \rangle = \left\langle \frac{r \cdot dV}{2 dr} \right\rangle \quad . \quad (1.17)$$

For a power-law potential

$$V(r) = \lambda r^v \quad , \quad (1.18)$$

the Virial Theorem yields

$$\begin{aligned} \langle T \rangle &= \frac{v}{2} \langle V \rangle = vE/(2+v) \quad ; \\ \langle V \rangle &= 2E/(2+v) \quad . \end{aligned} \quad (1.19)$$

For simple potentials, including power-laws and other monotonic wells, rather far-reaching results can be derived using quite elementary techniques. This mode of

analysis has been reviewed by Quigg and Rosner, [4] and exploited by many authors. I shall summarize here a few of the results with direct applications to experiment.

For the special case of a power-law potential, the equation (1.11) can be divested of all its dimensionful parameters. To see this, we first introduce a scaled measure of length

$$\rho = (M^2/2\mu|\lambda|)^{1/2} r \quad , \quad (1.20)$$

where the exponent p is to be chosen to eliminate dimensions from (1.11). The choice

$$p = -1/(2+v) \quad , \quad (1.21)$$

when accompanied by the substitutions

$$E = \left(\frac{\hbar^2}{2\mu}\right) \left(\frac{\hbar^2}{2\mu|\lambda|}\right)^{2p} \epsilon \quad , \quad (1.22)$$

where ϵ is dimensionless, and

$$w(\rho) = u(r) \quad (1.23)$$

accomplishes precisely this. The ensuing equation is

$$w''(\rho) + [\epsilon - \text{sgn}(\lambda)\rho^v - \lambda(\lambda+1)/\rho^2]w(\rho) = 0 \quad , \quad (1.24)$$

which depends only upon pure numbers.

Several consequences follow immediately from these manipulations. Lengths and quantities with the dimensions of lengths depend upon the constituent mass and coupling strength as

$$L = (\mu|\lambda|)^{-1/(2+v)} \quad . \quad (1.25)$$

As a result, the particle density at the origin of coordinates behaves as

$$|\Psi(0)|^2 \sim L^{-3} \propto (\mu|\lambda|)^{3/(2+v)} \quad . \quad (1.26)$$

Level spacings have a similarly definite behavior, according to (1.21):

$$\Delta E \propto \mu^{-v/(2+v)} |\lambda|^{2/(2+v)} \quad . \quad (1.27)$$

The limiting behavior of the scaled Schrödinger equation as $v \rightarrow 0$ is easily studied. The "power-law" potential corresponding to this limit is simply

$$V(r) = C \log(r) \quad . \quad (1.28)$$

The scaling laws (1.25)-(1.27) contain many well-known results. Recall, for example, that in the Coulomb potential, for which $v=-1$,

$$\Delta E(v=-1) \propto \mu\alpha^2 = \mu|\lambda|^2 \quad . \quad (1.29)$$

Likewise, the conclusion that in a linear potential

$$|\Psi(0)|^2 \Big|_{v=1} \propto \mu |\lambda| \quad (1.30)$$

can be derived at once using the identity

$$|\Psi(0)|^2 = \frac{\mu}{2\pi M^2} \left\langle \frac{dV}{dr} \right\rangle . \quad (1.31)$$

The scaling laws (1.25)-(1.27) have many applications in quarkonium physics. For the moment let us merely note that electric multipole matrix elements vary as

$$\langle n' | E_j | n \rangle \sim L^j \propto (\mu |\lambda|)^{-j/(2+v)} , \quad (1.32)$$

so that transition rates behave as

$$\Gamma(E_j) \sim k^{2j+1} \left| \langle n' | E_j | n \rangle \right|^2 , \quad (1.33)$$

where k is the energy of the radiated photon, which is just a level spacing ΔE . Using (1.25) and (1.27) we then deduce that

$$\Gamma(E_j) \propto \mu^{-[2j(1+v)+v]/(2+v)} |\lambda|^{2(j+1)/(2+v)} . \quad (1.34)$$

This has the interesting consequence that for fixed potential strength $|\lambda|$, $\Gamma(E_j)$ is a decreasing function of j as $\mu \rightarrow \infty$ for potentials less singular than the Coulomb potential.

Using the Van Royen-Weisskopf formula [5]

$$\Gamma(V^0 \rightarrow e^+ e^-) = \frac{16\pi\alpha^2}{M_V^2} |\Psi(0)|^2 \left\langle e^2 \right\rangle \quad (1.35)$$

for vector meson decay, one may easily show that for $v > -1$ (for which binding energies are asymptotically negligible compared with the quark mass)

$$\Gamma(E_j) / \Gamma(V^0 \rightarrow e^+ e^-) \propto \mu^{-(2j-1)(v+1)/(2+v)} |\lambda|^{2(j-1)/(2+v)} , \quad (1.36)$$

which implies the dominance of leptonic over radiative decays as $\mu \rightarrow \infty$ for fixed potential strength $|\lambda|$.

To investigate how observables depend upon the principal quantum number with some degree of generality it is convenient to adopt the semiclassical, or JWKB approximation. This turns out to be rather less of a compromise than one might at first surmise. Judiciously applied, the semiclassical approximation is in fact highly accurate for the sort of nonpathological potentials one hopes to encounter for quarkonium. This accuracy is documented in Ref. 4, where additional references may be found.

The semiclassical results all follow from the quantization condition

$$\int_0^{r_c} dr [2\mu(E-V(r))]^{\frac{1}{2}} = (n-\frac{1}{2})\pi\hbar \quad , \quad (1.37)$$

where n is the principal quantum number and the classical turning point r_c is defined through $V(r_c)=E$. Although it is both possible and useful to be more general, it is appropriate to retain the spirit of the preceding section and specialize to power-law potentials. For s -wave bound states of nonsingular potentials of the form (1.18), Eq. (1.37) can be integrated by elementary means to yield

$$E_n \propto (n-\frac{1}{2})^{2\nu/(2+\nu)} \quad (1.38)$$

where with an eye toward the intended applications I have suppressed the dependence on constituent mass and coupling strength given in (1.27). For singular potentials additional care is required near the origin. A simple modification of the usual procedure leads to

$$E_n \propto (n-\gamma(\nu))^{2\nu/(2+\nu)} \quad , \quad -2 < \nu < 0 \quad , \quad (1.39)$$

where

$$\gamma(\nu) = \frac{1}{2} \left(\frac{1+\nu}{2+\nu} \right) \quad . \quad (1.40)$$

Similar expressions may be obtained for orbitally-excited states.

By evaluating the expectation value in Eq. (1.31) with JKWB wavefunctions, it is also straightforward to derive

$$|\Psi_n(0)|^2 \propto \begin{cases} (n-\frac{1}{2})^{2(\nu-1)/(2+\nu)} \quad , & \nu > 0 \quad , \\ (n-\gamma(\nu))^{(\nu-2)/(2+\nu)} \quad , & 0 > \nu > -2 \quad . \end{cases} \quad (1.41a)$$

$$(1.41b)$$

For a general nonsingular potential, one may readily show that

$$|\Psi_n(0)|^2 = \frac{(2\mu E_n)^{\frac{1}{2}}}{4\pi^2 \hbar^3} \frac{\partial(2\mu E_n)}{\partial n} \quad . \quad (1.42)$$

Generalizations of these results to $l \neq 0$ have also been made, but we shall not require them here. Let us now see what can be learned by comparing these simple results with experimental information.

Inferences. The strategy embodied in the preceding paragraphs has been pursued explicitly by several authors [4,6-9] and implicitly by many others. The conclusion to be drawn from the data is that a potential of the form

$$V(r) = A + Br^\nu \quad (1.43)$$

with $\nu=0.1$ gives a good representation of the ψ and Υ spectra. This is based upon four distinct kinds of evidence.

First, we may note by comparing Figs. 1 and 2 that the level spacings are quite similar in the ψ and T families. Indeed, the observation that

$$M_{T'} - M_T = M_{\psi'} - M_{\psi} \quad (1.44)$$

provided an early motivation for the logarithmic potential [7]. A more detailed look at the intervals is given by Fig. 5, which indicates that

$$\Delta E(T) = 0.95 \Delta E(\psi) \quad (1.45)$$

Assuming that the potential strength does not vary between the ψ and T systems, this implies a small positive power for the effective potential. The precise value of the exponent depends upon the ratio of quark masses, which is imperfectly known.

The principal-quantum-number dependence of observables within one quarkonium system is free from the assumption that the potential strength λ is the same for different quark flavors. Effective powers may be inferred independently from the ψ and T levels and compared for consistency. The level structures $(E_3 - E_2)/(E_2 - E_1)$, etc. are characteristic of the potential shape. These ratios of intervals are the same for ψ

$$\left. \frac{E_3 - E_2}{E_2 - E_1} \right|_{\psi} = 0.58 \quad (1.46)$$

and T

$$\left. \frac{E_3 - E_2}{E_2 - E_1} \right|_T = 0.59 \quad (1.47)$$

states, and are again compatible with $v=0.1$, as shown in Fig. 6. The ratio

$$\left. \frac{E_4 - E_3}{E_2 - E_1} \right|_T = 0.39 \quad (1.48)$$

displayed in Fig. 7, indicates a similar potential shape.

The center-of-gravity of 3P_J levels,

$$\langle M(^3P_J) \rangle = [M(^3P_0) + 3M(^3P_1) + 5M(^3P_2)]/9 \quad (1.49)$$

is free of L-S and tensor force fine structure contributions. For the 3P_J levels, the mean masses are

$$\langle M(\chi_c) \rangle = 3524.9 \text{ MeV}/c^2 \quad (1.50)$$

$$\langle M(\chi_b) \rangle = 9903.3 \pm 3 \text{ MeV}/c^2 \quad ,$$

so that

$$\frac{M(\psi') - \langle M(\chi_c) \rangle}{M(\psi') - M(\psi)} = 0.27 \quad (1.51)$$

and

$$\frac{M(T') - \langle M(\chi_D) \rangle}{M(T') - M(T)} = 0.21 \quad (1.52)$$

As shown in Fig. 8, these imply respectively small positive and small negative powers.

Finally, the principal quantum number dependence of wavefunctions at the origin, or equivalently of the reduced leptonic widths

$$\bar{\Gamma}(V^0 \rightarrow e^+e^-) \equiv M_V^2 \Gamma(V^0 \rightarrow e^+e^-) \quad , \quad (1.53)$$

is approximately given by

$$|\Psi_n(0)|^2 \sim 1/(n-\frac{1}{2}) \quad (1.54)$$

for both ψ and T , as shown in Figs. 9 and 10. This behavior again corresponds to an effective potential which is a small positive power. It was this observation for the ψ family that led Machacek and Tomozawa [10] to investigate softer-than-linear confining potentials, including logarithmic forms. Taken together, these results on principal quantum number dependence would seem to exclude the bizarre possibility that the nearly equal spacing in the ψ and T families results from a potential strength which varies approximately as

$$\lambda \propto \mu^{1/2} \quad . \quad (1.55)$$

Martin [9] has shown that careful attention to hyperfine effects does not change the conclusions of this analysis, namely that the interquark potential is flavor-independent (as QCD would have it) and characterized by an effective power-law potential with a small positive exponent. This is also in agreement with the conclusions of all other analyses and fits: In the region of space between 0.1 fm and 1 fm, the interaction between heavy quarks is flavor-independent, and roughly logarithmic in shape [11,12].

We may characterize the inferred potential shapes in two convenient expressions: as a logarithmic shape [6]

$$V(r) = (0.71 \text{ GeV}) \ln(r/r_0) \quad , \quad (1.56)$$

for which level spacings ΔE are independent of the quark mass μ , lengths scale as $L \propto \mu^{-1/2}$, and wavefunctions vary as $|\Psi_n(0)|^2 \propto 1/(n-\frac{1}{2})$; or as a power-law [9]

$$V(r) = (5.82 \text{ GeV})(r/1 \text{ GeV}^{-1})^{0.104} - 6.377 \text{ GeV} \quad . \quad (1.57)$$

The two forms are numerically indistinguishable for

$$0.1 \text{ fm} \leq r \leq 1 \text{ fm} \quad .$$

$$(1.58)$$

Number of Narrow Levels. A semiclassical near-theorem relates the number of levels below flavor threshold to the mass of the constituents. This would seem to be a question ill-suited to a nonrelativistic approach because it is necessary to compute both quarkonium ($Q\bar{Q}$) masses and the mass of the lightest flavor ($Q\bar{q}$) state. The latter is unlikely to be governed by a potential theory description. However, a key simplifying observation was made by Eichten and Gottfried [13] who noted that the mass of the light quark-heavy quark state can be written as

$$M(Q\bar{q}) = M(Q) + M(q) + \text{binding} + \text{hyperfine} \quad . \quad (1.59)$$

Although the binding energy may not be calculable, it is reasonable to suppose that it depends upon the reduced mass of the constituents, which tends to $M(q)$ as $M(Q) \rightarrow \infty$. Thus the binding energy must become independent of the heavy quark mass. Furthermore, the hyperfine splitting of the 0^{-+} and 1^{--} ($Q\bar{q}$) levels must certainly vary as $1/M(Q)$. It therefore vanishes as $M(Q) \rightarrow \infty$. Hence in the limit of infinite quark mass, the difference

$$\delta(M(Q)) \equiv 2M(Q\bar{q}) - 2M(Q) \rightarrow \delta_\infty \quad , \quad (1.60)$$

independent of the heavy-quark mass.

In the regime in which $\delta(M(Q)) = \delta_\infty$ is a good approximation, the number of levels below flavor threshold is easily calculated [14]. Consider any confining potential. In semiclassical approximation the number of levels bound below $E = 2M(Q) + \delta_\infty$ is specified by the quantization condition

$$\int_0^{r_\delta} dr [M(Q)(\delta_\infty - V(r))]^{\frac{1}{2}} = (n - \frac{1}{2})\pi \quad , \quad (1.61)$$

where to save writing the zero of energy has been set at $2M(Q)$. The classical turning point r_δ , defined through

$$V(r_\delta) = \delta_\infty \quad (1.62)$$

is independent of $M(Q)$, so we have by inspection the result that

$$(n - \frac{1}{2}) \propto \sqrt{M(Q)} \quad (1.63)$$

It is likely that the limit (1.60) is already approached within 10% in the charmonium system, in which two 3S_1 levels lie below charm threshold. Thus there should be slightly less than four bound levels in the epsilon family, in agreement with the observation of three narrow vector states. The success of this prediction

provides another verification of flavor independence, which was the principal assumption.

It is interesting to see how the result (1.63) is realized in specific potentials. To make this plain, I show in Fig. 11 the evolution with constituent mass of the spectra of the potentials $V(r)=-r^{-1/2}$, $V(r)=\lambda \ln r$ and $V(r)=r$, for which $\Delta E \sim \mu^{1/3}$, μ^0 , and $\mu^{-1/3}$, respectively, according to (1.27). All the levels fall deeper into the wells as μ is increased. For the potential $V(r)=-r^{-1/2}$, singular at the origin, the levels spread apart as they sink into the well. For the linear potential, no such pit exists, but the levels are packed more densely as μ increases. The logarithmic potential represents an intermediate case in which the level spacing is independent of the mass and levels drop into the well at a common rate given by

$$E_j(\mu') = E_j(\mu) - \frac{1}{2} \lambda \ln(\mu'/\mu) \quad . \quad (1.64)$$

In each case the rate of accumulation of levels below any specific value of the energy is given by (1.63).

A corollary to the conclusion that the classical turning point of the last narrow level has become independent of quark mass is that the single-channel analysis cannot be extended past about 1 fm. Heavier (QQ) systems will extend our knowledge of the interaction to shorter distances, but are unlikely to address the nature of the confining potential.

How many narrow levels of toponium are to be expected? For a top-quark mass of 45 GeV/c², [15] scaling from $\sqrt{m_t/m_b}$ or $\sqrt{m_t/m_c}$ gives 10-11 narrow 3S_1 states. The full spectroscopy is much richer. For each s-wave, we expect a pair of hyperfine partners, the 1S_0 and 3S_1 levels. Similarly there will be four fine- and hyperfine-partners for each $\ell > 1$ -wave, corresponding to $^3\ell_{\ell+1}$, $^3\ell_{\ell}$, $^3\ell_{\ell-1}$, and $^1\ell_{\ell}$ levels. If there are N radial excitations, there will be (N-1) sets of p-waves, (N-2) sets of d-waves, etc. The total number of narrow states is thus [16]:

$$2N + 4 \sum_{\ell=1}^N (N-\ell) = 2N^2 \quad (1.65)$$

~ 200-250 levels.

To conclude this introduction to quarkonium physics, let us verify the consistency of the nonrelativistic approach. For a (QQ) bound state, the mean-squared velocity is

$$\langle \mathbf{v}^2 \rangle = \left\langle \frac{\mathbf{p}^2}{m^2} \right\rangle = \frac{1}{m} \left\langle \frac{\mathbf{p}^2}{2\mu} \right\rangle = \frac{\langle T \rangle}{m} \quad , \quad (1.66)$$

where m is the quark mass and $\mu=m/2$ is the reduced mass. For a logarithmic potential of the form

$$V(r) = C \ln(r) \quad , \quad (1.67)$$

the kinetic energy of any bound state is

$$\langle T \rangle = \left\langle \frac{r}{2} \cdot \frac{dV}{dr} \right\rangle = C/2 \quad , \quad (1.68)$$

so that

$$\langle \beta^2 \rangle = C/2m \approx \frac{350 \text{ MeV}}{m} \quad . \quad (1.69)$$

For the psion family, with $m_c \approx 1.5 \text{ GeV}/c^2$, we find

$$\langle \beta^2 \rangle_\psi \approx 0.23 \quad , \quad (1.70)$$

while for the upsilons, with $m_b \approx 5 \text{ GeV}/c^2$, we obtain

$$\langle \beta^2 \rangle_T \approx 0.07 \quad . \quad (1.71)$$

At least the second of these appears comfortably nonrelativistic. For the charmonium states, we must be open to the possibility of significant relativistic corrections.

LECTURE 2: MORE ON QUARKONIUM

The $(s\bar{s})$ System. Several authors have attempted to extend the successful description of the quarkonium spectrum to light mesons and baryons. This may be done either by abstracting the scaling laws from the ψ and T states or by transplanting the quarkonium potential to what would seem a manifestly relativistic regime. As a stimulus to thought along these lines I present in Fig. 12 a highly speculative spectrum of $(s\bar{s})$ states. Many of the assignments are uncertain, but the resemblance to the ψ and T spectra is remarkable. For a strange-quark mass $m_s = 0.5 \text{ GeV}/c^2$, the mean-squared velocity is

$$\langle \beta^2 \rangle_\psi \approx 0.7 \quad (2.1)$$

Whether the spectrum in Fig. 12 (if correct!) shows that a nonrelativistic analysis has a wider-then-expected range of validity, or that a deeper principle of hadron dynamics awaits recognition, I do not know.

Theorems. An excellent review of statements about bound-state properties which may be proved rigorously in nonrelativistic potential theory has been given by Grosse and Martin [17]. Many results have been deduced which pertain to the order of levels, inequalities for wavefunctions at the origin, bounds on quark mass

differences and so forth. The value of such statements is not only that they are true, but also that they provide a context for computations based upon explicit potentials. It is of great value to understand what must be true for any reasonable potential, or for any potential of a particular class, in order to distinguish the consequences that may be peculiar to a specific model. I shall cite one example that bears directly upon experimental results.

Consider a quarkonium potential which is monotonic,

$$dV/dr \geq 0 \quad (2.2)$$

and concave downward,

$$d^2V/dr^2 \leq 0 \quad (2.3)$$

The first property is motivated by simplicity, and the second by the expectation that the confining potential rises no faster than linearly. Both are satisfied by the effective power-law potentials just discussed. Then if $m > \mu$ are masses of the constituents of two $Q\bar{Q}$ systems, one may prove [18] that

$$|\Psi_m(0)|^2 \geq (m/\mu) |\Psi_\mu(0)|^2 \quad (2.4)$$

This result holds for the ground state under the assumptions stated, for all levels in power-law potentials (compare Eq. (1.26)), and for all levels in a general potential satisfying the assumptions, in WKB approximation [17]. It implies a lower bound on leptonic widths in the more massive system as, in the case at hand,

$$\Gamma(T_n \rightarrow e^+e^-) \geq \frac{m_b}{m_c} \cdot \frac{e_b^2}{e_c^2} \cdot \frac{M_{\psi_n}^2}{M_{T_n}^2} \Gamma(\psi_n \rightarrow e^+e^-) \quad (2.5)$$

The lower bounds on upilon leptonic widths are plotted in Fig. 13, together with the experimental measurements. A b-quark charge of 2/3 is seen to be incompatible with the bound. The conclusion that $|e_b| = 1/3$ is substantiated by the measurements of $R = \sigma(e^+e^- \rightarrow \text{hadrons})/\sigma(e^+e^- \rightarrow \mu^+\mu^-)$.

By extrapolating from the upsilons to higher masses one may bound from below the integrated cross section for the production of the ground state of the next quarkonium family in e^+e^- annihilations [19]. Using cross section measurements from PETRA [20] it is possible to exclude on this basis a $t\bar{t}$ resonance (charge 2/3 quarks) below $46.78 \text{ GeV}/c^2$.

The String Picture of Hadrons. Suppose that the interaction among quarks is so strong at large distances that a $(q\bar{q})$ pair is always created when the quarks are widely separated, as depicted in Fig. 14. By analogy with the hadronic clusters typically inferred from experiments on multiple production, it is reasonable to expect that a quark is accompanied by an antiquark in a typical hadron of mass

$\sim 1 \text{ GeV}/c^2$ at a separation of $\sim 1 \text{ fm}$. That would imply that between every quark and antiquark there is a linear energy density of order

$$k = \Delta E/\Delta r \approx 1 \text{ GeV}/\text{fm} \\ \approx 0.2 \text{ GeV}^2 \approx 5/\text{fm}^2 \quad . \quad (2.6)$$

This picture is supported by the evidence for linear Regge trajectories of the light hadrons, which are displayed in Figs. 15 and 16. For the families of hadrons composed entirely of light quarks, the Regge trajectories are given by

$$J(M^2) = \alpha_0 + \alpha' M^2 \quad , \quad (2.7)$$

with

$$\alpha' \approx 0.8-0.9(\text{GeV}/c^2)^{-2} \quad . \quad (2.8)$$

The connection between linear energy density and the linear Regge trajectories is provided by the string model formulated by Nambu [21].

Consider a massless quark and antiquark connected by a string of length r_0 , which is characterized by an energy density per unit length k . The situation is sketched in Fig. 17. For a given value of the length r_0 , the largest achievable angular momentum L occurs when the ends of the string move with the velocity of light. In this circumstance, the speed at any point along the string will be

$$v(r) = 2r/r_0 \quad . \quad (2.9)$$

The total mass of the system is then

$$M = 2 \int_0^{r_0/2} dr k [1 - v(r)^2]^{-1/2} = k r_0 \pi / 2 \quad , \quad (2.10)$$

while the orbital angular momentum of the string is

$$L = 2 \int_0^{r_0/2} dr k r v(r) c [1 - v(r)^2]^{-1/2} = k c r_0^2 \pi / 8 \quad , \quad (2.11)$$

Using the fact (2.10) that $r_0^2 = 4M^2/k^2\pi^2$, we find that

$$L = M^2/2\pi k \quad , \quad (2.12)$$

which corresponds to a linear Regge trajectory, with

$$\alpha' = 1/2\pi k \quad . \quad (2.13)$$

This connection yields

$$k = \begin{cases} 0.18 \text{ GeV}^2 \\ 0.20 \text{ GeV}^2 \end{cases} \quad \text{for } \alpha' = \begin{cases} 0.9 \text{ GeV}^{-2} \\ 0.8 \text{ GeV}^{-2} \end{cases} \quad , \quad (2.14)$$

consistent with our heuristic estimate of the energy density. Thus we see that a linear energy density implies linearly rising Regge trajectories, and that the connection makes quantitative sense. These results suggest that at separations of the order of 1 fm, we may characterize the interquark interaction by the linear potential

$$V(r) \approx kr \quad , \quad (2.15)$$

while recognizing that because of quark pair creation the situation is not one to which one-channel potential theory applies.

Guessing the Interquark Potential. It is of interest to construct phenomenological potentials that incorporate in some approximation the expected behavior of perturbative QCD at short distances and reproduce the string picture at large distances. We shall consider two simple examples. The Cornell model [22] is a simple superposition of Coulomb and linear potentials,

$$V(r) = -A/r + Br + C \quad . \quad (2.16)$$

A fit to the ψ and T spectra yields the parameters

$$\left. \begin{array}{l} A = 0.48 \\ B = 0.183 \text{ GeV}^2 \\ C = -0.25 \text{ GeV} \end{array} \right\} . \quad (2.17)$$

The slope B of the linear term is consistent with the string tension (2.14) inferred from the spectrum of light hadrons. The coefficient A , when interpreted [compare (1.4)] as $4\alpha_s/3$, corresponds to a strong coupling constant

$$\alpha_s = 0.36 \quad , \quad (2.18)$$

which is perhaps bigger than one would like, if the Born approximation is to be reliable. A second form inspired by QCD is the Richardson potential [23],

$$V(r) = \int \frac{d^3Q}{(2\pi)^3} e^{iQ \cdot r} \left[-\frac{4}{3} \frac{12\pi}{27Q^2 \log(Q^2/\Lambda^2 + 1)} \right] \quad , \quad (2.19)$$

where the 1 in the argument of the logarithm serves to make the integral easily calculable. A fit to the data gives for the QCD scale parameter the value

$$\Lambda = 400 \text{ MeV} \quad . \quad (2.20)$$

These two potentials are compared in Fig. 18 with the "data-inspired" potentials (1.56) and (1.57) discussed in the first lecture. In the region of space populated by the narrow ψ and T states, the four curves are essentially indistinguishable. On the basis of this and other determinations to be discussed in Lecture 8, we may assert that the interquark potential has been measured in the

interval

$$0.1 \text{ fm} \leq r \leq 1 \text{ fm} \quad . \quad (2.21)$$

We have already remarked that scans at PETRA for narrow resonances produced in e^+e^- annihilation into hadrons have excluded toponium states below $46.78 \text{ GeV}/c^2$ [20]. This implies that the top quark mass exceeds about $24 \text{ GeV}/c^2$. In addition, the UA-1 collaboration at the CERN Collider has presented preliminary evidence [15] for the decay sequence

$$W^+ \rightarrow \begin{array}{l} \bar{t}b \\ \downarrow \\ be^+\nu_e \end{array} \quad (2.22)$$

with

$$30 \text{ GeV}/c^2 \leq m_t \leq 60 \text{ GeV}/c^2 \quad . \quad (2.23)$$

We saw in Lecture 1 that for a top quark in the middle of this range, we expect 10 or 11 narrow 3S_1 levels. Now we are in a position to ask in more detail what we should expect for the next quarkonium family, and what we might learn from it [24-26].

Outside the region in which ψ and T spectra have measured the interquark force, the four potentials differ significantly, as shown in Fig. 19. The $1^3S_1(t\bar{t})$ level will have a radius

$$\langle r^2 \rangle_{t\bar{t}}^{1^3S_1} \approx 0.06 \text{ fm} \quad , \quad (2.24)$$

where distinctions can be made. As an example, consider the 2S-1S interval, for which the expectations are displayed in Fig. 20. We see at once that extrapolation from the $b\bar{b}$ to the $t\bar{t}$ system is risky for this quantity. Additional parameters are collected for the case of $m_t = 40 \text{ GeV}/c^2$ in Table 3. The 2S-1S splitting and the 1S leptonic width will be particularly revealing.

Suppose that we take seriously the Richardson potential as the right form at short distances, because it ties on gracefully to QCD. Using this as a standard, we may ask whether QCD perturbation theory alone would suffice for the $1S(t\bar{t})$ state. In other words, will the toponium system place us in the simple regime anticipated by Appelquist and Politzer [2]? The sketch in Fig. 21 shows that the answer is no: the long-range part of the QQ interaction is essential, even for the toponium ground state.

To close our tour of quarkonium systems, I show in Fig. 22 the anticipated spectrum of $(t\bar{t})$ bound states in the Richardson potential, for a top-quark mass of $45 \text{ GeV}/c^2$.

LECTURE 3: ASYMPTOTIC FREEDOM, CONFINEMENT, AND THE 1/N EXPANSION

Asymptotic Freedom. The physical origin of the antiscreening of color charges that characterizes QCD is indicated by calculations of the effective charge in a variety of gauges, cited in the Bibliography. A less familiar, but quite evocative, description of how asymptotic freedom arises is provided by the magnetic moment interpretation [27].

The interaction between charges in vacuum is described in momentum space by e_0^2/q^2 . In the presence of matter, this is modified to $e_0^2/q^2\epsilon(q)$, where $\epsilon(q)$ is the dielectric constant or, more properly, the dielectric function. It is convenient to define the "running charge" by

$$e^2(q) = e_0^2/\epsilon(q) \quad . \quad (3.1)$$

The magnetic permeability of the medium can be defined through the relation

$$\epsilon\mu = 1 \quad . \quad (3.2)$$

In ordinary matter, or in the QED vacuum, the dielectric constant is greater than unity,

$$\epsilon > 1 \quad , \quad (3.3)$$

so that the medium is "diamagnetic," with

$$\mu < 1 \quad . \quad (3.4)$$

In contrast, the antiscreening of QCD corresponds in this language to paramagnetism ($\mu > 1$).

We may write the q^2 -evolution of the magnetic permeability as

$$\mu = 1 + g^2\chi \log(q^2/q_0^2) \quad , \quad (3.5)$$

where $g^2 \rightarrow e^2$ for electrodynamics. The generalization to arbitrary spin of a standard condensed-matter formula for magnetic susceptibility (derived in a uniform background magnetic field) is

$$\chi = \frac{1}{16\pi^2} \text{Tr} \left[(2S_z)^2 - \frac{1}{3} \right] \cdot \begin{pmatrix} +1, \text{ bosons} \\ -1, \text{ fermions} \end{pmatrix} \quad . \quad (3.6)$$

The first term $(2S_z)^2$ in the trace is the Pauli paramagnetism, which arises from the interaction of the intrinsic dipole moments (with gyromagnetic ratio $g=2$) with the background field. The term $(-1/3)$ is the Landau diamagnetism, which arises from the quantization of orbital vacuum currents.

Using (3.6) we can quickly recover some familiar results:

(i) QED

$$\chi = \frac{-1}{16\pi^2} \left[1 - \frac{1}{3} \right] \times (2 \text{ spin states}) = -\frac{1}{12\pi^2} \quad , \quad (3.7)$$

so that

$$\mu(q^2) = 1 - \frac{\alpha}{3\pi} \log(q^2/q_0^2) \quad . \quad (3.8)$$

(ii) Scalar electrodynamics

$$\chi = \frac{1}{16\pi^2} \left[-\frac{1}{3} \right] = -\frac{1}{48\pi^2} \quad , \quad (3.9)$$

so that

$$\mu(q^2) = 1 - \frac{\alpha}{12\pi} \log(q^2/q_0^2) \quad . \quad (3.10)$$

(iii) Charged vectors

$$\chi = \frac{1}{16\pi^2} \left[4 - \frac{1}{3} \right] \times (2 \text{ spin states}) = \frac{1}{16\pi^2} \cdot \left(\frac{22}{3} \right) \quad , \quad (3.11)$$

so that

$$\mu(q^2) = 1 + \frac{11\alpha}{6\pi} \log(q^2/q_0^2) \quad . \quad (3.12)$$

(iv) QCD

$$\chi = \frac{1}{16\pi^2} \left[\frac{22}{3} \cdot \frac{3}{2} - \frac{4}{3} \cdot \frac{1}{2} \cdot n_f \right] \quad , \quad (3.13)$$

where we have weighted (3.7) and (3.11) by the effective color-charge-squared for triplets (for n_f quark flavors) and octets, respectively. The resulting evolution of the magnetic permeability is

$$\mu(q^2) = 1 + \frac{\alpha_s}{12\pi} \left[33 - 2n_f \right] \log(q^2/q_0^2) \quad , \quad (3.14)$$

which shows the expected paramagnetic behavior.

A Metaphor for Confinement [28]. It is typical in field theories that the coupling constant depend upon the distance scale. As we have seen, this dependence can be expressed in terms of a dielectric constant ϵ . We define

$$\epsilon(r_0) = 1 \quad , \quad (3.15)$$

and write

$$g^2(r) = g^2(r_0)/\epsilon(r) \quad . \quad (3.16)$$

We assert that the implication of asymptotic freedom is that in QCD the effective color charge decreases at short distances and increases at large distances. In other words, the dielectric "constant" will obey

$$\epsilon(r) > 1 \quad , \quad \text{for } r < r_0 \quad , \quad (3.17a)$$

$$\epsilon(r) < 1 \quad , \quad \text{for } r > r_0 \quad . \quad (3.17b)$$

Indeed, to second order in the strong coupling we may write

$$\epsilon(r) = \left[1 + \frac{1}{2\pi} \frac{g^2(r_0)}{4\pi} (11-2n_f/3) \ln(r/r_0) + O(g^4) \right]^{-1} \quad (3.18)$$

in QCD, where n_f is the number of active quark flavors.

Let us now consider an idealization based upon electrodynamics. In Quantum ElectroDynamics, we choose

$$\epsilon_{\text{vacuum}} = 1 \quad , \quad (3.19)$$

and can show [29] that physical media have $\epsilon > 1$. The displacement field is

$$\mathbf{D} = \mathbf{E} + 4\pi\mathbf{P} \quad , \quad (3.20)$$

and atoms are polarizable with \mathbf{P} parallel to the applied field \mathbf{E} , so that $|\mathbf{D}| > |\mathbf{E}|$. Since the dielectric constant is defined through

$$\mathbf{D} = \epsilon\mathbf{E}$$

in these simple circumstances, we conclude that $\epsilon > 1$. For a thorough treatment, see Dolgov et al. [30].

Now let us consider, in contrast to the familiar situation, the possibility of a dielectric medium with

$$\epsilon_{\text{medium}} = 0 \quad , \quad (3.21)$$

a perfect dia-electric, or at least

$$\epsilon_{\text{medium}} \ll 1 \quad , \quad (3.22)$$

a very effective dia-electric medium. We can easily show that if a test charge is placed within the medium, a hole will develop around it.

To see this, consider the arrangement depicted in Fig. 23a, a positive charge distribution ρ_+ placed in the medium. Suppose that a hole is formed. Then because the dielectric constant of the medium is less than unity, the induced charge on the inner surface of the hole will also be positive. The test charge and the induced

charge thus repel, and the hole is stable against collapse. In normal QED, the induced charge will be negative, as indicated in Fig. 23b, and will attract the test charge. The hole is thus unstable against collapse.

The radius R of the hole can be estimated on the basis of energetics. Within the hole the electrical energy W_{in} is finite and independent of the dielectric constant of the medium. The displacement field is radial and hence continuous across the spherical boundary. Thus it is given outside the hole by

$$\mathbf{D}_{out}(r>R) = \hat{\mathbf{r}}Q/r^2 \quad , \quad (3.23)$$

where Q is the total test charge. The induced charge density on the surface of the hole is

$$\sigma_{induced} = (1-\epsilon)|\mathbf{D}(R)|/4\pi\epsilon = (1-\epsilon)Q/4\pi\epsilon R^2 \quad , \quad (3.24)$$

which has the same sign as Q , as earlier asserted. Outside the hole, the electric field is determined by the total interior charge

$$Q + (1-\epsilon)Q/\epsilon = Q/\epsilon \quad , \quad (3.25)$$

so that

$$\mathbf{E}_{out}(r>R) = \hat{\mathbf{r}}Q/\epsilon r^2 \quad . \quad (3.26)$$

The energy stored in electric fields outside the hole is then

$$W_{out} = \frac{1}{8\pi} \int d^3r \mathbf{D}_{out}(r) \cdot \mathbf{E}_{out}(r) = \frac{1}{2} \int_R^\infty r^2 dr Q^2 / \epsilon r^4 = Q^2 / 2\epsilon R \quad . \quad (3.27)$$

As the dielectric constant of the medium approaches zero, W_{out} becomes large compared to W_{in} , so that the total electric energy

$$W_{el} \approx W_{in} + W_{out} \rightarrow W_{out} \quad , \quad \text{as } \epsilon \rightarrow 0 \quad . \quad (3.28)$$

One must consider as well the energy required to hew such a hole out of the medium. For a hole of macroscopic size, it is reasonable to suppose that

$$W_{hole} = \frac{4}{3} \pi R^3 v + 4\pi R^2 s + \dots \quad , \quad (3.29)$$

where v and s are non-negative constants. The total energy of the system,

$$W = W_{el} + W_{hole} \quad , \quad (3.30)$$

can now be minimized with respect to R . In the regime where the volume term dominates W_{hole} , the minimum occurs at

$$R = \left(\frac{Q^2}{2\epsilon} \cdot \frac{1}{4\pi v} \right)^{1/3} \neq 0 \quad , \quad (3.31)$$

for which

$$W_{e1} \approx \left(\frac{Q^2}{2\epsilon}\right)^{\frac{3}{2}} (4\pi v)^{\frac{1}{2}} \quad , \quad (3.32)$$

and

$$W_{hole} \approx \frac{1}{3} \left(\frac{Q^2}{2\epsilon}\right)^{\frac{3}{2}} (4\pi v)^{\frac{1}{2}} \quad , \quad (3.33)$$

so that

$$W \approx \frac{4}{3} \left(\frac{Q^2}{2\epsilon}\right)^{\frac{3}{2}} (4\pi v)^{\frac{1}{2}} \quad . \quad (3.34)$$

Thus, in a very effective dia-electric medium, a test charge will induce a bubble or hole of finite radius. Notice, however, that in the limit of a perfect dia-electric medium

$$W \rightarrow \infty \quad \text{as} \quad \epsilon \rightarrow 0 \quad . \quad (3.35)$$

An isolated charge in a perfect dia-electric thus has infinite energy.

If instead of an isolated charge, we place a test dipole within the putative hole in the medium, we can again show that the minimum energy configuration occurs for a hole of finite radius about the test dipole. In this case, however, the field lines need not extend to infinity, so the hole radius remains finite as $\epsilon \rightarrow 0$, and so does the total energy of the system. The analogy between the exclusion of chromoelectric flux from the QCD vacuum and the exclusion of magnetic flux from a superconductor is now obvious. To separate the dipole charges to $\pm\infty$ requires an infinite amount of work, as shown in the previous example. This is the would-be analog of quark confinement.

The 1/N Expansion in Particle Physics (or, Why QCD May Be the Solution to the Hadron Spectrum). The search for small parameters which can play the part of expansion parameters is a central element of the process of approximation and model making that is theoretical physics. In many physical situations, extremes of energy or distance suggest highly accurate and readily improved approximation schemes. In classical electrodynamics the indispensable far-field approximation is applicable when the size of a radiator is negligible compared to the distance between the radiator and receiver. The Born approximation for the scattering of charged-particle beams from atomic electrons is trustworthy for beam energies greatly in excess of the atomic binding energy. In Quantum ChromoDynamics, a perturbative treatment (which is to say an expansion in powers of the strong coupling parameter $\alpha_s(Q^2)$) is expected to be reliable when the invariant momentum

transfer Q^2 is large compared to a characteristic mass scale denoted by Λ^2 .

For the problem of hadron structure, no similar expansion is applicable. All of the relevant energies of the problem are on the order of the naturally occurring scale. In a typical hadron, the separation of the quarks is simply the hadronic size of approximately 1 fm—hardly a regime in which perturbative QCD is likely to make any sense. We may, of course, simply await the day when a very heavy quarkonium family is found, and then happily apply conventional perturbative measures. That insouciant course however leaves untouched the problem of the structure of all the hadrons now known, so other actions are called for.

The strategy of the $1/N$ expansion is a familiar one. When confronted with a problem we cannot solve, we invent a related problem that we can attack. If this is done adroitly, the new problem will not only be simpler but will also capture the physical essence of the original one. More specifically, the $1/N$ expansion represents an attempt to introduce a parameter that permits a simplification of the calculation at hand.

For QCD, this simplification is achieved [31] by generalizing the color gauge group from $SU(3)_c$ to $SU(N)_c$ and considering the limit in which N becomes very large. Although $SU(N)$ is in general more complicated than $SU(3)$, the hadron structure problem is simplified by two observations:

(i) At any order in the strong coupling constant, some classes of diagrams are found to be combinatorially negligible.

(ii) The remaining diagrams have common consequences, in large- N perturbation theory.

This technique does not entirely free us from the constraints of perturbative analysis. Since we shall find, by inspection, that entire classes of combinatorially favored diagrams have common features to all orders in the coupling constant, we shall have to assume that the content of the theory is accurately represented by the set of all diagrams. For QCD, the best evidence for the reliability of the $1/N$ expansion is that $SU(N)_c$ QCD seems to resemble the world we observe.

The combinatorial analysis of $SU(N)_c$ QCD is most transparent in terms of the double-line notation introduced for this purpose by 't Hooft [31], which is illustrated in Fig. 24. Several examples will suffice to make the main points.

Consider first the lowest-order vacuum polarization contributions to the gluon propagator, the quark loop illustrated in Fig. 25a and the gluon loop pictured in Fig. 25b, in conventional notation. These are redrawn in the double-line notation in Fig. 25c, d. For an initial gluon of type $i\bar{j}$, only a single color configuration is possible for the quark loop intermediate state: a quark of color i and an antiquark of color \bar{j} . For the gluon loop, however, the index k is free to take on any value $1, 2, \dots, N$. Thus the gluon loop diagram has a combinatoric factor N associated with it. This illustrates the general rule that gluon loops dominate over quark loops by a factor of N , as $N \rightarrow \infty$.

The presence of the factor N would seem to imply that the gluon loop diagram diverges as $N \rightarrow \infty$. This can be cured by choosing the coupling constant to be g/\sqrt{N} , with g fixed as $N \rightarrow \infty$. Then for any value of N , the contribution of the gluon loop goes as

$$(g/\sqrt{N})^2 \times N \rightarrow g^2 \quad , \quad (3.36)$$

a smooth limit.

That this device solves the divergence problem in general is indicated by an analysis of diagrams with more than one loop. The two-loop diagram depicted in Fig. 26 in (a) standard and (b) double-line notation is immediately seen to be proportional to

$$(g/\sqrt{N})^4 \times N^2 \rightarrow g^4 \quad . \quad (3.37)$$

Similarly, the three-loop diagram of Fig. 27 obviously goes as

$$(g/\sqrt{N})^6 \times N^3 \rightarrow g^6 \quad . \quad (3.38)$$

The situation is different for nonplanar graphs, however. The simplest such graph is shown in Fig. 28. The double-line notation makes it apparent that this graph contains but a single, tangled color loop, and therefore goes as

$$(g/\sqrt{N})^6 \cdot N \rightarrow g^6/N^2 \quad , \quad (3.39)$$

and is therefore suppressed by $1/N^2$ compared to its planar counterpart at the same order in g^2 . It is generally the case that nonplanar graphs are reduced by $1/N^2$, as $N \rightarrow \infty$.

These combinatorial arguments select planar graphs as an important subclass. To evaluate and sum all the graphs thus selected is no trivial task. Instead, we may identify their common features and speculate that these survive confinement. It is possible in this way to establish the following results in the large- N limit:

(i) Mesons are free, stable, and noninteracting. For each allowed combination of J^{PC} and flavor quantum numbers, there are an infinite number of resonances.

(ii) Zweig's rule is exact. Singlet-octet mixing (through virtual annihilations) and meson-gluon mixing are suppressed. Mesons are pure $(q\bar{q})$ states, with no quark-antiquark sea.

(iii) Meson-meson bound states, which would include particles with exotic quantum numbers, are absent.

(iv) Meson decay amplitudes are proportional to $1/\sqrt{N}$, so mesons are narrow structures.

(v) The meson-meson elastic scattering amplitude is proportional to $1/N$ and is given, as in Regge theory, by an infinite number of one-meson exchange diagrams.

(vi) Multibody decays of unstable mesons are dominated by resonant, quasi-two body channels whenever they are open. The partial width of an intrinsically k -body

final state goes as $1/N^{k-1}$.

(vii) For each allowed J^{PC} there are infinitely many glueball states, with widths of order $1/N^2$. They are thus more stable than $(q\bar{q})$ mesons, interact feebly with $(q\bar{q})$ mesons, and mix only weakly with $(q\bar{q})$ states.

Until QCD is actually solved, we will not know how closely the $N \rightarrow \infty$ limit of $SU(N)_C$ resembles the case of interest, which is color $SU(3)$. The preceding list of large- N results does bear, however, a quite striking resemblance to what is observed in experiments. To the extent that the $1/N$ expansion faithfully represents the consequences of QCD, much of the familiar phenomenology is explained, and many of the model approximations are justified.

It is worthwhile to indicate diagrammatically how some of these consequences arise. Two-body decay of a color-singlet into color-singlets is illustrated in Fig. 29. In fourth order, the amplitude is given by

$$A = (g/\sqrt{N})^4 \cdot N^3 \cdot (1/\sqrt{N})^3 \quad , \quad (3.40)$$

where the N^3 is the combinatorial factor for three loops, and a factor of $1/\sqrt{N}$ occurs for each color-singlet projection. The decay amplitude is therefore proportional to $1/\sqrt{N}$.

To the same order in the coupling constant, the propagator of a color singlet, indicated in Fig. 30, goes as

$$(g/\sqrt{N})^4 \cdot N^3 \cdot (1/\sqrt{N})^2 \sim g^4 \quad , \quad (3.41)$$

independent of N .

Compared to the allowed decay, the disconnected quark line diagram of Fig. 31 is suppressed by an additional power of $1/N$. In this case the amplitude is

$$A = (g/\sqrt{N})^4 \cdot N \cdot (1/\sqrt{N}) \propto g^4/N\sqrt{N} \quad . \quad (3.42)$$

As a final example, mixing between $(q\bar{q})$ -mesons and $(q^2\bar{q}^2)$ -exotics proceeds at fourth order by the diagrams of Fig. 32. The mixing amplitude goes as

$$A = (g/\sqrt{N})^4 \cdot N^2 \cdot (1/\sqrt{N})^2 \propto g^4/N \quad . \quad (3.43)$$

which vanishes in the large- N limit.

This brief survey shows that the $1/N$ analysis of $SU(N)_C$ reproduces some of the features of meson spectroscopy. It is of clear interest to learn to what extent these results are indeed representative of QCD, the theory based on $SU(3)_C$. To the extent the correspondence can be made, the $1/N$ analysis motivates the neglect of quark loops in lattice QCD.

LECTURE 4: TOWARD LATTICE GAUGE THEORY

In this lecture, we begin to formulate QCD on a lattice. Nonperturbative methods are called for on two accounts. Perturbation theory will not converge if coupling constants are large, and perturbation theory is not complete. It gives no hint of intrinsically nonperturbative phenomena such as barrier penetration, soliton solutions or (central to our purposes here) color confinement. There are also several reasons for introducing a space-time lattice. It provides an ultraviolet cutoff, allows us to bring the full arsenal of statistical-mechanical methods to bear on field theory, and gives a nonperturbative implementation of QCD.

Our goal in this lecture will be to make precise the connection between quantum mechanics and statistical mechanics. To do so, we review the path-integral formulation of quantum mechanics developed by Feynman [32]. It is helpful to proceed by example; we consider the harmonic oscillator in 1-dimension, for which the Lagrangian is

$$\mathcal{L} = \frac{1}{2}(m\dot{x}^2 - \omega^2 x^2) \quad . \quad (4.1)$$

The amplitude for the transition from the initial space-time point (x_a, t_a) to the final point (x_b, t_b) is

$$Z = \sum_{\text{paths}} e^{iS/\hbar} = \int \mathcal{D}x(t) e^{iS[x(t)]/\hbar} \quad , \quad (4.2)$$

where the classical action is

$$S = \int_{t_a}^{t_b} dt \mathcal{L} \quad . \quad (4.3)$$

To give meaning to (4.2) we must provide a sensible operational definition of the sum over paths.

We first introduce a space-time lattice so various paths may be labelled simply. It is convenient to regard time as a discrete variable, and to choose a lattice with equal time slices

$$t_{i+1} - t_i = \epsilon \quad (4.4)$$

as shown in Fig. 33. The expression (4.2) for the amplitude contains rapidly oscillating phases from the factor $e^{iS/\hbar}$. To tame these, we continue to imaginary time by writing

$$t = -i\tau \quad , \quad (4.5)$$

so that

$$S \rightarrow \frac{i}{2} \int d\tau \left[m(dx/d\tau)^2 + \omega^2 x^2 \right] \quad . \quad (4.6)$$

The phase factor $e^{iS/\hbar}$ is therefore replaced by $e^{-\hat{S}/\hbar}$, where the Euclidean action is given by

$$\hat{S} = \int d\tau \frac{1}{2} \left[m(dx/d\tau)^2 + \omega^2 x^2 \right] . \quad (4.7)$$

If the integral is replaced by a sum over discrete time slices, the Euclidean action becomes

$$\hat{S} = \frac{\epsilon}{2} \sum_i \left\{ \frac{(x_{i+1} - x_i)^2}{\epsilon^2} + \omega^2 x_i^2 \right\} . \quad (4.8)$$

The similarity between the Schrödinger problem and a one-dimensional statistical system is now evident. The partition function

$$Z \equiv \sum_{\text{states}} e^{-\beta E_{\text{state}}} , \quad (4.9)$$

with $\beta=1/kT$, is a sum over Boltzmann weights for all possible configurations of the system. We may compare this with the quantum mechanical transition amplitude

$$Z = \sum_{\text{paths}} e^{-\hat{S}/\hbar} = \int_{-\infty}^{\infty} dx_1 \int_{-\infty}^{\infty} dx_2 \dots \int_{-\infty}^{\infty} dx_N e^{-\hat{S}/\hbar} . \quad (4.10)$$

We see at once the correspondences:

Quantum Mechanics

Euclidean action \hat{S}
 \hbar

Statistical Mechanics

Hamiltonian \mathcal{H}
 $1/\beta \sim T$

The limit $\hbar \rightarrow 0$ picks out the classical trajectory, without quantum fluctuations, just as $T \rightarrow 0$ is a frozen point in statistical mechanics, free of thermal fluctuations.

In the particular case of our example, there is a correspondence between the quantum mechanical problem of the harmonic oscillator and a statistical mechanics problem involving nearest-neighbor interactions. This is exhibited more clearly if we rewrite the partition function as

$$Z = \int_{-\infty}^{\infty} \prod_i [dx_i T(x_{i+1}, x_i)] , \quad (4.11)$$

where

$$T(x_{i+1}, x_i) = \exp \left\{ -\frac{1}{2\hbar} \left[\frac{(x_{i+1} - x_i)^2}{\epsilon} + \frac{\omega^2 \epsilon x_{i+1}^2}{2} + \frac{\omega^2 \epsilon x_i^2}{2} \right] \right\} \quad (4.12)$$

is the transfer matrix. To establish the equivalence with the Hamiltonian formulation of quantum mechanics, choose operators x and p such that

$$\underline{x}|x\rangle = x|x\rangle \quad , \quad (4.13)$$

with

$$\langle x'|x\rangle = \delta(x'-x) \quad . \quad (4.14)$$

The basis is assumed to be complete, so that

$$I = \int dx |x\rangle\langle x| \quad . \quad (4.15)$$

The conjugate momentum operator \underline{p} satisfies

$$[\underline{p}, \underline{x}] = -i\hbar \quad , \quad (4.16)$$

and so generates translations:

$$e^{-i\underline{p}a/\hbar}|x\rangle = |x+a\rangle \quad . \quad (4.17)$$

Using these operators we construct the transfer operator \underline{I} with matrix elements

$$\langle x'|\underline{I}|x\rangle = T(x',x) \quad , \quad (4.18)$$

which evidently corresponds to the time-evolution operator of quantum mechanics, and must therefore be related to the Hamiltonian. The partition function may be written in terms of the transfer operator as

$$\begin{aligned} Z &= \int_{-\infty}^{\infty} \prod_i dx_i \langle x_{i+1}|\underline{I}|x_i\rangle \\ &= \int \langle x_b|\underline{I}|x_{N-1}\rangle dx_{N-1} \langle x_{N-1}|\underline{I}|x_{N-2}\rangle \dots \langle x_1|\underline{I}|x_a\rangle \\ &= \langle x_b|\underline{I}^N|x_a\rangle \quad , \end{aligned} \quad (4.19)$$

where N is the number of time slices and the last step follows from the completeness property (4.15). As a final preliminary to expressing $T(x',x)$ in operator form, we note that

$$\begin{aligned} \langle x'|\exp(-\epsilon p^2/2)|x\rangle &= \int dp dp' \langle x'|p'\rangle \langle p'|\exp(-\epsilon p^2/2)|p\rangle \langle p|x\rangle \\ &= \frac{1}{2\pi} \int dp dp' e^{ip'x'/\hbar} e^{-\epsilon p^2/2} e^{-ipx/\hbar} \delta(p'-p) \\ &= \frac{1}{2\pi} \int dp e^{ip(x'-x)/\hbar} e^{-\epsilon p^2/2} \\ &= \frac{1}{\sqrt{2\pi\epsilon}} \exp\left\{-\frac{(x'-x)^2}{2\epsilon\hbar^2}\right\} \quad . \end{aligned} \quad (4.20)$$

The transfer operator satisfying (4.18) may therefore be written as

$$\underline{I} = \exp(-\epsilon\omega^2\underline{x}^2/4\hbar)\exp(-\epsilon\underline{p}^2/2\hbar)\exp(-\epsilon\omega^2\underline{x}^2/4\hbar)\cdot\text{constant} \quad . \quad (4.21)$$

Using the operator identity

$$e^{\underline{A}}e^{\underline{B}} = \exp\{\underline{A} + \underline{B} + \frac{1}{2}[\underline{A},\underline{B}] + \dots\} \quad , \quad (4.22)$$

we find that

$$\underline{I} = \text{constant}\cdot\exp\left[-\epsilon(\underline{p}^2+\omega^2\underline{x}^2)/2\hbar + O(\epsilon^2)\right] \quad . \quad (4.23)$$

In the limit of vanishing lattice spacing $\epsilon\rightarrow 0$, the transfer operator approaches

$$\underline{I} \rightarrow \text{constant}\cdot\exp(-\epsilon\underline{\mathcal{H}}/\hbar) \quad , \quad (4.24)$$

with

$$\underline{\mathcal{H}} = \frac{1}{2}(\underline{p}^2+\omega^2\underline{x}^2) \quad . \quad (4.25)$$

To see the equivalence of the transfer formalism to the Schrödinger equation, consider the evolution of an arbitrary state $\psi(x,\tau)$. We may write

$$\begin{aligned} \psi(x',\tau') &\equiv \langle x'|\psi\rangle = \int dx Z(x',\tau',x,\tau)\psi(x,\tau) \\ &= \int dx \langle x'|\underline{I}|x\rangle\langle x|\psi\rangle_{\tau} \quad . \end{aligned} \quad (4.26)$$

For an infinitesimal time interval

$$\tau' - \tau = \epsilon \quad (4.27)$$

we have

$$\begin{aligned} \psi(x',\tau') &= \int dx \langle x'|\exp(-\epsilon\underline{\mathcal{H}}/\hbar)|x\rangle\langle x|\psi\rangle_{\tau} \\ &\approx \int dx \langle x'|(1-\epsilon\underline{\mathcal{H}}/\hbar)|x\rangle\langle x|\psi\rangle_{\tau} \\ &= \psi(x',\tau) - \frac{\epsilon}{\hbar}\underline{\mathcal{H}}\psi(x',\tau) \quad , \end{aligned} \quad (4.28)$$

so that

$$\frac{\hbar}{\epsilon}[\psi(x',\tau')-\psi(x',\tau)] = \hbar \frac{\partial\psi}{\partial\tau}(x',\tau) = -\underline{\mathcal{H}}\psi(x',\tau) \quad , \quad (4.29)$$

which we recognize as the Euclidean form of the Schrödinger equation.

We may give a more general definition of the Hamiltonian as

$$\underline{\mathcal{H}}_{\epsilon} = (-\hbar/\epsilon)\ln \underline{I} \quad , \quad (4.30)$$

the coefficient of the term in $\ln \underline{I}$ linear in the lattice spacing ϵ . As $\epsilon\rightarrow 0$, $\underline{\mathcal{H}}_{\epsilon} \rightarrow \underline{\mathcal{H}}$. In this picture, operators are independent of τ , and all the τ -dependence is carried by the state functions.

Let us close with a few general observations. In statistical mechanics,

thermodynamic properties are determined by the largest eigenvalue of the transfer matrix. In quantum mechanics, the corresponding eigenvector has the lowest eigenvalue of \mathcal{H} : it is the vacuum, or ground state, of the system. Notice that if we impose periodic boundary conditions and integrate over all initial positions,

$$Z = \langle x_b | \underline{I}^N | x_a \rangle \rightarrow \text{tr } \underline{I}^N \quad , \quad (4.31)$$

which emphasizes the importance of the largest eigenvalue.

The path-integral and Hamiltonian formulations of quantum mechanics are equivalent. Roughly speaking, the path-integral approach is more efficient for scattering problems, and the Hamiltonian language is superior for bound-state problems.

LECTURE 5: FIELD THEORY ON THE LATTICE

In this lecture we shall make the connection between statistical mechanics and quantum field theory. The same general ideas that we have exploited in Lecture 4 will apply here. Let us first recall the correspondence between quantum mechanics and field theory:

<u>Quantum Mechanics</u>	<u>Quantum Field Theory</u>
position x	dynamical variables
particle trajectory	path
	$\psi(x)$: field values at each point x in $d-1$ dimensional space
	space-time history of the field

In seeking the precise correspondence between statistical mechanics and field theory we shall once again proceed by example, this time studying scalar field theory in d -dimensions, for which the Lagrangian is

$$\mathcal{L} = \int d^{d-1}x \left[\frac{1}{2} \left(\frac{\partial \phi}{\partial t} \right)^2 - \frac{1}{2} (\nabla \phi)^2 - \frac{1}{2} \mu^2 \phi^2 - \frac{\lambda |\phi|^4}{4} \right] \quad . \quad (5.1)$$

As before, the classical action is

$$S = \int_{t_a}^{t_b} dt \quad (5.2)$$

and the path integral can be defined as

$$Z = \sum_{\text{paths}} e^{iS/\hbar} = \int [\mathcal{D}\phi(x)] e^{iS[\phi(x)]/\hbar} \quad , \quad (5.3)$$

and our task is to give a meaning to the path integral.

To begin, we continue to imaginary time,

$$t \rightarrow -i\tau \quad . \quad (5.4)$$

We assume this can be done. A demonstration that this is permissible was given order-by-order in perturbation theory for all Green's functions by Schwinger [33]. We next formulate the theory on an isotropic, Euclidean space-time lattice with lattice spacing a . This regularizes ultraviolet divergences because no wavelengths shorter than a (no momenta in excess of π/a) appear. The Euclidean action becomes

$$\hat{S} = a^d \sum_{\text{lattice sites } \mathbf{n}} \left\{ \frac{1}{2} \frac{[\Delta_0 \phi(\mathbf{n})]^2}{a^2} + \frac{1}{2} \sum_{k=1}^{d-1} \frac{[\Delta_k \phi(\mathbf{n})]^2}{a^2} + \frac{1}{2} \mu^2 [\phi(\mathbf{n})]^2 + \frac{|\lambda|}{4} [\phi(\mathbf{n})]^4 \right\} , \quad (5.5)$$

where $\mathbf{n} = (n_0; n_1, n_2 \dots n_{d-1})$ labels lattice sites. We denote by the "unit vector" $\hat{\mathbf{n}}_\mu$ one lattice step along the μ -direction. The difference operator is defined as

$$\Delta_\mu f(\mathbf{n}) = f(\mathbf{n} + \hat{\mathbf{n}}_\mu) - f(\mathbf{n}) \quad . \quad (5.6)$$

We may rewrite the Euclidean action more compactly as

$$\hat{S} = \sum_{\mathbf{n}} \left\{ K \sum_{\mu=0}^{d-1} [\Delta_\mu \phi(\mathbf{n})]^2 + b [\phi(\mathbf{n})]^2 + u [\phi(\mathbf{n})]^4 \right\} , \quad (5.7)$$

where

$$K = \frac{1}{2} a^{d-2} \quad (5.8)$$

is the nearest-neighbor coupling, and

$$\left. \begin{aligned} b &= \mu^2 a^d / 2 \quad , \\ u &= |\lambda| a^d / 4 \quad . \end{aligned} \right\} \quad (5.9)$$

The path integral for the lattice theory is (hereafter we set $\hbar=1$)

$$Z = \prod_{\mathbf{n}} \int_{-\infty}^{\infty} d\phi(\mathbf{n}) e^{-\hat{S}} \quad , \quad (5.10)$$

which corresponds to the partition function of a d -dimensional statistical mechanics problem, with boundary conditions on the path integral specifying ϕ on initial and final temporal slices.

As we did in quantum mechanics, we define a transfer matrix to propagate the field $\phi(\mathbf{n})$ in the time direction, from ϕ on one time slice to ϕ' on the next:

$$\begin{aligned}
\langle \phi' | \mathbb{I} | \phi \rangle = \exp \left[- \sum_{\mathbf{n}} \left\{ K [\phi'(\mathbf{n}) - \phi(\mathbf{n})]^2 + \right. \right. \\
\left. \left. + \frac{K}{2} \sum_{\mu=1}^{d-1} \left([\phi'(\mathbf{n} + \hat{\mathbf{n}}_{\mu}) - \phi'(\mathbf{n})]^2 + [\phi(\mathbf{n} + \hat{\mathbf{n}}_{\mu}) - \phi(\mathbf{n})]^2 \right) \right. \right. \\
\left. \left. + \frac{b}{2} [\phi'(\mathbf{n})^2 + \phi(\mathbf{n})^2] + \frac{u}{2} [\phi'(\mathbf{n})^4 + \phi(\mathbf{n})^4] \right\} \right] .
\end{aligned} \quad (5.11)$$

To obtain an operator expression, define second-quantized conjugate fields $\phi(\mathbf{n})$, $\pi(\mathbf{n})$ satisfying

$$[\pi(\mathbf{n}'), \phi(\mathbf{n})] = -i\delta_{\mathbf{n}', \mathbf{n}} . \quad (5.12)$$

Manipulations parallel to those of the quantum mechanical case yield

$$\begin{aligned}
\mathbb{I} = \exp \left[-\frac{1}{2} \sum_{\mathbf{n}} \left\{ K \sum_{\mu=1}^{d-1} [\phi'(\mathbf{n} + \hat{\mathbf{n}}_{\mu}) - \phi'(\mathbf{n})]^2 + b\phi'(\mathbf{n})^2 + u\phi'(\mathbf{n})^4 \right\} \right] \\
\times \exp \left[-K \sum_{\mathbf{n}} \pi(\mathbf{n})^2 \right] \times \\
\exp \left[-\frac{1}{2} \sum_{\mathbf{n}} \left\{ K \sum_{\mu=1}^{d-1} [\phi(\mathbf{n} + \hat{\mathbf{n}}_{\mu}) - \phi(\mathbf{n})]^2 + b\phi(\mathbf{n})^2 + u\phi(\mathbf{n})^4 \right\} \right] .
\end{aligned} \quad (5.13)$$

Just as for quantum mechanics, we can identify the lattice Hamiltonian operator \mathcal{H}_S by

$$\mathbb{I} = e^{-\mathcal{H}_S a} . \quad (5.14)$$

We are now in a position to relate field theory on a lattice to a statistical mechanics analog with greater precision. We will show the correspondence

Statistical Mechanics

Free energy density

Correlation function

1/Correlation length

Quantum Field Theory

Vacuum energy density

Propagator

Mass gap

We begin by expanding the transfer operator in a set of orthonormal eigenvectors with real energy eigenvalues E_i :

$$\mathbb{I} = \mathbb{I}^\dagger = \sum_i |i\rangle e^{-E_i a} \langle i| . \quad (5.15)$$

The partition function corresponds to

$$Z = \text{tr } \mathbb{I}^{N+1} \quad (5.16)$$

for evolution through $N+1$ time slices. The trace in (5.16) arises from identifying, and summing over, the initial and final fields.

In this basis,

$$\mathbb{I}^{N+1} = \sum_i |i\rangle \exp[-(N+1)E_i a] \langle i| \quad . \quad (5.17)$$

Consider the limit of infinitely many time slices ($N \rightarrow \infty$), and suppose there is a unique (vacuum) state of minimum energy E_0 , corresponding to the largest eigenvalue of \mathbb{I} :

$$\lim_{N \rightarrow \infty} \mathbb{I}^{N+1} \rightarrow |0\rangle e^{-E_0 \Delta t} \langle 0| \quad , \quad (5.18)$$

where Δt is the difference between final and initial times. In this limit, the path integral is

$$Z = e^{-E_0 \Delta t} \quad . \quad (5.19)$$

This is to be compared with the connection in statistical mechanics between the partition function and the free energy,

$$Z = e^{-\beta F} = e^{-F/kT} \quad . \quad (5.20)$$

The free energy can be expressed as the free energy density times the space-time volume,

$$F = U - TS = fV\Delta t \quad . \quad (5.21)$$

If in analogy we write the vacuum energy eigenvalue as

$$E_0 = \omega_0 V \quad , \quad (5.22)$$

where ω_0 is the energy density of the vacuum, we may identify

$$\beta f = \omega_0 \quad , \quad (5.23)$$

the desired connection.

Next, we construct the field theory propagator in Minkowski space,

$$\Delta(t; \mathbf{x}) = \langle 0 | \mathcal{T} \phi(t; \mathbf{x}) \phi(0; \mathbf{0}) | 0 \rangle \quad , \quad (5.24)$$

where the Heisenberg-picture field operators are related to the Schrödinger-picture operators by

$$\phi(t; \mathbf{x}) = e^{i\mathcal{H}_S t} \phi(\mathbf{x}) e^{-i\mathcal{H}_S t} \quad (5.25)$$

and \mathcal{T} denotes "time-ordering." In terms of the Schrödinger-picture fields, the propagator is

$$\Delta(t; \mathbf{x}) = \langle 0 | \phi(\mathbf{x}) e^{-i\mathcal{H}_S t} \phi(\mathbf{0}) | 0 \rangle e^{iE_0 t} \quad (5.26)$$

Now consider the correlation function in statistical mechanics, which is defined by

$$C(n) = C(n_0; \mathbf{n}) = (1/Z) \prod_{n_0, \mathbf{n}'} \int d\phi(n_0, \mathbf{n}') \phi(n_0, \mathbf{n}) \phi(0, \mathbf{0}) e^{-\hat{S}} \quad (5.27)$$

We organize the sums over configurations so that for each time slice n_0' we integrate over all the spatial sites \mathbf{n}' . Except for the initial and final time slices $n_0'=0$ and $n_0'=n_0$, the reorganized sums are identical to those appearing in the definition of the partition function Z . By the usual steps, we obtain the operator expression for the correlation function,

$$C(n_0, \mathbf{n}) = \frac{\text{tr}\{\mathbb{I}^P \phi(\mathbf{n}) \mathbb{I}^{n_0} \phi(\mathbf{0}) \mathbb{I}^L\}}{\text{tr}\{\mathbb{I}^{N+1}\}} \quad (5.28)$$

where $P + n_0 + L = N+1$.

Now let $P, n_0, L \rightarrow \infty$ so we may use (cf. (5.18))

$$\mathbb{I}^N = |0\rangle e^{-E_0 \Delta t} \langle 0| \quad .$$

We find

$$C(n_0, \mathbf{n}) = \langle 0 | \phi(\mathbf{n}) e^{-n_0 \mathcal{H}_S a} \phi(\mathbf{0}) | 0 \rangle e^{n_0 E_0 a} \quad (5.29)$$

Comparing with the field theory propagator (5.26) we see that

$$C(n_0; \mathbf{n}) \sim \Delta(-in_0 a; \mathbf{n} a) \quad (5.30)$$

This establishes the correspondence between the correlation function in statistical mechanics and the field theory propagator for imaginary times.

For a statistical system not at a critical point, the correlation function falls exponentially:

$$C(n_0; \mathbf{0}) \sim \exp[-|n_0|/\xi] \text{ for } |n_0| \gg \xi \quad , \quad (5.31)$$

where ξ is the correlation length. Compute the imaginary-time propagator in the same approximation:

$$\begin{aligned} \Delta(-in_0 a; \mathbf{0}) &= \langle 0 | \phi(\mathbf{0}) e^{-\mathcal{H}_S n_0 a} \phi(\mathbf{0}) | 0 \rangle e^{E_0 n_0 a} \\ &= \sum_{\lambda} \langle 0 | \phi(\mathbf{0}) e^{-\mathcal{H}_S n_0 a} | \lambda \rangle \langle \lambda | \phi(\mathbf{0}) | 0 \rangle e^{E_0 n_0 a} \\ &= \sum_{\lambda} \exp[-n_0 a (E_{\lambda} - E_0)] |\langle 0 | \phi(\mathbf{0}) | \lambda \rangle|^2 \\ &\xrightarrow{n_0 a \gg 1} \exp[-n_0 a (E_1 - E_0)] |\langle 0 | \phi(\mathbf{0}) | 1 \rangle|^2 \quad , \end{aligned} \quad (5.32)$$

where $|1\rangle$ is the particle state of smallest energy, the lightest particle state at zero momentum. If we identify the mass gap, or particle mass, as

$$m = E_1 - E_0 \quad , \quad (5.33)$$

we have

$$\Delta(-in_0a; \mathbf{0}) \sim \exp(-n_0am) |\langle 0 | \phi(\mathbf{0}) | 1 \rangle|^2 \quad . \quad (5.34)$$

Consequently, so long as the matrix element $\langle 0 | \phi(\mathbf{0}) | 1 \rangle$ is nonvanishing, we may identify the mass gap with the correlation length through $1/\xi \leftrightarrow am$, or

$$m = 1/a\xi \quad . \quad (5.35)$$

A nonzero mass corresponds to a finite correlation length, which is to say an uncritical statistical system. The correspondences between statistical mechanics, quantum mechanics, and quantum field theory reviewed in this lecture and the preceding one are summarized in Fig. 34.

LECTURE 6: GAUGE SYMMETRIES ON THE LATTICE

In this lecture, we consider models with global or local discrete or continuous symmetries on the lattice. Our objectives are to learn how to formulate gauge invariant theories on the lattice, and to see how the methods of statistical mechanics lend themselves to the study of QCD.

The Ising Model [34]. A simple and informative spin system is the Ising Model of a ferromagnetic material in two dimensions. Consider a two-dimensional square lattice as shown in Fig. 35 with a spin $\sigma = \pm 1$ on each site. In the absence of an applied magnetic field, the theory is determined by its nearest-neighbor interactions. The configuration energy, or Euclidean action, is given by

$$\hat{S}[\sigma] = \beta E[\sigma] = -\beta \sum_{\langle ij \rangle} \sigma_i \sigma_j \quad , \quad (6.1)$$

where $\langle ij \rangle$ denotes a sum over nearest-neighbor pairs, or "bonds," and the minus sign (which favors alignment of neighboring spins) is appropriate for a ferromagnetic substance. The model has a global up-down symmetry. That is, the configuration energy is unchanged if all spins are reversed. The partition function is

$$Z = \sum_{\text{spin configurations}} e^{-\beta E[\sigma]} = \sum_{[\sigma]} e^{\beta \sum_{\langle ij \rangle} \sigma_i \sigma_j} . \quad (6.2)$$

The Ising model in two dimensions is exactly solvable, most simply by transfer matrix methods. It displays a second-order phase transition — spontaneous magnetization — at a critical temperature $\beta_c = 0.4407$, corresponding to the condition $\sinh(2\beta_c) = 1$. The behavior of the net magnetization $M = \langle \sigma \rangle$ is sketched in Fig. 36. The sign of the spontaneous magnetization is random, which is to say unpredictable. This is characteristic of spontaneous symmetry breaking.

It is quite illuminating to watch a Monte Carlo simulation of the Ising model. Some representative configurations are shown in Fig. 37. At zero temperature, the system is completely ordered, so that $|M| = 1$, and the up-down symmetry is broken. As the temperature is raised, small bubbles of flipped spins arise. When the temperature exceeds the critical temperature, the bubbles expand and merge, so that $M \approx 0$. The system is then disordered, and the up-down symmetry is restored.

If we think of the lattice as a space-time lattice, the connection with field theory becomes apparent. Bubble formation corresponds, in the language of Feynman diagrams, to vacuum fluctuations. A domain boundary can be regarded as the world line of a (virtual) particle-antiparticle pair.

Z_2 Lattice Gauge Theory. A spin system with local up-down symmetry was constructed by Wegner [35]. Consider a cubic lattice in d -dimensional space-time, as indicated in Fig. 38. Lattice sites are labelled by the coordinate n , and links are labelled by the site n and a lattice unit vector $\hat{\mu}$ leaving the site. An Ising spin $\sigma = \pm 1$ is placed on each link. In the two-dimensional sketch of Fig. 38, the spins at site n are

$$\sigma(n, \hat{x}) \quad , \quad \sigma(n, \hat{y}) \quad , \quad \sigma(n, -\hat{x}) \quad , \quad \sigma(n, -\hat{y}) \quad .$$

A local spin flip (or rotation), which is to say a gauge transformation $\mathcal{F}(n)$ at site n changes these spins to

$$-\sigma(n, \hat{x}) \quad , \quad -\sigma(n, \hat{y}) \quad , \quad -\sigma(n, -\hat{x}) \quad , \quad -\sigma(n, -\hat{y}) \quad .$$

A nontrivial action invariant under local spin flips is given by the product of spins around elementary squares (plaquettes) of the lattice,

$$S = \sum_{\mathbf{n}} \sigma(n, \hat{x}) \sigma(n + \hat{x}, \hat{y}) \sigma(n + \hat{x} + \hat{y}, -\hat{x}) \sigma(n + \hat{y}, -\hat{y}) \quad , \quad (6.3)$$

as shown in Fig. 39. A plaquette involves two links at each lattice site. Under a local spin flip $\mathcal{F}(n)$,

$$\left. \begin{aligned} \sigma(\mathbf{n}, \hat{\mathbf{x}}) &\rightarrow -\sigma(\mathbf{n}, \hat{\mathbf{x}}) \\ \sigma(\mathbf{n} + \hat{\mathbf{y}}, -\hat{\mathbf{y}}) &= \sigma(\mathbf{n}, \hat{\mathbf{y}}) \rightarrow -\sigma(\mathbf{n}, \hat{\mathbf{y}}) = -\sigma(\mathbf{n} + \hat{\mathbf{y}}, -\hat{\mathbf{y}}) \end{aligned} \right\} , \quad (6.4)$$

so $S \rightarrow S$. The same invariance holds for any closed curve used to define the action. The plaquette is the most local definition one can devise.

Using the freedom conferred by the local spinflip invariance, it is easy to show that the Z_2 theory in two dimensions is equivalent to the one-dimensional Ising model. We choose all the links $\sigma(\mathbf{n}, \pm \hat{\mathbf{y}}) = 1$, whereupon

$$\begin{aligned} S &\rightarrow \sum_{\mathbf{n}} \sigma(\mathbf{n}, \hat{\mathbf{x}}) \sigma(\mathbf{n} + \hat{\mathbf{x}} + \hat{\mathbf{y}}, -\hat{\mathbf{x}}) \\ &= \sum_{\mathbf{n}} \sigma(\mathbf{n}, \hat{\mathbf{x}}) \sigma(\mathbf{n} + \hat{\mathbf{y}}, \hat{\mathbf{x}}) . \end{aligned} \quad (6.5)$$

This theory has no phase transition: the spins are always disordered, with $\langle \sigma \rangle = 0$, except at $T=0$.

A Lattice Theory with Continuous Symmetry. A representative model with a global continuous symmetry is the planar spin model. On each site of a (two-dimensional) square lattice, we place a planar spin

$$\hat{\mathbf{s}}(\mathbf{n}) = \begin{pmatrix} \cos \theta(\mathbf{n}) \\ \sin \theta(\mathbf{n}) \end{pmatrix} . \quad (6.6)$$

A nearest-neighbor action is

$$\begin{aligned} S &= -K \sum_{\mathbf{n}, \hat{\boldsymbol{\mu}}} \hat{\mathbf{s}}(\mathbf{n}) \cdot \hat{\mathbf{s}}(\mathbf{n} + \hat{\boldsymbol{\mu}}) \\ &= -K \sum_{\mathbf{n}, \hat{\boldsymbol{\mu}}} \cos[\theta(\mathbf{n}) - \theta(\mathbf{n} + \hat{\boldsymbol{\mu}})] . \end{aligned} \quad (6.7)$$

With the finite-difference, or lattice-derivative, notation

$$\Delta_{\boldsymbol{\mu}} \theta(\mathbf{n}) = \theta(\mathbf{n} + \hat{\boldsymbol{\mu}}) - \theta(\mathbf{n}) , \quad (6.8)$$

we may write

$$S = -K \sum_{\mathbf{n}, \boldsymbol{\mu}} \cos[\Delta_{\boldsymbol{\mu}} \theta(\mathbf{n})] , \quad (6.9)$$

which is manifestly invariant under a global phase rotation

$$\theta(\mathbf{n}) \rightarrow \theta(\mathbf{n}) + \alpha . \quad (6.10)$$

The generalization to a locally symmetric theory is easily made by following

the example of Wegner's Z_2 theory. We place angular variables characterizing planar spins on each link of a lattice, as shown in Fig. 40. The sum of angles around a plaquette,

$$\begin{aligned} P_n &= \theta_x(\mathbf{n}) + \theta_y(\mathbf{n}, \hat{x}) + \theta_{-x}(\mathbf{n} + \hat{x} + \hat{y}) + \theta_{-y}(\mathbf{n} + \hat{y}) \\ &= \theta_x(\mathbf{n}) - \theta_x(\mathbf{n} + \hat{y}) + \theta_y(\mathbf{n} + \hat{x}) - \theta_y(\mathbf{n}) \quad , \end{aligned} \quad (6.11)$$

is unchanged by local angular rotations

$$\theta_\mu(\mathbf{n}) \rightarrow \theta_\mu(\mathbf{n}) + \alpha(\mathbf{n}) \quad . \quad (6.12)$$

Notice that the sum of angles around a directed plaquette is simply the discrete curl

$$P_n = \Delta_x \theta_y - \Delta_y \theta_x \quad (6.13)$$

or, in an arbitrary dimension,

$$\mathcal{F}_{\mu\nu} = \Delta_\nu \theta_\mu - \Delta_\mu \theta_\nu \quad . \quad (6.14)$$

The sum of angles along an open string is changed by angular rotations only by the phase changes at the endpoints.

Now consider simultaneous gauge transformations

$$\left. \begin{aligned} \theta_\mu(\mathbf{n}) &\rightarrow \theta_\mu(\mathbf{n}) + \chi(\mathbf{n}) \\ \theta_\mu(\mathbf{n} + \hat{\mu}) &\rightarrow \theta_\mu(\mathbf{n} + \hat{\mu}) + \chi(\mathbf{n} + \hat{\mu}) \end{aligned} \right\} \quad . \quad (6.15)$$

The net change in $\theta_\mu(\mathbf{n})$ is

$$\begin{aligned} \theta_\mu(\mathbf{n}) &\rightarrow \theta_\mu(\mathbf{n}) + \chi(\mathbf{n}) - \chi(\mathbf{n} + \hat{\mu}) \\ &= \theta_\mu(\mathbf{n}) - \Delta_\mu \chi(\mathbf{n}) \quad , \end{aligned} \quad (6.16)$$

while

$$\mathcal{F}_{\mu\nu} \rightarrow \mathcal{F}_{\mu\nu} \quad . \quad (6.17)$$

This is a spatially discrete form of the local gauge invariance of electrodynamics:

$$\left. \begin{aligned} A_\mu &\rightarrow A_\mu - \partial_\mu \chi \\ F_{\mu\nu} &\rightarrow F_{\mu\nu} \end{aligned} \right\} \quad . \quad (6.18)$$

This similarity suggests that we base a locally phase-invariant lattice action on the phase factor

$$\exp \left[- \frac{ie}{\hbar} \oint dx_\mu A^\mu \right]$$

that leads to QED [36]. A possible form is to take the phase factor around the edges of a plaquette:

$$S_{\text{plaquette}} = K[U(1)U(2)U(3)U(4) + \text{c.c.}] \quad , \quad (6.19)$$

where

$$U(j) = \exp \left[ie \int_{\text{side } j} dx_{\mu} A^{\mu} \right] = \exp [i\theta_j] \quad (6.20)$$

is an element of the group $U(1)$, and the sides are labelled as shown in Fig. 41. We saw earlier that the sum of angles around a plaquette is the locally gauge-invariant quantity $\mathcal{F}_{\mu\nu}(\mathbf{n})$. Comparing with the nearest-neighbor action (6.9), we have

$$S_p = -K \cos(\mathcal{F}_{\mu\nu}) \approx -K \left[1 - \mathcal{F}_{\mu\nu}^2/2 + \dots \right] \quad . \quad (6.21)$$

The constant term is free of dynamics, so we redefine the plaquette action without it, as

$$S_p = K \left[1 - \cos(\mathcal{F}_{\mu\nu}) \right] \quad . \quad (6.22)$$

We may write the lattice action in terms of a sum over plaquettes, as

$$\begin{aligned} S &= \sum_{\mathbf{n}, \mu, \nu} K \left[1 - \cos(\mathcal{F}_{\mu\nu}(\mathbf{n})) \right] \\ &\rightarrow \sum \left(\frac{K \mathcal{F}_{\mu\nu}^2}{2} + \dots \right) \quad . \end{aligned} \quad (6.23)$$

In four dimensions, let $\Sigma \rightarrow \int d^4x/a^4$; the lattice action goes over to

$$S = \frac{K}{a^4} \int d^4x \frac{\mathcal{F}_{\mu\nu}^2}{2} \quad . \quad (6.24)$$

If we identify [37]

$$\left. \begin{aligned} \mathcal{F}_{\mu\nu} &= a^2 e F_{\mu\nu} \\ \theta_{\mu} &= ea A_{\mu} \\ K &= 1/2e^2 \end{aligned} \right\} \quad , \quad (6.25)$$

then

$$S \rightarrow \frac{1}{2} \int d^4x F_{\mu\nu} F^{\mu\nu} \quad , \quad (6.26)$$

the Euclidean action of electrodynamics. This identification fixes the plaquette action as

$$S_p = \frac{1}{2e^2} \left[1 - \cos(\mathcal{F}_{\mu\nu}) \right] \quad . \quad (6.27)$$

Implementing Non-Abelian Gauge Symmetries on the Lattice. We consider as an example the group SU(2) on a four-dimensional hypercubic Euclidean lattice with lattice spacing a . On each link we place an SU(2) group element [38]

$$U_{\mu}(\mathbf{n}) = \exp \left[iB_{\mu}(\mathbf{n}) \right] \quad , \quad (6.28)$$

a 2×2 matrix, where the gauge field is

$$B_{\mu}(\mathbf{n}) = \frac{ag}{2} \vec{\tau} \cdot \vec{A}_{\mu}(\mathbf{n}) \quad . \quad (6.29)$$

[The corresponding form for SU(N) is an $N \times N$ matrix. The gauge field \vec{A}_{μ} has N^2-1 components, and $(\vec{\tau}/2)$ is replaced by the normalized generators of SU(N).] Just for the Abelian case, each link carries a directional sense $(\mathbf{n}, \hat{\mu})$, and a backward link carries

$$U_{-\mu}(\mathbf{n} + \hat{\mu}) = U_{\mu}^{-1}(\mathbf{n}) \quad . \quad (6.30)$$

Under a local gauge transformation characterized by

$$G[\vec{\chi}(\mathbf{n})] = \exp \left[\frac{-i\vec{\tau} \cdot \vec{\chi}(\mathbf{n})}{2} \right] = G(\mathbf{n}) \quad (6.31)$$

the link variables transform as

$$U_{\mu}(\mathbf{n}) \rightarrow G(\mathbf{n})U_{\mu}(\mathbf{n})G^{-1}(\mathbf{n} + \hat{\mu}) \quad . \quad (6.32)$$

This is the simplest local generalization of a global gauge transformation (cf. (6.16)). As in the Abelian theory, a string of link variables transforms by a gauge rotation at each end.

A product of link variables around a closed loop is locally gauge invariant. The most local color singlet on which to base a lattice action is the elementary Wilson loop [38]

$$\text{Tr} \left\{ U_{\mu}(\mathbf{n})U_{\nu}(\mathbf{n} + \hat{\mu})U_{-\mu}(\mathbf{n} + \hat{\mu} + \hat{\nu})U_{-\nu}(\mathbf{n} + \hat{\nu}) \right\} \quad . \quad (6.33)$$

Wilson's lattice action is

$$S = -(1/2g^2) \sum_{\mathbf{n}, \mu, \nu} \left\{ \text{tr} \left[U_{\mu}(\mathbf{n})U_{\nu}(\mathbf{n} + \hat{\mu})U_{-\mu}(\mathbf{n} + \hat{\mu} + \hat{\nu})U_{-\nu}(\mathbf{n} + \hat{\nu}) \right] + \text{h.c.} \right\} \quad . \quad (6.34)$$

We shall now show that in the classical continuum limit $a \rightarrow 0$ (the "naive continuum limit") this lattice action becomes the Euclidean action for Yang-Mills theory.

We begin by making a Taylor expansion of the gauge fields around site \mathbf{n} :

$$\begin{aligned}
B_\nu(\mathbf{n}+\hat{\mu}) &\approx B_\nu(\mathbf{n}) + a\partial_\mu B_\nu(\mathbf{n}) + O(a^2) \quad , \\
B_{-\mu}(\mathbf{n}+\hat{\mu}+\hat{\nu}) &= -B_\mu(\mathbf{n}+\hat{\nu}) \\
&\approx -\left[B_\mu(\mathbf{n}) + a\partial_\nu B_\mu(\mathbf{n}) + O(a^2) \right] \quad , \\
B_{-\nu}(\mathbf{n}+\hat{\nu}) &= -B_\nu(\mathbf{n}) \quad .
\end{aligned}
\tag{6.35}$$

The Wilson loop is then approximately

$$\begin{aligned}
UUUU &\approx \exp\left[iB_\mu(\mathbf{n}) \right] \exp\left[i\left(B_\nu(\mathbf{n}) + a\partial_\mu B_\nu(\mathbf{n}) \right) \right] \\
&\quad \times \exp\left[-i\left(B_\mu(\mathbf{n}) + a\partial_\nu B_\mu(\mathbf{n}) \right) \right] \exp\left[-iB_\nu(\mathbf{n}) \right] \quad .
\end{aligned}
\tag{6.36}$$

Using the operator identity

$$e^{\frac{X}{e} \frac{Y}{e}} = \exp\left[\frac{X+Y}{e} + \frac{1}{2} [X, Y] + \dots \right] \quad ,
\tag{6.37}$$

we find

$$\begin{aligned}
UUUU &= \exp\left[i\left(B_\mu + B_\nu + a\partial_\mu B_\nu \right) - \frac{1}{2} [B_\mu, B_\nu] \right] \\
&\quad \times \exp\left[-i\left(B_\mu + B_\nu + a\partial_\nu B_\mu \right) - \frac{1}{2} [B_\mu, B_\nu] \right] \\
&\approx \exp\left[ia\left(\partial_\mu B_\nu - \partial_\nu B_\mu \right) - [B_\mu, B_\nu] \right] \quad .
\end{aligned}
\tag{6.38}$$

Recalling the definition (6.29) of the gauge field, we let

$$A_\mu(\mathbf{n}) = \frac{\vec{t}}{2} \cdot \vec{A}_\mu(\mathbf{n}) \quad ,
\tag{6.39}$$

whereupon

$$UUUU = \exp\left[ia^2 g \left(\partial_\mu A_\nu - \partial_\nu A_\mu + ig [A_\mu, A_\nu] \right) \right] \quad .
\tag{6.40}$$

The expression in parentheses is minus the Yang-Mills field-strength tensor $G_{\mu\nu}$, so we may write

$$UUUU = \exp\left[-ia^2 g G_{\mu\nu} + \text{higher order in } a \right] \quad .
\tag{6.41}$$

Now take the classical continuum limit of smooth fields by considering

$$a^2 g G_{\mu\nu} \ll 1 \quad ,
\tag{6.42}$$

so that

$$\begin{aligned}
\text{Tr}(UUUU) &= \text{Tr} \left(\exp[-ia^2 g G_{\mu\nu}] \right) \\
&\approx \text{Tr} \left(1 - ia^2 g G_{\mu\nu} - \frac{1}{2} a^4 g^2 G_{\mu\nu}^2 + \dots \right) \\
&\approx \text{Tr}(1) - \frac{1}{2} a^4 g^2 \text{tr}(G_{\mu\nu} G^{\mu\nu}) + \dots
\end{aligned}
\tag{6.43}$$

In this limit, the lattice action becomes

$$\begin{aligned}
S &= (-1/2g^2) \sum_{\mathbf{n}, \hat{\mu}, \hat{\nu}} \left[\text{Tr}(UUUU) + \text{h.c.} \right] \\
&\longrightarrow \frac{1}{2g^2} \int \frac{d^4x}{a^4} \frac{a^4 g^2}{2} \frac{\vec{G}_{\mu\nu} \cdot \vec{G}^{\mu\nu}}{2} \cdot 2 + O(a^2) \quad ,
\end{aligned}
\tag{6.44}$$

where the (+h.c.) contributes the overall factor of 2. Simplifying the expression, we find

$$S \approx \frac{1}{2} \int d^4x \vec{G}_{\mu\nu} \cdot \vec{G}^{\mu\nu} \quad ,
\tag{6.45}$$

the Euclidean action of classical Yang-Mills theory.

Observe that the final result has a Euclidean $O(4)$ invariance, whereas the original lattice action had only a hypercubic symmetry. The $O(4)$ symmetry breaking resides in terms that are higher order in the lattice spacing a , and do not affect the continuum limit. This emphasizes that the Wilson action is not a unique choice. Many possible lattice actions have the same continuum limit. For example, we may replace the elementary plaquettes by more complicated loops, or add other gauge-invariant quantities which vanish with additional powers of a . All such lattice actions should have the same critical behavior, and reproduce the same continuum field theory — up to renormalization constants. The final classical continuum result involves the standard locally gauge invariant Yang-Mills field strength tensor $\vec{G}_{\mu\nu}$. This is guaranteed by the local gauge invariance of the lattice action.

LECTURE 7: THE STRONG COUPLING EXPANSION AND CONFINEMENT

An important attribute of lattice gauge theory is that we can easily study properties of the theory in the strong coupling limit $g^2 \rightarrow \infty$. Recalling that the lattice action is schematically given by

$$S \sim \beta \sum_p \text{tr}(UUUU)
\tag{7.1}$$

with $\beta=1/g^2$, we are reminded that $1/g^2$ is the analog of $1/kT$ in statistical mechanics. The strong coupling expansion is therefore akin to the high temperature expansion. As we noted in our survey of the Ising model, the high-temperature phase characterizes a very disordered system. We shall see in the course of this lecture that there is a deep connection between disorder and confinement.

Physical observables are given by the expectation values of gauge-invariant quantities on the lattice. An example is the Wilson loop,

$$W(\mathcal{C}) = \left\langle \text{tr} \left(\prod_{\mathcal{C}} U \right) \right\rangle = \frac{1}{Z} \int [dU] \text{Tr} \left(\prod_{\mathcal{C}} U \right) e^{-S} \quad , \quad (7.2)$$

where \mathcal{C} defines a closed path on the lattice. For $g^2 \rightarrow \infty$ ($\beta \rightarrow \infty$), we may expand

$$e^{-S} \sim 1 - \beta \sum_p \text{tr}(UUUU) + \dots \quad (7.3)$$

To proceed further, we must be more precise about the integral $\int [dU]$ over the group volume at each link. For a $U(1)$ gauge theory, this represents an integral over the phase angle on each link. If we write $U_j = e^{i\theta_j}$, then

$$\int [dU] = \int_0^{2\pi} \frac{d\theta_1}{2\pi} \int_0^{2\pi} \frac{d\theta_2}{2\pi} \dots \int_0^{2\pi} \frac{d\theta_M}{2\pi} \quad (7.4)$$

for a lattice of M links. Notice in particular that

$$\left. \begin{aligned} \int_0^{2\pi} \frac{d\theta}{2\pi} &= 1 \quad , \\ \int_0^{2\pi} \frac{d\theta}{2\pi} e^{i\theta} &= 0 \quad . \end{aligned} \right\} \quad (7.5)$$

For the general case of $SU(n)$, the invariant Haar measure has the properties

$$\left. \begin{aligned} \int [dU] &= 1 \\ \int [dU] U_{ij} &= 0 \\ \int [dU] U_{ij} U_{kl}^\dagger &= \frac{1}{n} \delta_{ij} \delta_{kl} \end{aligned} \right\} \quad (7.6)$$

and

$$\int [dU] f(U) = \int [dU] f(U_0 U) \quad , \quad (7.7)$$

for $U_0 \in SU(n)$. For the rotation group $O(3)$,

$$\int [dU] = \int \frac{d\Omega}{4\pi} \quad . \quad (7.8)$$

With these rules for group integration, we can expand e^{-S} in strong coupling, and evaluate integrals for the Wilson loops.

As an example, let us calculate the leading behavior of $\langle \text{tr}(UU) \rangle$. Consider a rectangular loop of dimension $M \times N$ in lattice units, as shown in Fig. 42. For each link in the contour \mathcal{C} , we must bring down at least one corresponding link from the expansion of e^{-S} in order to avoid the zeroes from $\int [dU] U_{ij} = 0$. It is fruitful to think of each plaquette term $\beta \text{tr}(UUUU)$ as a tile on plaquette p . The first nonvanishing term in the strong coupling limit $\beta \rightarrow 0$ is obtained when the minimum surface enclosed by the contour \mathcal{C} is tiled. The leading behavior of the Wilson loop is therefore

$$\begin{aligned} W(\mathcal{C}) &= \text{constant} \times \beta^{M \cdot N} \\ &= \text{constant} \times e^{-M \cdot N \ln(1/\beta)} \end{aligned} \quad (7.9)$$

We see that the Wilson loop follows an area law

$$\begin{aligned} W(\mathcal{C}) &\sim \exp(-\ln(1/\beta) \times \text{area of loop}) \\ &= e^{-\sigma A} \end{aligned} \quad (7.10)$$

The exponential falloff reflects the disordered character of the system.

The Area Law and Confinement. We may measure the gauge interaction between two test charges representing a massive quark and antiquark in a color singlet state as follows:

- Introduce test charges at Euclidean time $T=0$, and pull them apart a distance L .
- Let them remain in fixed positions for a length of time T .
- Bring them back together again at time T .

The path traced out by the test charges is a rectangular Wilson loop of area

$$A = LT \quad , \quad (7.11)$$

and we have just seen that in the strong coupling limit,

$$W(\mathcal{C}) \sim e^{-\sigma LT} \quad . \quad (7.12)$$

We identify this behavior with the evolution in Euclidean time of an energy eigenstate $\sim e^{-ET}$. Thus the system of two test charges separated by a distance L has an energy

$$E = \sigma L \quad . \quad (7.13)$$

This result is suggestive of the string picture of hadrons. The energy of the string joining the quark and antiquark is proportional to its length L . The string tension is

$$\sigma = \log(1/\beta) = \log(g^2) \quad . \quad (7.14)$$

The quark-confining string suggested by the area law is made of "gauge glue." In this picture, the string tension is determined (through g^2) by the color charges of the test quarks. We therefore expect the same string tension for mesons ($3-3^*$ quark-antiquark systems) as for baryons ($3-3^*$ quark-diquark systems). This provides an understanding of the equal slopes of meson and baryon Regge trajectories evident in Figs. 15 and 16.

Confinement in Abelian and Non-Abelian Gauge Theory. We have demonstrated that confinement occurs in the strong coupling limit of lattice gauge theory. However, in the strong coupling limit, confinement is a universal property of gauge theories, true for $U(1)$ as well as $SU(3)$. The experimental evidence that electrons are unconfined suggests that our understanding is incomplete. The resolution of this puzzle is that in $U(1)$ gauge theory on the lattice a deconfining phase transition occurs at some finite value of $g^2 = g_{cr}^2$. For $g^2 > g_{cr}^2$, charge is confined, in agreement with the strong coupling result. For $g^2 < g_{cr}^2$, large Wilson loops obey a perimeter law instead of an area law:

$$W(\mathcal{C}) \sim e^{-2mP(\mathcal{C})} \rightarrow e^{-2mL} \quad , \quad (7.15)$$

so that the potential approaches a constant at large separations,

$$V(R) \rightarrow 2m \quad , \quad (7.16)$$

where m is the self-energy in gauge fields around an isolated point source. This means that charges can be separated with only a finite cost in energy, characteristic of the QED phase. In contrast, we expect QCD to be a confining theory, with no phase transition at finite values of the coupling constant. We shall see at once that this different behavior is consistent with the asymptotic freedom of non-Abelian theories. In Lecture 9 we will review some numerical evidence for the deconfining phase transition in the $U(1)$ lattice theory.

The Renormalization Group, Confinement, and Asymptotic Freedom. To recover the consequences of continuum field theory, we must let the lattice spacing $a \rightarrow 0$ while holding physical quantities fixed. Consider the case of the confining phase of pure gauge theory. For a given value of g , we identify the string tension σ from the behavior of large Wilson loops,

$$W(\mathcal{C}) \sim e^{-\sigma A} \quad . \quad (7.17)$$

Dimensional analysis shows that we may write the string tension as

$$\sigma(g, a) = \frac{1}{a^2} \tilde{\sigma}(g) \quad , \quad (7.18)$$

where $\bar{\sigma}$ is the string tension in lattice units. We now require that $\sigma(g,a)$ remain fixed while we vary both g and a :

$$\frac{\partial \sigma}{\partial a} \delta a + \frac{\partial \sigma}{\partial g} \frac{\partial g}{\partial a} \delta a = 0 \quad . \quad (7.19)$$

The change in g^2 necessary to keep σ fixed as a is varied is therefore

$$\frac{\partial g}{\partial a} = - \frac{\partial \sigma / \partial a}{\partial \sigma / \partial g} \quad . \quad (7.20)$$

This required variation in g^2 is conventionally described by the dimensionless Callan-Symanzik beta function

$$\beta(g^2) = -a \frac{\partial g}{\partial a} = - \frac{2\bar{\sigma}(g)}{\partial \bar{\sigma}(g) / \partial g} \quad . \quad (7.21)$$

This function is of fundamental importance to the phase structure of the theory. Critical values of the coupling g_{cr}^2 are determined by zeroes of the beta function,

$$\beta(g_{cr}^2) = 0 \quad . \quad (7.22)$$

To go to the continuum limit, we let $a \rightarrow 0$ and continuously adjust g^2 accordingly. For g^2 to remain finite in this limit, we must reach a point where an incremental change in $\ln(1/a^2)$ induces a negligible change in g^2 .

The β -Function in Abelian and Non-Abelian Gauge Theory. In the strong-coupling limit of both Abelian and non-Abelian theories, the Wilson loop behaves as

$$W(\mathcal{C}) \sim \text{constant} \times e^{-A \ln g^2} \quad , \quad (7.23)$$

so the string tension in lattice units goes as

$$\bar{\sigma}(g) \sim \ln g^2 \quad , \quad (7.24)$$

which means that the beta-function is

$$\beta(g^2) \sim -g^2 \ln g^2 \quad . \quad (7.25)$$

In the limit of small lattice spacing $a \rightarrow 0$, there are two possibilities:

- If $\beta(g^2) > 0$, then g^2 increases as $a \rightarrow 0$;
- If $\beta(g^2) < 0$, then g^2 decreases as $a \rightarrow 0$.

The beta-function is negative in the strong-coupling regime. Therefore if we begin in the strong-coupling regime and try to go to the continuum limit by letting $a \rightarrow 0$, it forces us toward the weak coupling regime. This makes it difficult to base quantitative predictions about the continuum theory upon results derived from the strong coupling expansion.

In the weak coupling limit, we may use perturbation theory either on the lattice or in the continuum, with a momentum-space cutoff if necessary. To any order in perturbation theory, there is no confinement [39] and consequently no string tension, so we cannot rely on the definition (7.21) of the beta function. We can, of course, still define a Callan-Symanzik function by holding fixed some "physical" quantity other than the string tension. Different definitions of $\beta(g^2)$ may differ in detail, but the sign of $\beta(g^2)$ and the location of its zeroes are universal.

In the weak coupling limit, QCD is asymptotically free ($\beta(g^2) < 0$), but QED is not ($\beta(g^2) > 0$). Thus, the β -function for QED changes sign somewhere between strong coupling and weak coupling, while the β -function for QCD does not. The behavior of the β -function in the two cases is sketched in Fig. 43. The phase structure suggested by this analysis has been borne out by Monte Carlo data, and by analytic proofs.

LECTURE 8: THE INVERSE BOUND-STATE PROBLEM FOR QUARKONIUM

We interrupt our survey of lattice gauge theory to look one final time at what may be learned from the spectroscopy of heavy quark systems about the force between quarks. In Lectures 1 and 2 we reviewed some of the motivation for an interest in heavy-quark spectroscopy, and investigated a few of the ways in which elementary methods of quantum mechanics can be useful. In this lecture we shall approach similar issues using different techniques. We seek answers to the following questions:

- How, and to what extent, does the spectrum of a quarkonium system measure the interquark potential?
- Where do we know the potential, and what is its form? The elementary analyses suggested that a form

$$V(r) = (710 \text{ MeV}) \log(r) \tag{8.1}$$

is a convenient summary for the ψ and T states.

- What information do we need to know the potential better?
- What conclusions may we draw about the force between quarks?

Our tool in this lecture will be the inverse scattering formalism.

We are all familiar with the direct problem of scattering theory, which consists in calculating the S-matrix from the equation of motion and the interaction. In typical nonrelativistic applications the quantities to be computed are the bound-state positions and wavefunctions and the scattering amplitudes or phase shifts.

The inverse problem of scattering theory is complementary: given the equation of motion and the S-matrix, deduce the interaction. This is not the place for a thorough treatment of the inverse scattering problem, which has an immense literature, nor even to give a complete derivation of the results we shall use. Instead, we shall present some examples to make plausible the utility of the inverse formalism. We shall next pass on to a statement of the quantum mechanical problem first for finite potentials and then for confining potentials. There follows a review of the methodology followed in applications to quarkonium, and a study of the associated phenomenology of the ψ and Υ families. The lecture concludes with a summary of what has been learned and an outlook on future prospects. Two examples will illustrate the sort of information (and assumptions!) required to determine a potential.

The Classical Inverse Problem. In classical mechanics, knowledge of the period of oscillation as a function of energy is sufficient to determine uniquely a symmetric, monotonic potential. Consider a one-dimensional potential well of the kind shown in Fig. 44. The energy of a particle moving in such a well is given by

$$E = \frac{m\dot{x}^2}{2} + V(x) \quad . \quad (8.2)$$

Solving for

$$\dot{x} = \left[\frac{2(E-V)}{m} \right]^{\frac{1}{2}} \quad (8.3)$$

gives an expression for dt/dx which may be integrated to give the period

$$\begin{aligned} T(E) &= 4 \left(\frac{m}{2} \right)^{\frac{1}{2}} \int_0^{x(E)} \frac{dx}{\sqrt{E-V}} \\ &= 2(2m)^{\frac{1}{2}} \int_0^E \frac{dV(dx/dV)}{\sqrt{E-V}} \quad . \end{aligned} \quad (8.4)$$

If we divide this equation by $\sqrt{\alpha-E}$, where α is for the moment a parameter satisfying

$$0 \leq V \leq E \leq \alpha \quad , \quad (8.5)$$

integrate over the energy $\int_0^\alpha dE$, and interchange the order of integration, we find

$$\begin{aligned} \int_0^\alpha \frac{dE T(E)}{\sqrt{\alpha-E}} &= 2(2m)^{\frac{1}{2}} \int_0^\alpha dV(dx/dV) \underbrace{\int_V^\alpha dE [(E-V)(\alpha-E)]^{-\frac{1}{2}}}_{\pi} \\ &= 2\pi(2m)^{\frac{1}{2}} x(\alpha) \quad . \end{aligned} \quad (8.6)$$

Now replacing $\alpha \rightarrow V$, we obtain an expression for the shape of the potential in terms of the period,

$$x(V) = \frac{1}{2\pi(2m)^{\frac{1}{2}}} \int_0^V \frac{dE T(E)}{\sqrt{V-E}} \quad . \quad (8.7)$$

If, for example, the period is independent of energy, we readily find that

$$x(V) \propto \sqrt{V} \quad , \quad (8.8)$$

or, in other words,

$$V(x) \propto x^2 \quad . \quad (8.9)$$

This is a familiar result.

The Semiclassical Inverse Problem. Very similar arithmetic leads to the reconstruction, in semiclassical approximation, of a symmetric, monotonic potential in one dimension. In this instance we begin with the quantization condition

$$2 \int_0^{x_0} dx \left[2\mu(E_n - V(x)) \right]^{\frac{1}{2}} = (n + \frac{1}{2})\pi \quad . \quad (8.10)$$

Differentiating both sides with respect to the principal quantum number n , we have

$$(2\mu)^{\frac{1}{2}} \int_0^x \frac{dx(\partial E/\partial n)}{\sqrt{E-V}} = \pi \quad , \quad (8.11)$$

which may be rewritten as

$$\int_{V(0)=0}^E dV(dx/dV) \left[\frac{2\mu}{E-V} \right]^{\frac{1}{2}} = \frac{\pi}{\partial E/\partial n} \quad . \quad (8.12)$$

This is quite similar in form to Eq. (8.4), and so we follow the same steps as before. Operating on the equation with $\int_0^\alpha dE(\alpha-E)^{-\frac{1}{2}}$ and interchanging the order of integration, we find

$$\int_0^\alpha dV(dx/dV) \int_V^\alpha \frac{dE}{(\alpha-E)^{\frac{1}{2}}(E-V)^{\frac{1}{2}}} = \pi \int_0^\alpha \frac{dE}{[2\mu(\alpha-E)]^{\frac{1}{2}}(\partial E/\partial n)} \quad . \quad (8.13)$$

The $\int dE$ on the left-hand side is a Beta function whose value is π . Consequently upon renaming $\alpha \rightarrow V$ we are left with the result

$$x(V) = \int_0^V \frac{dE}{[2\mu(V-E)]^{\frac{1}{2}}(\partial E/\partial n)} \quad . \quad (8.14)$$

Again it is worthwhile to examine an elementary case. Consider a constant level density

$$\partial E/\partial n = 2 \quad , \quad (8.15)$$

with mass

$$2\mu = 1 \quad . \quad (8.16)$$

An elementary computation gives the well-known result

$$x = \sqrt{V} \quad , \quad (8.17)$$

or

$$V = x^2 \quad . \quad (8.18)$$

With these two examples to provide plausibility, we now turn to the general case in one-dimensional quantum mechanics.

The Quantum Mechanical Inverse Problem. The general inverse problem in one-dimensional quantum mechanics as governed by the Schrödinger equation is highly developed. A finite potential which binds N bound states is completely specified by $2N$ bound-state parameters plus knowledge of the phase shift everywhere in the continuum [40]. The procedure, roughly speaking, is to write a dispersion relation for the Schrödinger wavefunction, for which one must specify the position and wavefunction normalization of each bound state (as poles and residues) and the reflection coefficient in the continuum (as a dispersion integral). Having such a representation of the wavefunction $\psi(x)$ and knowing the (Schrödinger) equation of motion, one may solve for the potential $V(x)$.

An interesting special case is that of a symmetric potential, for which the required bound-state information is reduced to N parameters — one for each bound state. A further simplification is obtained in the case of a symmetric potential which is also reflectionless, which is to say that an incident wave is completely transmitted, throughout the continuum. The simplest such potential is

$$V(x) = \frac{-2\kappa^2}{\cosh^2 \kappa x} \quad . \quad (8.19)$$

For a particle of reduced mass ($2\mu=1$) it binds a single level at

$$E_1 = -\kappa^2 \quad (8.20)$$

and has a vanishing reflection coefficient everywhere in the continuum. For potentials of this class, the dispersion integral disappears, and we are left with an N -parameter algebraic equation for a potential which binds N levels. Consequently, a symmetric, reflectionless potential is completely specified by the set of binding energies of its levels. The inverse Schrödinger problem for reflectionless potentials has a deep and interesting connection with soliton solutions to the Korteweg-de Vries equation [41].

The extensive development of the inverse scattering formalism has been concentrated on finite potentials, i.e., those which bind a finite number of levels.

What can be done for a confining potential? It is natural [42] to try to build up a confining potential by a sequence of reflectionless approximations. A reflectionless approximant $V_N(x)$ is constructed to reproduce the first N levels of the true potential $V(x)$, and one hopes that in the limit of a large number of bound states,

$$\lim_{N \rightarrow \infty} V_N(x) \rightarrow V(x) \quad (8.21)$$

in some suitable sense.

It is intuitively reasonable that this procedure should provide a faithful representation of the true potential. This expectation is supported by a number of numerical examples, some of which are shown in Figs. 45-47. In the case of confining potentials, we must supplement the bound-state information with a choice of the ionization point $V_N(\pm\infty)$ for each approximant. We have found (through numerical experiments as well as analytic studies) that the choice

$$V_N(\pm\infty) = \frac{1}{2}(E_N + E_{N+1}) \quad (8.22)$$

yields sensible approximations. It satisfies the obvious requirements

$$E_N \leq V_N(\pm\infty) \leq E_{N+1} \quad , \quad (8.23)$$

and has the advantage of being easy to remember. In the limit as $N \rightarrow \infty$, the details of this choice become unimportant.

Take first the case of the harmonic oscillator potential

$$V(x) = x^2 \quad , \quad (8.24)$$

which supports bound states at energies

$$E_n = 2n+1 \quad , \quad n = 0,1,2,\dots \quad . \quad (8.25)$$

The first five reflectionless approximations to (8.24), with $V_N(\pm\infty)$ given by (8.22), are compared with the true potential in Fig. 45(a)-(e). The agreement is excellent in the region of x relevant to the specified energy levels. Successive approximations to the bound-state wave functions are plotted in Fig. 45(f)-(j). They are seen to converge rapidly toward the exact solutions shown in Fig. 45(k).

As a second example, consider the linear potential

$$V(x) = |x| \quad , \quad (8.26)$$

for which the bound-state energies are given by the zeros of Airy functions

$$\begin{aligned} \text{Ai}'(-E_n) &= 0 \quad , \quad n = 1,3,5,\dots \\ \text{Ai}(-E_n) &= 0 \quad , \quad n = 2,4,6,\dots \end{aligned} \quad (8.27)$$

This energy spectrum gives rise to the approximate potentials and wavefunctions displayed in Fig. 46. The agreement is again extremely encouraging.

Finally, it is well to examine the pathological case of an infinitely deep square-well potential

$$V(x) = \begin{cases} 0, & |x| < \pi/2 \\ \infty, & |x| > \pi/2 \end{cases} \quad (8.28)$$

which has bound states at

$$E_n = n^2, \quad n = 1, 2, \dots \quad (8.29)$$

The reconstructed potentials are shown in Fig. 47(a)-(e). The agreement between exact and approximate forms is rather less striking than for the two preceding examples. The manner in which the approximate wavefunctions plotted in Fig. 47(f)-(j) are increasingly excluded from the forbidden region of space is noteworthy, however.

These examples, which suggest the convergence of reflectionless approximations to nonpathological potentials, also indicate an acceptable rate of convergence. It has been possible to prove a number of limited statements about the fact of convergence [43-45], but nothing is known about the rate of convergence beyond what is indicated by the numerical experiments. In the numerical experiments reported here the potentials have been reconstructed from the binding energies of the levels of both odd and even parity. Alternatively, one may base the reconstruction on the states of either parity, in which case the binding energies must be supplemented with wave function information such as the value of slope of the wave function at the origin. Some of the proofs of convergence have been carried through for all three sets of input information.

Determinations of the Quarkonium Potential. In a series of publications, [46-48] Rosner, Thacker, and I have extended the inverse scattering formalism for reflectionless potentials to the reconstruction of central potentials in three space dimensions, and have derived approximate interquark potentials from the quarkonium data. In this section I will briefly summarize what we have done and what we think we have learned about the force between quarks.

The reduced radial Schrödinger equation for s-waves,

$$\frac{1}{2\mu} u''(r) + [E - V(r)]u(r) = 0, \quad (8.30)$$

is identical in form to the one-dimensional Schrödinger equation. As a consequence, the one-dimensional inverse scattering formalism can be applied to the study of quarkonium systems. However, because of the boundary condition

$$u(0) = 0 \quad (8.31)$$

imposed by the finiteness of the radial wave function at the origin, only the

odd-parity levels in one dimension correspond to physical states. Therefore, in order to apply our one-dimensional formalism to the psions, we must regard the ψ and ψ' as the second and fourth levels of a symmetric one-dimensional potential $V(r) = V(-r)$. The even-parity levels which appear in the one-dimensional problem are interleaved with the physical psions, one below the ψ , one between the ψ and ψ' , and so on.

To substitute in the reconstruction algorithm for the fictitious levels we require information about the slopes of the odd-parity reduced radial wavefunctions, or equivalently, the values of the three-dimensional wavefunctions at the origin. These are related in principle to the measured leptonic decay widths through the connection

$$|\Psi_n(0)|^2 = (1/16\pi\alpha^2 e_Q^2) \cdot \rho \cdot M_n^2 \Gamma(V_n \rightarrow e^+ e^-) \quad (8.32)$$

With the parameter $\rho=1$, this is simply the Van Royen-Weisskopf formula [5] of nonrelativistic potential scattering. In a purely Coulombic quarkonium system, quantum chromodynamics yields a correction

$$\rho = \left[1 - \frac{16\alpha_s}{\pi} + O(\beta^2) \right]^{-1}, \quad (8.33)$$

where α_s is the strong coupling constant and β is the speed of the bound quark. Although the known quarkonium families are decidedly non-Coulombic, the belief that the strong coupling constant may be as large as $\alpha_s=0.2-0.3$ has led many authors to suspect that ρ may be appreciably greater than one.

In the most recent analysis, [48] we use as inputs to the charmonium potential the masses and leptonic widths of ψ and ψ' , and choose the "ionization point" as

$$E_0 = V(\pm\infty) = 3.8 \text{ GeV} \quad (8.34)$$

This is halfway between the ψ' and the first omitted fictitious (even-parity) level, estimated by

$$E_0 = \frac{3M(\psi') + M(4.028)}{4} \quad (8.35)$$

To explore the effects of our ignorance of strong radiative corrections to the decay rate, we take as representative values of the multiplicative correction to the van Royen-Weisskopf formula $\rho=1$ (which corresponds to no correction), and $\rho=1.4$ and 2. We believe, but cannot prove, that $\rho=2$ represents a larger correction than is plausible, and intend that the extremes $\rho=(1,2)$ bracket the true value.

Although only s-wave information is used systematically in the inverse-scattering algorithm, information about other partial waves may be used to discriminate among potentials constructed under varying assumptions for the quark mass. For each value of ρ , we select the value of the charmed quark mass m_c which

correctly reproduces the center of gravity of the 2^3P_J χ states. The resulting potentials are shown in Fig. 48. For each potential we choose a value of the b-quark mass which reproduces the mass of the T ground state, and then compute the complete upsilon spectrum. The agreement with experiment is quite satisfying.

The three charmonium potentials are compared in Fig. 49. In the range $0.5 \text{ GeV}^{-1} \leq r \leq 5 \text{ GeV}^{-1}$, the potentials vary approximately logarithmically with the interquark separation, as expected on the basis of the scaling arguments reviewed in the first lecture. The local fluctuations are artifacts of the reflectionless approximant technique. Also shown in Fig. 49 (as the short-dashed line) is the shape of the QCD-inspired potential of Buchmüller and Tye [23], which is typical of explicit potentials that provide a good representation of ψ and T data. In the region of space to which charmonium observables are sensitive, it provides a smooth interpolation of the inverse-scattering results.

The method of constructing potentials from the upsilon family differs only slightly in detail. In this case we took as inputs the masses and leptonic widths of the 1S-4S levels, and chose as ionization point the value

$$E_0 - \frac{5M(4S) - M(3S)}{4} = 10.6 \text{ GeV} \quad . \quad (8.36)$$

Since the spectrum of p-wave states was not yet well established, we were not able to use the P-states to select the "best" value of the b-quark mass. We therefore chose m_b for each ρ rather arbitrarily to be close to the value needed to reproduce the T(1S) mass in the corresponding charmonium potential. Although this does not lead to appreciable ambiguity in our conclusions, it represents an indefiniteness that one would hope eventually to overcome. [Our expectations for the $3P(b\bar{b})$ center of gravity are in reasonable accord with the subsequent measurements. The scale for the upsilons should be shifted upward by about 25 MeV, because of a recalibration of the CESR energy scale after this analysis was carried out.] The resulting potentials are shown in Fig. 50. For each of them we choose a value of the charmed quark mass m_c which reproduces the mass of the ψ ground state. Again, the agreement between prediction and observation is satisfactory.

The three T potentials are compared in Fig. 51. They are essentially indistinguishable for interquark separations larger than 0.4 GeV^{-1} . They also approximately coincide with other potentials that reproduce the data. Like the charmonium potentials of Fig. 41, the T potentials behave approximately logarithmically in the interval $0.5 \text{ GeV}^{-1} \leq r \leq 5 \text{ GeV}^{-1}$. At distances smaller than 0.4 GeV^{-1} there is considerable variation among the potentials. This provides a measure of our current ignorance of the interaction between quarks at short distances.

The potentials constructed from the ψ and T families are compared with one another for equal values of the parameter ρ in Fig. 52, where they have been

superposed by requiring that the $\psi(3097)$ levels coincide. The agreement in each case is excellent for $r \geq 0.5 \text{ GeV}^{-1}$ (0.1 fm), where both quarkonium systems provide information. The comparison provides direct evidence that the strong (quark-antiquark) interaction is flavor-independent in the range $0.1 \text{ fm} < r < 1 \text{ fm}$. This conclusion is supported by the quantitative agreement of predictions from ψ potentials with Υ observables and of predictions from Υ potentials with ψ observables.

A number of refinements to this analysis can be envisaged. Knowledge of the positions of the 2^3P_J , 3^3P_J , and 4^3P_J levels in the upsilon family and improved measurements of the leptonic widths of all the 3S_1 quarkonium levels will make possible more precise determinations of the potential. Detailed studies of the E1 transition rates for the upsilon will test in a different manner the nonrelativistic picture of quarkonium. The fine structure of the 3P states and locations of the 1P states hold important clues to the Lorentz structure of the interquark interaction.

Outlook. The ψ and Υ quarkonium systems have made accessible to us a considerable amount of new information about the force between quarks. What has been learned ranges from the qualitative insight that nonrelativistic methods are apt to a rather precise determination of the interquark potential at distances between about 0.1 fm and 1 fm. Some of the analysis techniques which lead to a determination of the potential have been reviewed in these lectures. There are other important issues that we have not touched on here. Among them are the general problem of fine structure and the spacetime form of the interaction, and the quantitative application of perturbative QCD to quarkonium decay rates. Both of these seem ripe for significant development. In all areas we would benefit enormously from the observation and detailed study of one more quarkonium family below the mass of the Z^0 .

LECTURE 9: MONTE CARLO SIMULATIONS OF LATTICE GAUGE THEORY

The lattice formulation reduces the Feynman path formula for the gauge theory into a multiple ordinary integral. The high multidimensionality of the integrals makes conventional mesh techniques for the numerical evaluation of integrals completely impractical, however. A lattice of size N^d upon which periodic boundary conditions have been imposed carries dN^d link variables. For a 10^4 lattice, for example, there will be 4×10^4 link variables. For the simplest gauge theory, Z_2 , the number of distinct configurations is

$$2^{40,000} \approx 1.6 \times 10^{12041} \quad . \quad (9.1)$$

Comparison with the age of the Universe (6×10^{17} sec.) quickly convinces us that it is hopeless to actually evaluate the path integral. We need instead to devise a reliable approximation method.

The goal of the Monte Carlo approach is to provide a tractably small number of configurations which are typical of thermal equilibrium in the system under study. Monte Carlo techniques are used to evaluate path integrals by the method known as "importance sampling." We wish to evaluate expectation values and correlation functions of the form

$$\langle \{\phi\} \rangle = \frac{\int [dU] \{\phi\} e^{-S}}{\int [dU] e^{-S}}, \quad (9.2)$$

a weighted average of $\{\phi\}$ over all possible configurations of the link variables, each configuration being weighted by the Boltzmann factor e^{-S} . Instead of evaluating the sum over configurations directly, the Monte Carlo method generates a statistical ensemble of configurations and calculates the average of $\{\phi\}$ over this ensemble.

Generating an Ensemble. We may begin a Monte Carlo simulation with any particular configuration. Two simple conventional choices are

- "Cold start," with the unit matrix $U_i = I$ placed on each link, and
- "Hot start," with the U_i chosen randomly from a uniform distribution in group space.

These possibilities are represented for the two-dimensional Ising model in Fig. 53. For the cold (ordered) start, with all spins up, the initial value of the magnetization is $|M|=1$. For the random (hot) start, the magnetization approximately vanishes. In the example depicted, we see that $M=-0.2$, in the range of typical values ($\sim 1/N$ for an $N \times N$ lattice) to be expected.

Having chosen a starting configuration, we cycle sequentially through the lattice, link by link, using some statistical algorithm to make pseudorandom changes in the link variables. Each "sweep" through the lattice produces a new configuration somewhat different from the preceding one. The algorithm for updating links must be constructed so that the probability of a configuration with action S is proportional to the Boltzmann weight e^{-S} . Two such algorithms are representative of those commonly in use.

- Metropolis algorithm [49]: Starting with the old value of the link matrix U_{old} , construct an updated value U_{new} . Compute the actions $S_{old}(U_{old})$ and $S_{new}(U_{new})$. If $S_{new} < S_{old}$, accept U_{new} . If $S_{new} > S_{old}$, select a random $0 < r < 1$. Accept U_{new} if

$$\exp \left[-(S_{new} - S_{old}) \right] > r. \quad (9.3)$$

- Heat bath algorithm [50,51]: Starting with the old value of the link matrix U_{old} , construct an updated value U_{new} chosen statistically with a distribution $e^{-S_{new}}$. This is best illustrated by example in the Ising model. First compute the probability of a given site to have spin up:

$$P(+)=\frac{e^{-\beta S(+)}}{e^{-\beta S(+)}+e^{-\beta S(-)}} \quad (9.4)$$

Then select a random number $0 < r < 1$. If $P(+)>r$, assign spin up; otherwise, assign spin down.

Either the Metropolis algorithm or the heat bath algorithm will produce a statistically distributed ensemble of configurations. These configurations are highly correlated from sweep to sweep. Near a critical point, configurations must be separated by hundreds or even thousands of sweeps in order to ensure their statistical independence.

The number of sweeps required to reach equilibrium from a hot or cold start depends on the lattice size, and on physical circumstances. The mean plaquette values $\langle 1-\frac{1}{4}\text{tr}(UUUU) \rangle$ displayed in Fig. 54 show that for the pure SU(2) theory in four dimensions, which has no critical point, equilibrium is reached within 20-30 sweeps. [Other, "long wavelength," quantities may equilibrate more slowly.] In contrast, the simulation of a system near a critical point exhibits a very slow convergence to equilibrium known as "critical slowing down." This is illustrated in Fig. 55 for the U(1) theory in four dimensions.

The phenomenon of critical slowing down suggests a tool for searching out critical points. Thermally cycle the system. Since convergence is rapid away from critical points and slow close to critical points, regions of slow convergence will appear as hysteresis loops. This is illustrated for U(1) gauge theory in four dimensions in Fig. 56. Longer runs in the critical region result in the single-values mean plaquette energies shown in Fig. 57. Using these Monte Carlo data, Lautrup and Nauenberg [54] evaluated the specific heat ρ of the lattice U(1) theory as a function of the coupling strength β and the lattice size L . Their results, reproduced in Fig. 53, show that ρ has a maximum as a function of β which increases rapidly as a function of L , characteristic of a second order (or higher) phase transition.

Corresponding studies of SU(2) and SU(3) gauge theories in four dimensions do not display hysteresis loops. Typical results for SU(3) are shown in Fig. 59. This is representative of the evidence that QCD is a confining theory for all values of the coupling constant.

Measuring the String Tension. We have seen in Lecture 7, in the derivation of the area law for Wilson loops, how the evaluation of a rectangular Wilson loop such as that shown in Fig. 60 leads to a determination of the string tension. Identifying

$$\langle W(M,N) \rangle \sim e^{-V(M) \cdot N} \quad (9.5)$$

as $e^{-E \cdot T}$, we obtain the heavy quark potential as

$$V(M) = \frac{1}{N} \ln \langle W(M,N) \rangle \quad (9.6)$$

for M fixed and large, as $N \rightarrow \infty$. Although conceptually clear, this procedure may not be practical, because $\langle W(M,N) \rangle$ becomes infinitesimal for large N , and because the results may be significantly distorted by a perimeter-law factor $e^{-2m(M+N)}$. We may eliminate the dependence on the perimeter of the loop and overall constant factors by forming the combination

$$R(M,N) = \frac{\langle W(M,N) \rangle \langle W(M-1,N-1) \rangle}{\langle W(M,N-1) \rangle \langle W(M-1,N) \rangle} \sim e^{-\bar{\sigma}} \quad (9.7)$$

where the correspondence is expected to hold for large loops or strong couplings. The quantity

$$\chi(M,N) \equiv -\ln R(M,N) \rightarrow \bar{\sigma} \quad (9.8)$$

should therefore directly measure the string tension in lattice units, provided the area law dominates.

Results from the simulation of $SU(2)$ gauge theory on 8^4 and 10^4 lattices are shown in Fig. 61. At strong coupling, the numerical results accurately reproduce our expectation that

$$\bar{\sigma}(g) \sim \ln g^2 \quad (7.24)$$

To analyze the behavior in the weak-coupling regime, we may exploit the fact that the string tension has dimensions of $(\text{mass})^2$, and so may be expressed as

$$\sigma(g,a) = \text{constant} \cdot \Lambda_L^2 \quad (9.9)$$

where Λ_L is a physical scale of the lattice theory. The requirement that Λ_L remain fixed as the coupling g and lattice spacing a are varied to approach the continuum limit, i.e., the requirement that Λ_L be a cutoff-independent physical mass scale

$$a \frac{d\Lambda_L}{da} = 0 \quad (9.10)$$

as $a \rightarrow 0$, then prescribes the dependence of $\bar{\sigma}$ upon g . Renormalization group analysis leads to a unique prescription for the g -dependence of Λ_L , as follows. Write

$$\Lambda_L = \frac{1}{a} \cdot f(g) \quad (9.11)$$

then the requirement (9.10) leads immediately to a first-order differential equation

for f ,

$$f(g) + \beta(g^2) \frac{df}{dg} = 0 \quad , \quad (9.12)$$

where $\beta(g^2)$ is the Callan-Symanzik function defined in (7.21). The leading behavior of $\beta(g^2)$ in the weak-coupling limit is known from perturbative calculations [3,56] as

$$\beta(g) = -\beta_0 g^3 - \beta_1 g^5 \quad , \quad (9.13)$$

with

$$\left. \begin{aligned} \beta_0 &= \frac{11}{3} \left(\frac{N}{16\pi^2} \right) \\ \beta_1 &= \frac{34}{3} \left(\frac{N}{16\pi^2} \right)^2 \end{aligned} \right\} . \quad (9.14)$$

for $SU(N)$. Direct integration of (9.12) then yields

$$\Lambda_L = \frac{1}{a} \left(\beta_0 g^2 \right)^{-\beta_1/2\beta_0^2} e^{-1/2\beta_0 g^2} \left(1 + O(g^2) \right) \quad . \quad (9.15)$$

This means that in the weak-coupling regime, we anticipate

$$\begin{aligned} \bar{\sigma}(g) &= \text{Constant} \cdot a^2 \cdot \Lambda_L^2 \\ &\approx \text{Constant} \cdot (\beta_0 g^2)^{-\beta_1/\beta_0^2} e^{-1/\beta_0 g^2} \end{aligned} \quad (9.16)$$

Precisely this trend is seen for large loops in Fig. 61. Making a fit of (9.16) to the Monte Carlo data determines the constant of proportionality between Λ_L and the (square root of the) physical string tension as

$$\Lambda_L = (1.3 \pm 0.2) \times 10^{-2} \sqrt{\sigma} \quad . \quad (9.17)$$

For small loops, $\chi(I,J)$ departs from the trend (9.16) in the weak-coupling regime, reflecting deviations from the area law. Thus we interpret the envelope of $\chi(I,J)$ for all I and J , plotted as a function of the coupling strength as the true measure of $\bar{\sigma}(g)$.

We show in Fig. 62 the result of a Monte Carlo simulation for the physically interesting case of $SU(3)$, on a 6^4 lattice. In this instance, a fit to the data yields

$$\Lambda_L = (6 \pm 1) \times 10^{-3} \sqrt{\sigma} \quad . \quad (9.18)$$

An auxiliary calculation [58] relates the lattice parameter Λ_L to a conventional definition of the QCD scale parameter in the continuum:

$$\Lambda_{\text{mom}} = \begin{cases} 57.5 \Lambda_L & (\text{for SU}(2)) \\ 83.5 \Lambda_L & (\text{for SU}(3)) \end{cases} . \quad (9.19)$$

Assembling the pieces, we have

$$\Lambda_{\text{mom}} \approx \begin{cases} \frac{1}{2}\sqrt{\sigma} & \text{for SU}(2) \\ \frac{1}{3}\sqrt{\sigma} & \text{for SU}(3) \end{cases} . \quad (9.20)$$

With the observed value of the string tension (from the light hadron spectrum, cf. (2.12)) $\sigma = 0.18 \text{ GeV}^2$, we estimate

$$\Lambda_{\text{mom}} \approx 225 \text{ MeV} \quad (9.21)$$

in reasonable agreement with determinations from deeply inelastic scattering and other sources. Although the relationship we have found between observables is far from precise, it is quite suggestive and encouraging.

Calculating the Interquark Potential, We need not be content with a computation of the string tension, since we interpret the Wilson loop as

$$W(R,T) \sim \exp[-V(R)T] \quad , \quad (9.22)$$

at large times T . An extensive study has been carried out by Otto and Stack [59] using the Caltech "Cosmic Cube," a hypercubic array of 64 Intel 8086 microprocessors equipped with 8087 coprocessors [60]. Their calculation required 2500 hours on this device, which is approximately equivalent to 8 VAX-11/780 superminicomputers for this problem. Having first verified that $W(R,T)$ indeed behaves exponentially in T , the authors extract an interquark potential. As was the case in our discussion of the string tension, quantities emerge naturally in "lattice units." Until a scale is chosen — for example, by fixing a dimensionful quantity such as Λ_{mom} or σ — what is determined is a relationship between dimensionless quantities. Fig. 63 shows the scaled lattice potential $V/\sqrt{\sigma}$ as a function of the scale lattice distance $R\sqrt{\sigma}$.

Before comparing these results with the phenomenological potentials, let us note that the effects of internal (light) quark loops are neglected in this calculation, and we do not know how their inclusion will modify the results. Furthermore, because of our limited experience we do not yet know how to assign systematic errors to lattice calculations in a definitive manner. With those apologies, we compare in Fig. 64 the lattice potential with a logarithmic form representative of the shape of the phenomenological potentials in the interval $0.1 \text{ fm} < R < 1 \text{ fm}$. Over a significant range, the lattice potential indeed follows the logarithmic reference curve. If the lattice potential is to reproduce the phenomenological potential quantitatively, we must choose

$$\sqrt{\sigma} \approx 0.3 \text{ GeV} \quad , \quad (9.23)$$

which at least resembles the true value of the string tension,

$$\sqrt{\sigma} = (0.4 - 0.45)\text{GeV} \quad .$$

Evidently the computation of the interquark potential on the lattice is in a highly preliminary state. Much work is needed to make possible a quantitatively reliable calculation. At the same time, this example shows us the way to more detailed studies, and provides considerable encouragement to carry them out. As we have seen in Lectures 1, 2, and 8, much has been achieved in the phenomenological determination of the interquark force. There, too, past work is mere prologue to what might be accomplished.

ACKNOWLEDGMENT

It is a pleasure to thank Chris Engelbrecht for his warm hospitality at the Stellenbosch School, and to record my appreciation to him and to the students for animated and informative discussions about physics and life. I am grateful to the Theory Group at Lawrence Berkeley Laboratory for their hospitality during the summer of 1985, when the writing of these notes was completed. I thank Hank Thacker for comments on the manuscript.

Table 1. The ψ family ($c\bar{c}$) bound states.

	State	Mass(MeV/c ²)	Γ_{tot} (keV)	Γ_{ee} (keV)
1^1S_0	η_c	2981.1±6.0		
1^3S_1	ψ/J	3096.9±1	63±9	4.60±0.39
2^3P_0	$\chi(3415)$	3415.0±1.0		
2^3P_1	$\chi(3510)$	3510.0±0.6		
2^3P_2	$\chi(3555)$	3555.8±0.6		
2^3S_1	ψ'	3686±1	215±40	2.05±0.21
3^3D_1	$\psi(3770)$	3770±3	25±3 MeV	0.257±0.046
3^3S_1	$\psi(4030)$	4028.7±2.8	52±10 MeV	0.75±0.15
$?^3S_1$	$\psi(4160)$	4157±20	78±20 MeV	0.77±0.23
$?^3S_1$	$\psi(4415)$	4415±6	43±20 MeV	0.49±0.13

Table 2. The Υ family ($b\bar{b}$) bound states.

	State	Mass(MeV/c ²)	Γ_{tot} (keV)	Γ_{ee} (keV)
1^3S_1	Υ	9460.0±0.3	44.3±6.6	1.10±0.12
2^3P_0	$\chi_b(9870)$	9872.9±5.8		
2^3P_1	$\chi_b(9895)$	9894.5±3.5		
2^3P_2	$\chi_b(9915)$	9914.6±2.4		
2^3S_1	Υ'	10023.4±0.3	29.6±4.7	0.507±0.051
3^3P_0				
3^3P_1	$\chi_b(10255)$	10253.7±3.4		
3^3P_2	$\chi_b(10270)$	10271.0±2.4		
3^3S_1	Υ''	10355.5±0.5	17.7±5.1	0.362±0.050
4^3S_1	Υ'''	10573±4	14.4±5.2 MeV	0.240±0.053
5^3S_1	? Υ	10860		
6^3S_1	? Υ	11030		

Table 3. Toponium observables in phenomenological potentials, for $m_t = 40 \text{ GeV}/c^2$ (after Ref. 26).

potential observable	potential			
	Power-law	Richardson	Coulomb	Log
$M(2S)-M(1S) \text{ (MeV}/c^2)$	520	958		
$M(3S)-M(2S) \text{ (MeV}/c^2)$	303	372		
$M(4S)-M(3S) \text{ (MeV}/c^2)$	217	231		
$M(2S)-\langle M(2P) \rangle \text{ (MeV}/c^2)$	145	105		
$M(3S)-\langle M(3P) \rangle \text{ (MeV}/c^2)$	107	66		
$\Gamma_{ee}(2S)/\Gamma_{ee}(1S)$	0.55	0.27	0.12	0.43
$\Gamma_{ee}(3S)/\Gamma_{ee}(1S)$	0.39	0.15	0.04	0.27
$\Gamma_{ee}(3S)/\Gamma_{ee}(2S)$	0.71	0.56	0.30	0.63
$\Gamma_{ee}(1S) \text{ (keV)}$	1.3	6.5	35	1.6
$\Gamma_{tot}(1S) \text{ (keV)}$		127		
$\Gamma_{tot}(2S) \text{ (keV)}$		66		
$\Gamma_{tot}(3S) \text{ (keV)}$		56		
$\Gamma_{tot}(4S) \text{ (keV)}$		52		

} SIGNIFICANT CONTRIBUTION
 FROM $t \rightarrow b + X$

BIBLIOGRAPHY

Hadron Spectroscopy.

F.E. Close, *An Introduction to Quarks and Partons*, Academic Press, New York, 1979.

O.W. Greenberg, *Ann. Rev. Nucl. Part. Sci.* **28**, 327(1978).

C. Quigg, "Models for Hadrons," in *Gauge Theories in High Energy Physics*, edited by M.K. Gaillard and R. Stora (Les Houches, 1981), North-Holland, Amsterdam, 1983, p.645.

J.L. Rosner, "Quark Models," in *Techniques and Concepts of High Energy Physics* (St. Croix, 1980), edited by T. Ferbel, Plenum, New York, 1981.

Particle Data Group, *Rev. Mod. Phys.* **56**, S1(1984).

Quarkonium.

C. Quigg and J.L. Rosner, *Phys. Rep.* **56**, 167(1979).

H. Grosse and A. Martin, *Phys. Rep.* **60**, 341(1980).

R.N. Cahn (editor), *e^+e^- Annihilation: New Quarks and Leptons* (Annual Reviews Special Collections Program), Benjamin/Cummings, Menlo Park, California, 1985.

E. Eichten, "The Last Hurrah for Quarkonium Physics: The Top System," in *The Sixth Quark*, Proceedings of the 1984 SLAC Summer Institute in Particle Physics, edited by Patricia M. McDonough, Stanford Linear Accelerator Center Report SLAC-281, January, 1985, p.1.

M.E. Peskin, "Aspects of the Dynamics of Heavy Quark Systems," in *Dynamics and Spectroscopy at High Energy*, Proceedings of the 1983 SLAC Summer Institute in Particle Physics, edited by Patricia M. McDonough, Stanford Linear Accelerator Report SLAC-267, p.151.

Asymptotic Freedom (The effective color charge in QCD).

J. Frenkel and J.C. Taylor, *Nucl. Phys.* **B109**, 439(1976); **B117**, 546E(1976).

J.D. Bjorken, "Elements of Quantum Chromodynamics," in *Quantum Chromodynamics*, Proceedings of the 1979 SLAC Summer Institute in Particle Physics, edited by Anne Mosher, Stanford Linear Accelerator Center Report SLAC-224, January, 1980, p.219.

S.D. Drell, in *A Festschrift for Maurice Goldhaber*, *Trans. NY Acad. Sci. Series II*, **40**, 76(1980).

V.N. Gribov, SLAC-Trans-176(1977).

A. Duncan, *Phys. Rev. D* **13**, 2866(1976).

C. Quigg, *Gauge Theories of the Strong, Weak, and Electromagnetic Interactions*, Benjamin/Cummings, Reading, Massachusetts, 1983, §8.3.

Path-Integral Formulation of Quantum Mechanics.

R.P. Feynman, *Rev. Mod. Phys.* **20**, 367(1948).

R.P. Feynman and A.R. Hibbs, *Quantum Mechanics and Path Integrals*, McGraw-Hill, New York, 1965.

Lattice Gauge Theories.

K.G. Wilson, *Phys. Rev.* **D10**, 2445(1974).

R.C. Brower, "Discrete Quantum Chromodynamics," in *Gauge Theories in High Energy Physics* (Les Houches, 1981), edited by M.K. Gaillard and R. Stora, North-Holland, Amsterdam, 1983, p.555.

M. Creutz, *Quarks, Gluons, and Lattices*, Cambridge University Press, Cambridge and New York, 1983.

C. Rebbi (editor), *Lattice Gauge Theories and Monte Carlo Simulations*, World Scientific, Singapore, 1983.

A. Hasenfratz and P. Hasenfratz, "Lattice Gauge Theories," Florida State University preprint FSU-SCRI-85-2.

J.-M. Drouffe and C. Itzykson, *Phys. Rep.* **38C**, 133(1978).

J.B. Kogut, *Rev. Mod. Phys.* **51**, 659(1979); **55**, 775(1983).

L.P. Kadanoff, *Rev. Mod. Phys.* **49**, 267(1977).

FOOTNOTES AND REFERENCES

1. Particle Data Group, *Rev. Mod. Phys.* **56**, S1(1984).
2. T. Appelquist and H.D. Politzer, *Phys. Rev. Lett.* **34**, 43(1975).
3. D.J. Gross and F. Wilczek, *Phys. Rev. Lett.* **30**, 1343(1973); H.D. Politzer, *ibid.*, p.1346.
4. C. Quigg and J.L. Rosner, *Phys. Rep.* **56**, 167(1979).
5. R. Van Royen and V.F. Weisskopf, *Nuovo Cimento* **50**, 617(1967); **51**, 583(1967).
6. C. Quigg and J.L. Rosner, *Phys. Lett.* **71B**, 153(1977).
7. C. Quigg and J.L. Rosner, *Comments Nucl. Part. Phys.* **8**, 11(1978).

8. C. Quigg, in *Proceedings of the 1979 International Symposium on Lepton and Photon Interactions at High Energies*, edited by T.B.W. Kirk and H.D.I. Abarbanel, Fermilab, Batavia, 1980, p.239;
J.L. Rosner, in *Particles and Fields-1979*, edited by B. Margolis and D.G. Stairs, American Institute of Physics, New York, p.325; in *Techniques and Concepts of High Energy Physics*, edited by T. Ferbel, Plenum, New York, 1981, p.1.
9. A. Martin, Phys. Lett. **93B**, 338(1980).
10. M. Machacek and Y. Tomozawa, Ann. Phys. (NY) **110**, 407(1978).
11. W. Buchmüller and S.-H.H. Tye, Phys. Rev. D**24**, 132(1981).
12. C. Quigg and J.L. Rosner, Phys. Rev. D**23**, 2625(1981).
13. E. Eichten and K. Gottfried, Phys. Lett. **66B**, 286(1977).
14. C. Quigg and J.L. Rosner, Phys. Lett. **72B**, 462(1978).
15. For suggestions that the top-quark mass lies in this range, see Phys. Lett. **147B**, 493(1984).
16. There could in fact be additional orbitally excited states below the flavor threshold. For estimates in specific potentials, see E. Eichten in *The Sixth Quark*, Proceedings of the 1984 SLAC Summer Institute in Particle Physics, edited by Patricia M. McDonough, SLAC-281, p.1. Note that his estimates do not count fine- and hyperfine-structure partners as distinct states.
17. H. Grosse and A. Martin, Phys. Rep. **60**, 341(1980).
18. J.L. Rosner, C. Quigg, and H.B. Thacker, Phys. Lett. **74B**, 350 (1978);
C.N. Leung and J.L. Rosner, J. Math. Phys. **20**, 1435(1979).
19. See, for example, Fig. 10 of C. Quigg, Ref. 8.
20. For a summary see S. Konamiya, in *Proceedings of the 1985 SLAC Summer Institute* (to be published).
21. Y. Nambu, Phys. Rev. D**10**, 4262(1974).
22. E. Eichten, et al., Phys. Rev. D**17**, 3090(1979); D**21**, 203(1980).
23. J. Richardson, Phys. Lett. **82B**, 272(1979). For an extension of this model see
W. Buchmüller and S.-H.H. Tye, Phys. Rev. D**24**, 132(1981).
24. E. Eichten, Ref. 16.
25. P. Moxhay, J.L. Rosner, and C. Quigg, Phys. Rev. D**23**, 2638(1981).
26. P. Moxhay and J.L. Rosner, Phys. Rev. D**31**, 1762(1985).
27. N.K. Nielsen, Am. J. Phys. **49**, 1171(1981);
R.J. Hughes, Phys. Lett **97B**, 246(1980); Nucl. Phys. **B186**, 376(1981);
K. Johnson, in *Asymptotic Realms of Physics*, edited by A. Guth, K. Huang, and
R.L. Jaffe, MIT Press, Cambridge, Mass., 1983.
28. J.B. Kogut and L. Susskind, Phys. Rev. D**9**, 3501(1974);
T.D. Lee, *Particle Physics and Introduction to Field Theory*, Harwood
Academic, Chur, London, New York, 1981, c.17.

29. L.D. Landau and E.M. Lifshitz, *Electrodynamics of Continuous Media*, Addison-Wesley, Reading, Mass., 1960, §14.
30. O.V. Dolgov, D.A. Kirzhnits, and E.G. Maksimov, *Rev. Mod. Phys.* **53**, 81 (1981).
31. G. 't Hooft, *Nucl. Phys.* **B72**, 461(1974); **B75**, 461(1974).
32. R.P. Feynman, *Rev. Mod. Phys.* **20**, 367(1948);
R.P. Feynman and A.R. Hibbs, *Quantum Mechanics and Path Integrals*, McGraw-Hill, New York, 1965.
See also M. Creutz, *Phys. Rev.* **D15**, 1128(1977);
J.B. Kogut, *Rev. Mod. Phys.* **51**, 659(1979).
33. J. Schwinger, *Proc. Nat. Acad. Sci.* **44**, 956(1958).
See also J. Schwinger, *Phys. Rev.* **115**, 721(1959);
G.C. Wick, *Phys. Rev.* **96**, 1124(1954).
34. E. Ising, *Z. Phys.* **31**, 253(1925). For an exhaustive treatment, see B.M. McCoy and T.T. Wu, *The Two-Dimensional Ising Model*, Harvard University Press, Cambridge, 1973.
35. F. Wegner, *J. Math. Phys.* **12**, 2259(1971).
36. Compare the analysis of the Bohm-Aharonov effect in C. Quigg, *Gauge Theories of the Strong, Weak, and Electromagnetic Interactions*, Benjamin/Cummings, Reading, Mass., 1983 §3.4.
37. The appearance of the coupling constant as written is justified by the inclusion of matter on the lattice.
38. K.G. Wilson, *Phys. Rev.* **D10**, 2445(1974).
39. See, for example, T. Appelquist, J. Carazzone, H. Kluberg-Stern, and M. Roth, *Phys. Rev. Lett.* **36**, 768(1976); **36**, 1161E(1976).
40. A partial bibliography includes I.M. Gel'fand and B.M. Levitan, *Am. Math. Soc. Trans.* **1**, 253(1955);
I. Kay and H.E. Moses, *J. Appl. Phys.* **27**, 1503(1956).
41. C.S. Gardner, J.M. Greene, M.D. Kruskal, and R.M. Miura, *Phys. Rev. Lett.* **19**, 1095(1967); *Comm. Pure Appl. Math.* **27**, 97(1974).
42. H.B. Thacker, C. Quigg, and J.L. Rosner, *Phys. Rev.* **D18**, 274(1978).
43. H. Grosse and A. Martin, *Nucl. Phys.* **B148**, 413(1979).
44. J.F. Schonfeld, et al., *Ann. Phys. (NY)* **128**, 1(1980).
45. I. Sabba Stefanescu, Karlsruhe preprint TKP-81-1.
46. H.B. Thacker, C. Quigg, and J.L. Rosner, *Phys. Rev.* **D18**, 287(1978).
47. C. Quigg, H.B. Thacker, and J.L. Rosner, *Phys. Rev.* **D21**, 234(1980).
48. C. Quigg and J.L. Rosner, *Phys. Rev.* **D23**, 2625(1981).
49. N. Metropolis, A.W. Rosenbluth, M.N. Rosenbluth, A.H. Teller, and E. Teller, *J. Chem. Phys.* **21**, 1087(1953).
50. M. Creutz, *Phys. Rev.* **D21**, 2308(1980).

51. E. Pietarinen, Nucl. Phys. **8190** [FS3], 349(1981);
E. Marinari and N. Cabibbo, Phys. Lett. **119B**, 387(1982).
52. M. Creutz, *Quarks, Gluons, and Lattices*, Cambridge University Press,
Cambridge and New York, 1983.
53. M. Creutz, Phys. Rev. Lett. **43**, 553 (1979).
54. B. Lautrup and M. Nauenberg, Phys. Lett. **95B**, 63(1980).
55. M. Creutz, Phys. Rev. Lett. **45**, 313(1980).
56. W. Caswell, Phys. Rev. Lett. **33**, 244(1974);
D.R.T. Jones, Nucl. Phys. **875**, 531(1974).
57. M. Creutz and K.J.M. Moriarty, Phys. Rev. **D26**, 2166(1982).
58. A. Hasenfratz and P. Hasenfratz, Phys. Lett. **93B**, 165(1980); Nucl. Phys.
8193, 210(1981);
R. Dashen and D. Gross, Phys. Rev. **D23**, 2340(1981);
H. Kawai, R. Nakayama, and K. Seo, Nucl. Phys. **8189**, 40(1981).
For the connection between $\Lambda_{\overline{MS}}$ and $\Lambda_{\overline{MS}}$, see W. Celmaster and R.J. Gonsalves,
Phys. Rev. **D20**, 1420(1979).
59. S. Otto and J. Stack, Phys. Rev. Lett. **52**, 2328(1984); **53**, 1028E(1984).
60. E. Brooks, III, et al., Phys. Rev. Lett. **52**, 2324(1984).

CAPTIONS

- Fig. 1: The spectrum of charmonium ($c\bar{c}$ bound states).
- Fig. 2: The upsilon spectrum ($b\bar{b}$ bound states).
- Fig. 3: Schematic level scheme for $(\sigma\sigma)$ bound states.
- Fig. 4: Schematic level scheme for $(f\bar{f})$ bound states.
- Fig. 5: Level spacings in the ψ and Υ families.
- Fig. 6: Semiclassical (curve) and exact (small dots) ratios $(E_3-E_2)/(E_2-E_1)$ for s-wave levels in potentials $V(r)=\lambda r^\nu$ (from Ref. 4).
- Fig. 7: Semiclassical (curve) ratios $(E_4-E_3)/(E_2-E_1)$ for s-wave levels in potentials $V(r)=\lambda r^\nu$. The datum is the value in the upsilon system.
- Fig. 8: The quantity $(E_{2S}-E_{2P})/(E_{2S}-E_{1S})$ for power-law potentials $V(r)=\lambda r^\nu$, $-1 \leq \nu \leq 2$. The data points are the values in the ψ and Υ systems.
- Fig. 9: Square of the wavefunction at the origin for the psions. Possible mixing between the $2^3S_1(3686)$ and $3^3D_1(3770)$ levels has been neglected. (a) A best fit proportional to $(n-\frac{1}{2})^p$, with $p = -0.83 \pm 0.11$ ($\nu=0.12 \pm 0.08$), assuming the conventional 4S assignment for $\psi(4415)$. (b) An alternative 5S assignment for $\psi(4415)$, which corresponds to $p = -0.79 \pm 0.10$ ($\nu=0.15 \pm 0.08$). In plotting the data against $(n-\frac{1}{2})$, we have anticipated the result $p > -1$ ($\nu > 0$).
- Fig. 10: Same as Fig. 9 for the upsilons. The best fit is for $p = -0.79 \pm 0.10$ ($\nu=0.15 \pm 0.08$).
- Fig. 11: Comparison of mass dependence of energy levels in three potentials: (a) $V(r)=-r^{-\frac{1}{2}}$; (b) $V(r)=\ln r$; (c) $V(r)=r$. (From Ref. 4.)
- Fig. 12: A possible spectrum of strangeonium ($s\bar{s}$) levels. Identification of $E(1418)$ and $\phi(1634)$ as pure $s\bar{s}$ states may be disputed. The dotted 0^{-+} entry is impressionistic, having been invented from the ϕ mass and the π - ρ splitting, appropriately rescaled.
- Fig. 13: Lower bounds for leptonic decays of Υ and Υ' (after Rosner, Quigg, and Thacker, Ref. 18), together with the data cited in Table 2. The bounds are computed from Eq. (2.5) using ψ leptonic widths 1σ below the central values and $m_b/m_c \geq 3$.
- Fig. 14: Attempting to separate a quark and antiquark results in the creation of a

quark-antiquark pair from the vacuum, so that color is always neutralized locally.

- Fig. 15: Regge trajectories of the natural-parity mesons. Uncertain states are indicated by open circles.
- Fig. 16: Regge trajectories of the nucleon, Δ , Λ resonances.
- Fig. 17: A massless quark and antiquark connected by a linear string.
- Fig. 18: Phenomenological potentials for quarkonium systems. The rms radii of the observed ψ and T states are indicated. (After Eichten, Ref. 24.)
- Fig. 19: Extrapolations of the four phenomenological potentials to short distances. The rms radii of toponium ground states are indicated for top quark masses of 30 and 60 GeV/c². (from Ref. 24).
- Fig. 20: The 2S-1S interval as a function of quark mass in four phenomenological potentials (from Ref. 24).
- Fig. 21: Comparison of Richardson's potential (dashed curve) with the expectations of perturbative QCD (solid curves) for $\Lambda_{\overline{MS}} = 0.1, 0.2, 0.3, 0.4$ GeV (from Ref. 24).
- Fig. 22: The spectrum of $(t\bar{t})$ states in Richardson's potential for $m_t = 45$ GeV/c² (from Ref. 24). All states below threshold with $L \leq 4$ are shown explicitly. The maximum angular momentum for which at least one state lies below flavor threshold is $L_{\max} = 17$.
- Fig. 23: Charge induced by a positive test charge placed at the center of a hole in a dielectric medium. (a) Dia-electric case $\epsilon_{\text{medium}} < 1$ hoped to resemble QCD. (b) Dielectric case $\epsilon_{\text{medium}} > 1$ of normal electrodynamics.
- Fig. 24: Double-line notation for quarks, gluons, and their interactions, useful for $1/N_c$ analyses.
- Fig. 25: Lowest order vacuum polarization contributions to the gluon propagator. (a) quark loop; (b) gluon loop; (c) quark loop in the double-line notation; (d) gluon loop in the double-line notation.
- Fig. 26: A two-loop diagram in (a) conventional and (b) double-line notation.
- Fig. 27: A three-loop diagram in (a) conventional and (b) double-line notation.
- Fig. 28: A nonplanar graph in (a) conventional and (b) double-line notation.
- Fig. 29: OZI-allowed decay of a meson, at order g^4 , in (a) conventional and (b) double-line notation. The crossed lines represent color singlet projections.

- Fig. 30: Propagation of a color-singlet meson, at order g^4 , in (a) conventional and (b) double-line notation.
- Fig. 31: A mechanism for OZI-forbidden decay, at order g^4 , in (a) conventional and (b) double-line notation.
- Fig. 32: Meson-exotic mixing, at order g^4 , in (a) conventional and (b) double-line notation.
- Fig. 33: Discrete time lattice for the evaluation of the quantum mechanical sum over paths.
- Fig. 34: Links between quantum mechanics, field theory, and statistical physics.
- Fig. 35: The Ising lattice.
- Fig. 36: Spontaneous magnetization in the two-dimensional Ising model.
- Fig. 37: Representative configurations of the two-dimensional Ising model. (a) $T=0$; (b) $0 < T < T_c$; (c) $T > T_c$.
- Fig. 38: Two-dimensional lattice for Z_2 gauge theory.
- Fig. 39: An elementary plaquette for the Z_2 gauge theory in two dimensions.
- Fig. 40: Link variables for the lattice $U(1)$ theory.
- Fig. 41: Elementary plaquette for the lattice $U(1)$ theory.
- Fig. 42: Contour for the derivation of the area law.
- Fig. 43: Callan-Symanzik beta functions for QED and QCD.
- Fig. 44: A symmetric, monotonic potential in one dimension.
- Fig. 45: Approximate reconstruction of the harmonic oscillator potential. (a)-(e): $N=1,2,3,4,5$ reflectionless approximations to the potential. The true potential is shown for comparison. (f)-(j): wave functions obtained in the $N=1,2,3,4,5$ reflectionless approximations; (k) exact wave functions (from Ref. 42).
- Fig. 46: Approximate reconstruction of the linear potential. See the caption to Fig. 45 (from Ref. 42).
- Fig. 47: Approximate reconstruction of the infinite square-well potential. See the caption to Fig. 45 (from Ref. 42).

- Fig. 48: Potentials constructed from the ψ and ψ' . (a) $\rho=1$, $m_c=1.1 \text{ GeV}/c^2$; (b) $\rho=1.4$, $m_c=1.4 \text{ GeV}/c^2$; (c) $\rho=2$, $m_c=1.7 \text{ GeV}/c^2$. Levels of the charmonium (T) system are plotted on the left (right). Solid lines denote the 3S_1 states; dashed lines indicate the mean mass of the 2^3P_J states. The right-hand scale (for the T 's) is shifted by an amount $2(m_b-m_c)$ with respect to the left-hand (ψ) scale (from Ref. 48).
- Fig. 49: Comparison of the charmonium potentials of Fig. 48. Dot-dashed line: $\rho=1$, $m_c=1.1 \text{ GeV}/c^2$; solid line: $\rho=1.4$, $m_c=1.4 \text{ GeV}/c^2$; long-dashed line: $\rho=2$, $m_c=1.7 \text{ GeV}/c^2$. The short-dashed line is the "asymptotic freedom" potential of Ref. 23 (from Ref. 48).
- Fig. 50: Potentials reconstructed from the T spectrum (a) $\rho=1$, $m_b=4.5 \text{ GeV}/c^2$; (b) $\rho=1.4$, $m_b=4.75 \text{ GeV}/c^2$; (c) $\rho=2$, $m_b=5 \text{ GeV}/c^2$. Levels of the upsilon (charmonium) system are plotted on the right (left). Solid lines denote the 3S_1 states; dashed lines indicate the mean mass of the 2^3P_J states. The left-hand scale (for the ψ 's) is shifted by an amount $2(m_c-m_b)$ with respect to the right-hand (upsilon) scale (from Ref. 48).
- Fig. 51: Comparison of the upsilon potentials of Fig. 50. Dot-dashed line: $\rho=1$, $m_b=4.5 \text{ GeV}/c^2$; solid line: $\rho=1.4$, $m_b=4.75 \text{ GeV}/c^2$; long-dashed line: $\rho=2$, $m_b=5 \text{ GeV}/c^2$. The short-dashed line is the "asymptotic freedom" potential of Ref. 23 (from Ref. 48).
- Fig. 52: Comparison of potentials deduced from the ψ and T families. The energy scale is appropriate for the ψ spectrum. In each graph, the label on the left-hand ordinate refers to the potential constructed using T data (solid curve). The label on the right-hand ordinate refers to the potential constructed using ψ data (dashed curve). (a) $\rho=1$; (b) $\rho=1.4$; (c) $\rho=2$ (from Ref. 48).
- Fig. 53: (a) Ordered and (b) random starts for the Ising model on a 5×5 lattice.
- Fig. 54: Approach to equilibrium for $SU(2)$ gauge theory on 4^4 , 6^4 , 8^4 , and 10^4 lattices, with $\beta=2.3$ (from Ref. 50).
- Fig. 55: Approach to equilibrium for $U(1)$ gauge theory on a 6^4 lattice, with $\beta=1.0$. The theory has a critical point at $\beta_{cr}=1.012$, for a lattice of infinite size (from Ref. 52).
- Fig. 56: Hysteresis in thermal cycles of the mean plaquette for $U(1)$ [$SU(2)$] gauge theory on a 5^4 lattice (from Ref. 53).
- Fig. 57: The $U(1)$ mean plaquette energy as a function of β for a 5^4 lattice (from Ref. 54).

- Fig. 58: The normalized specific heat ρ of the U(1) theory as a function of β in the critical region for lattices of size 4^4 , 5^4 , and 6^4 (from Ref. 54).
- Fig. 59: The mean plaquette energy for SU(3) gauge theory on 4^4 and 6^4 lattices (from Ref. 52).
- Fig. 60: Wilson loop for the evaluation of the string tension.
- Fig. 61: The quantities $\chi(I,I)$ for SU(2) gauge theory as a function of $1/g^2$ (from Ref. 55).
- Fig. 62: The quantities $\chi(I,I)$ for SU(3) gauge theory as a function of $1/g^2$ (from Ref. 57).
- Fig. 63: The SU(3) heavy quark potential determined on a $12^3 \times 16$ lattice (from Ref. 59). The string tension is denoted by σ .
- Fig. 64: Comparison of a smooth curve drawn through the lattice potential of Fig. 63 with a logarithmic form (dashed line) (from Ref. 16).

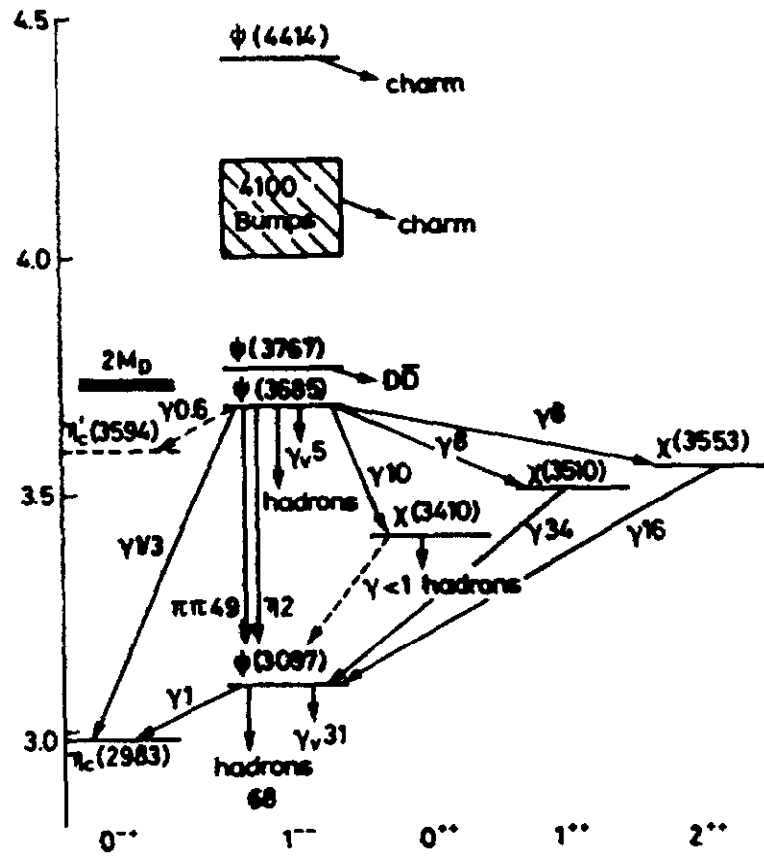


Fig. 1

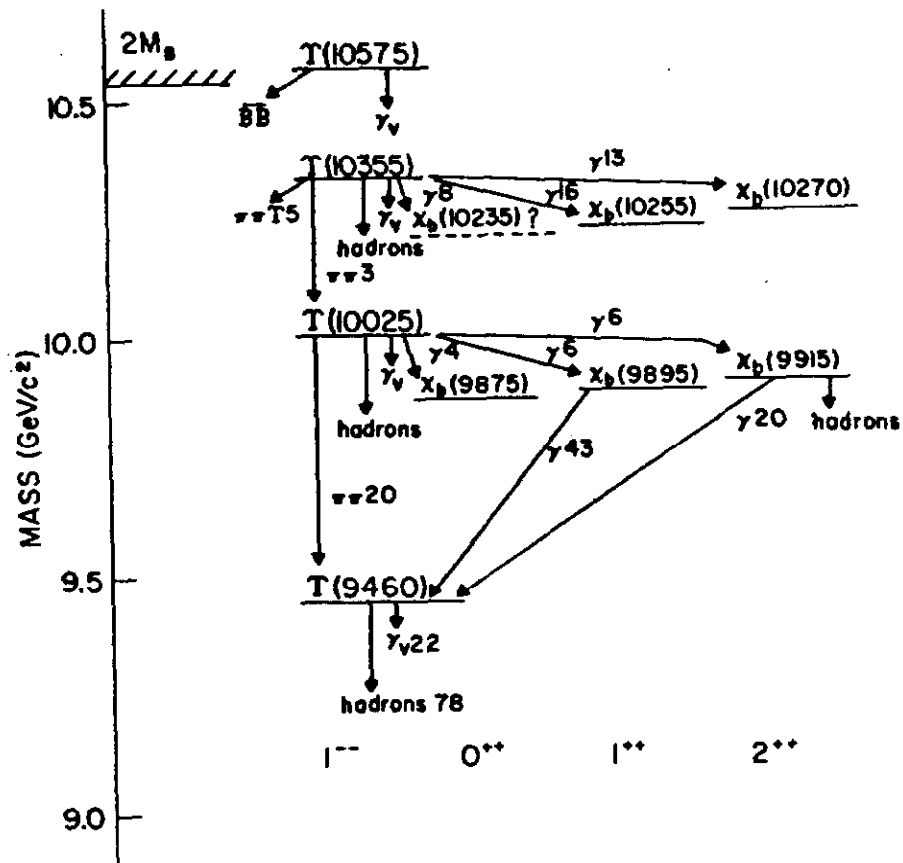


Fig. 2

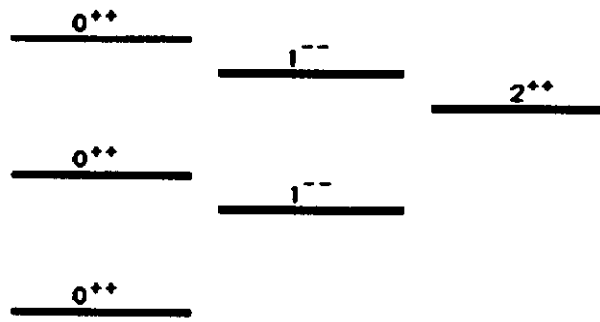


Fig. 3

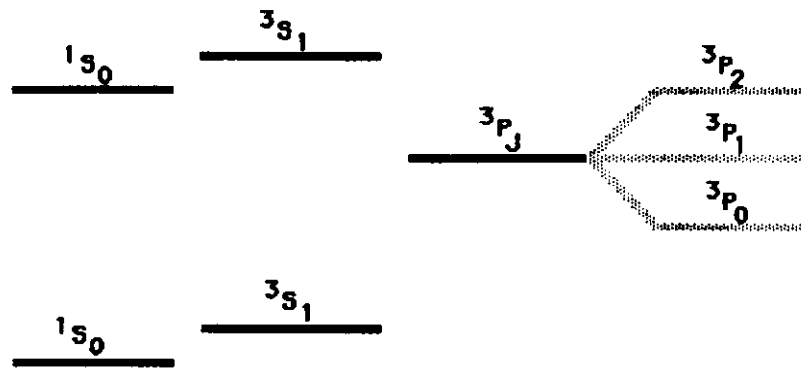


Fig. 4

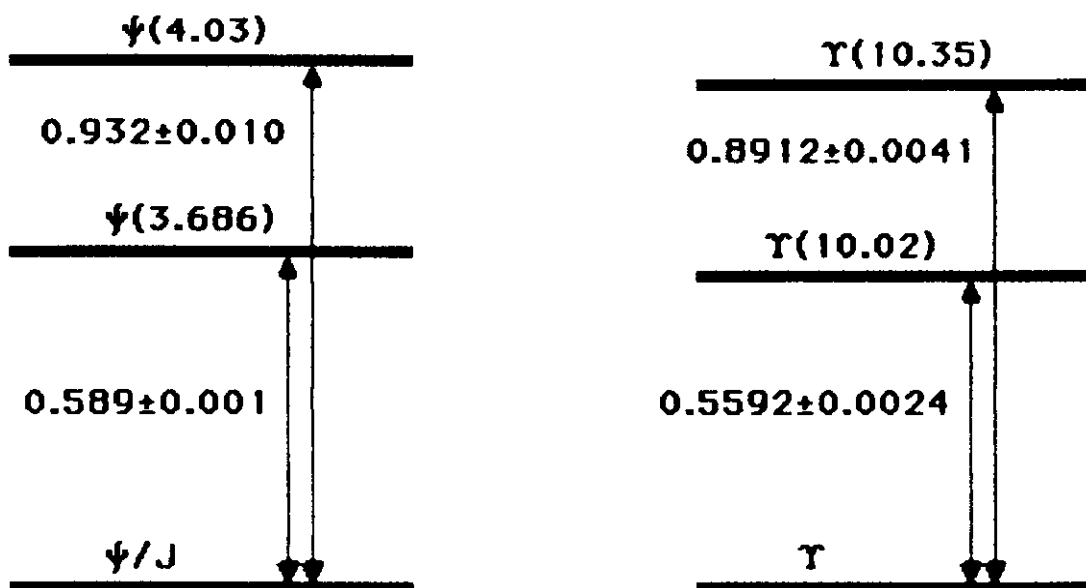


Fig. 5

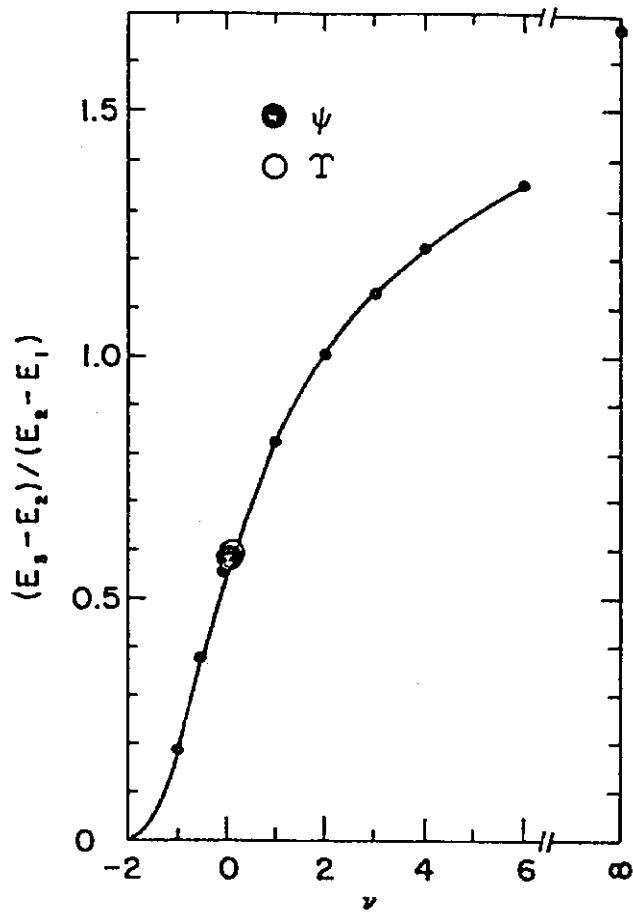


Fig. 6

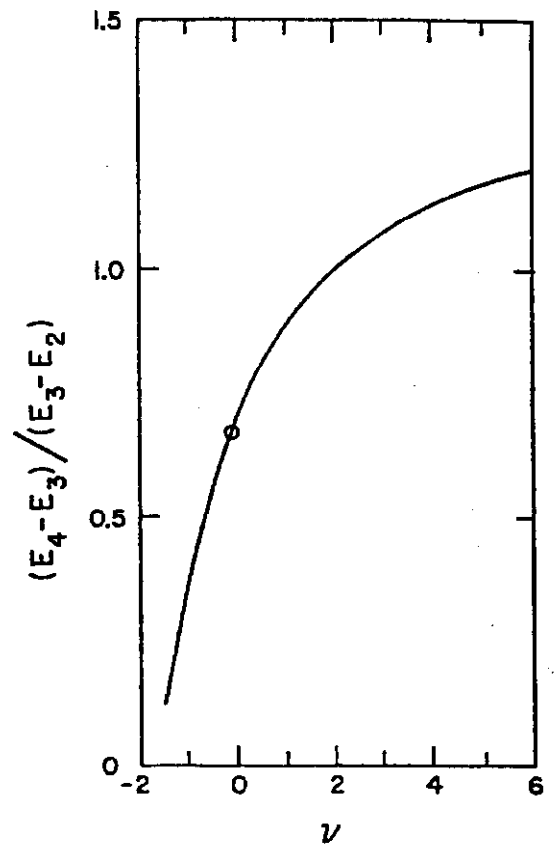


Fig. 7

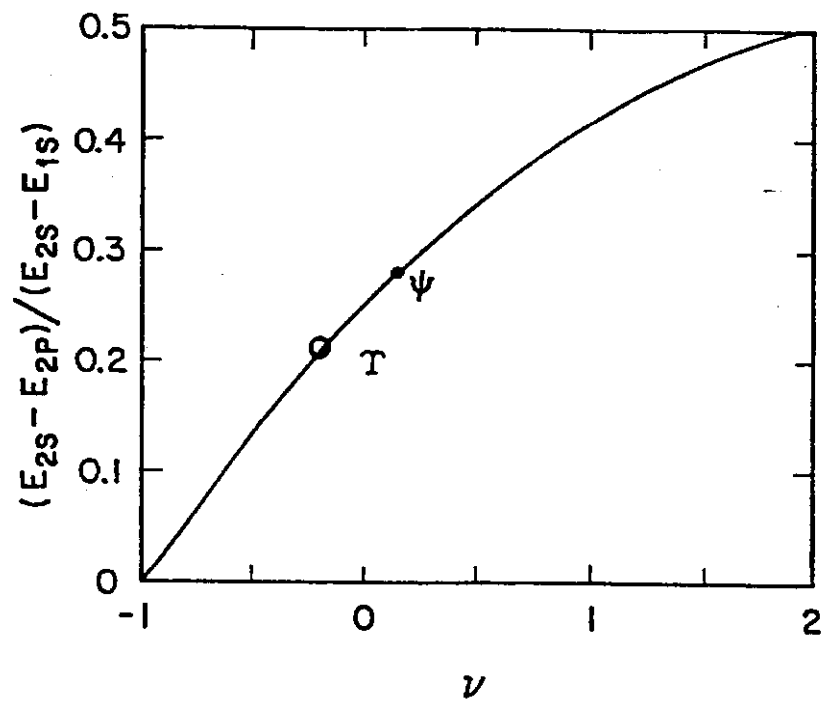


Fig. 8

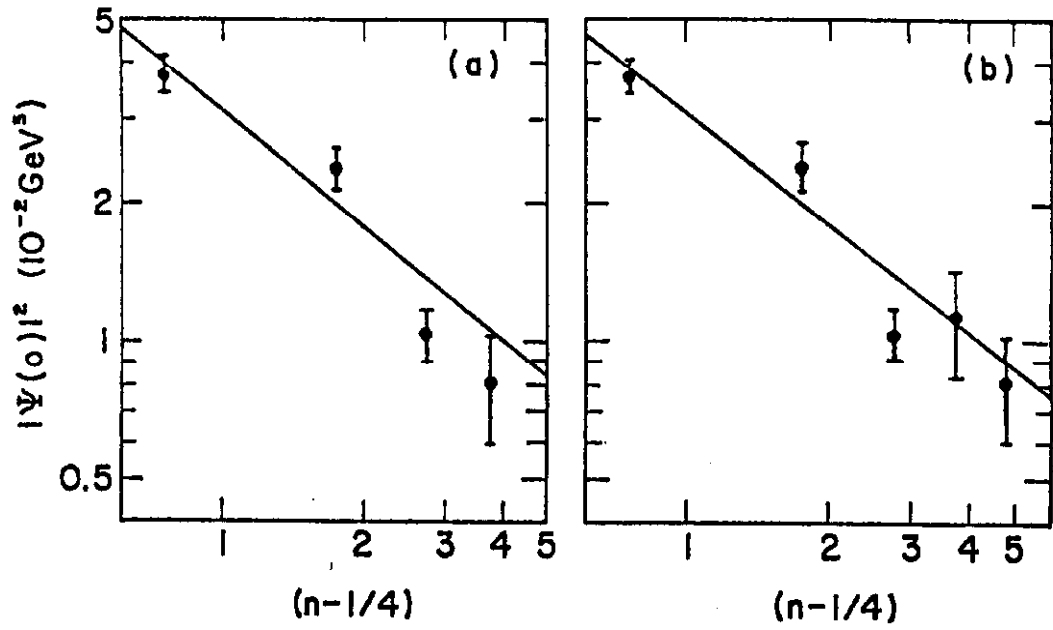


Fig. 9

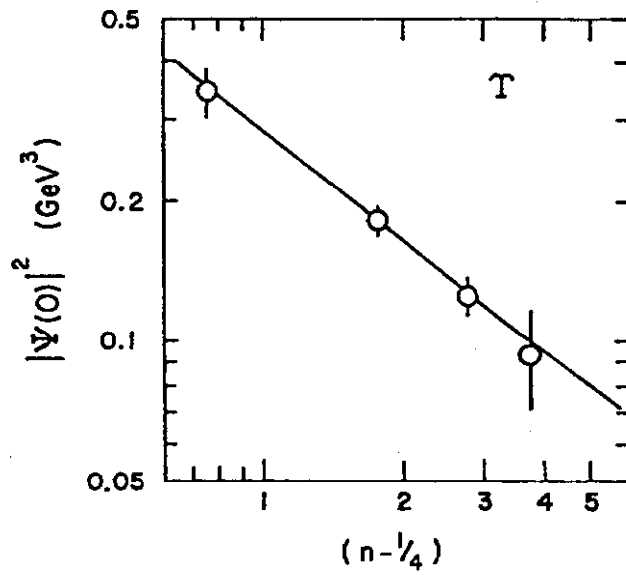


Fig. 10

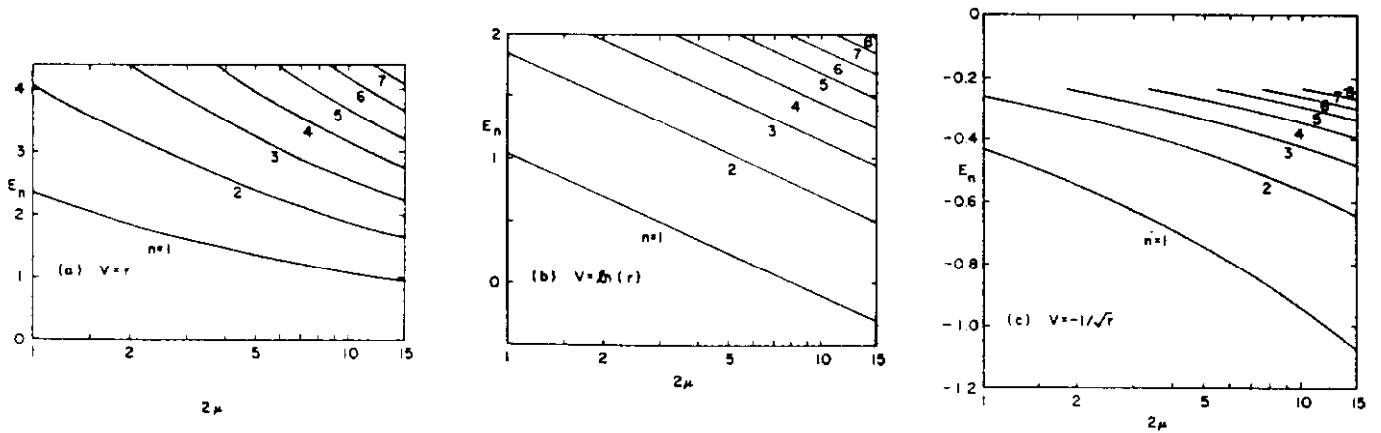


Fig. 11

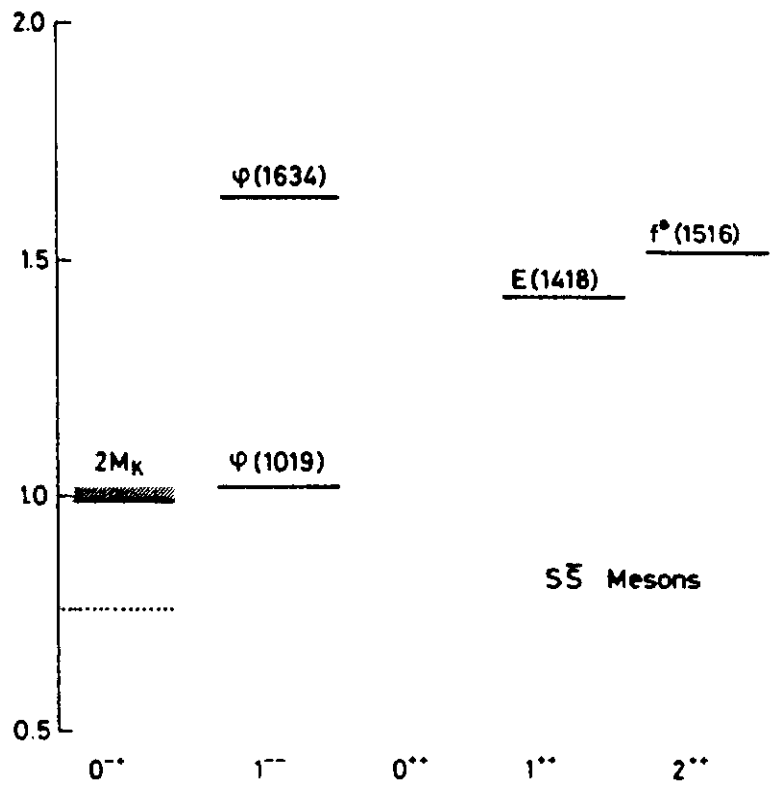


Fig. 12

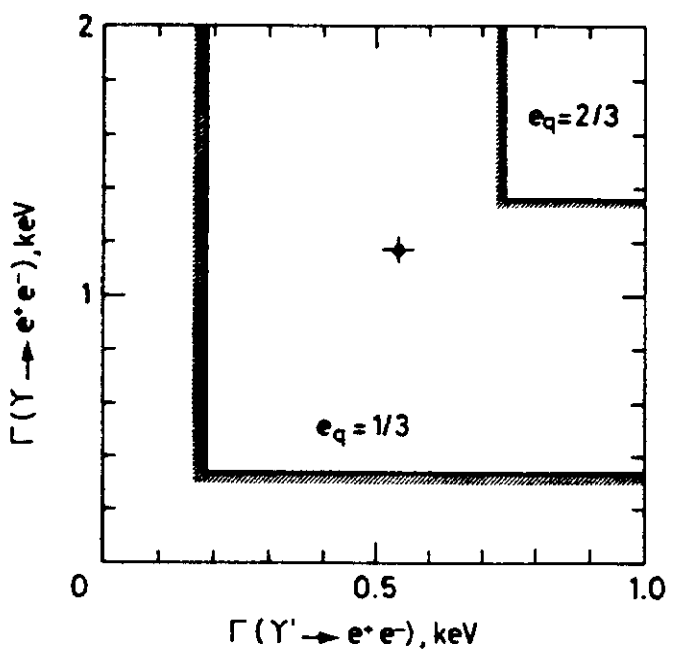


Fig. 13

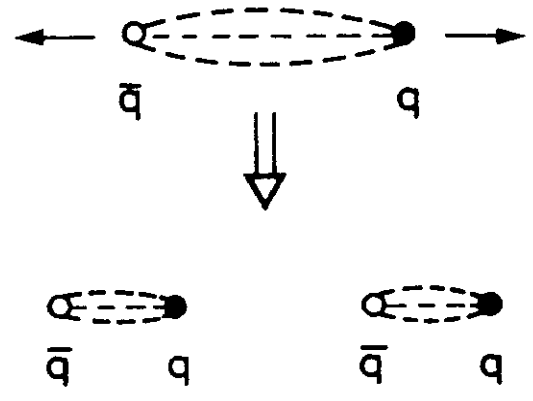


Fig. 14

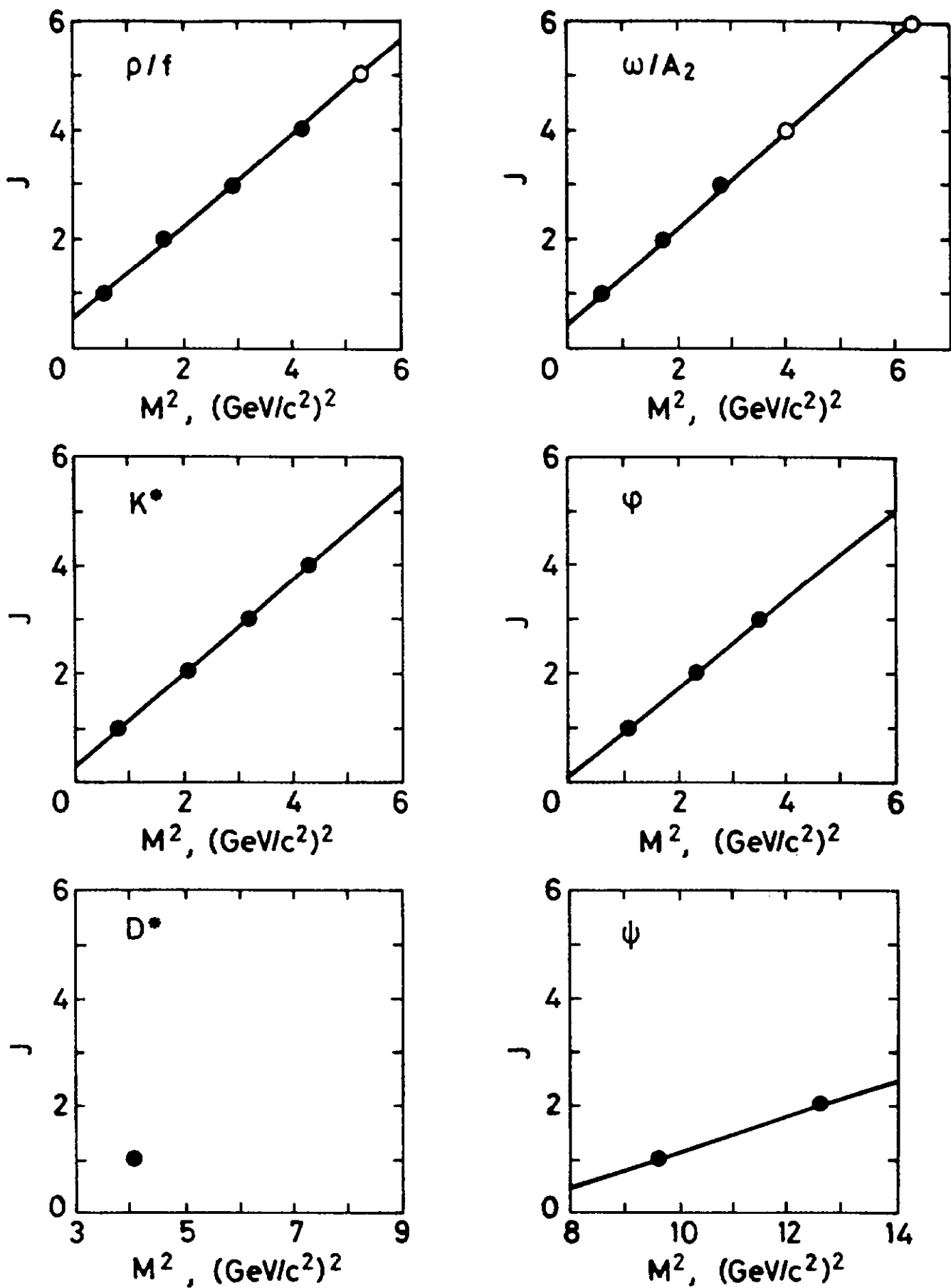


Fig. 15

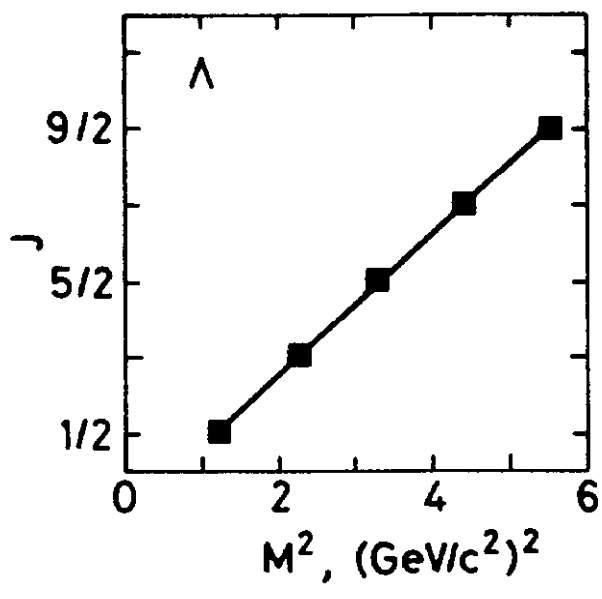
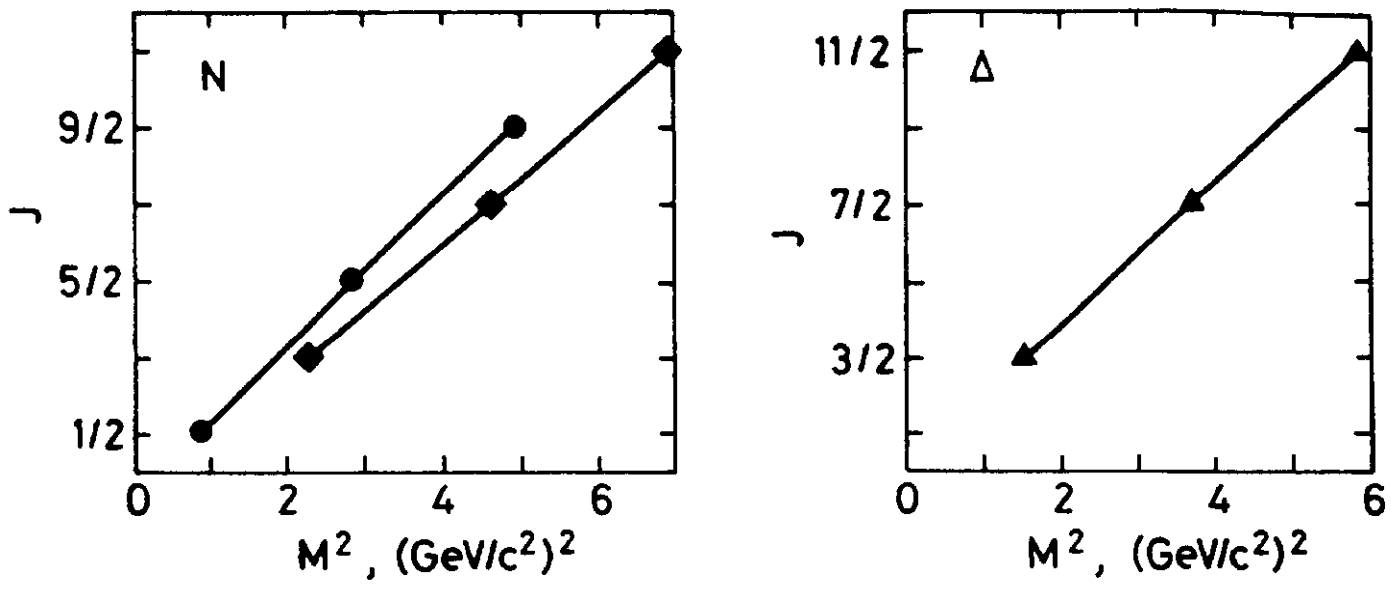


Fig. 16

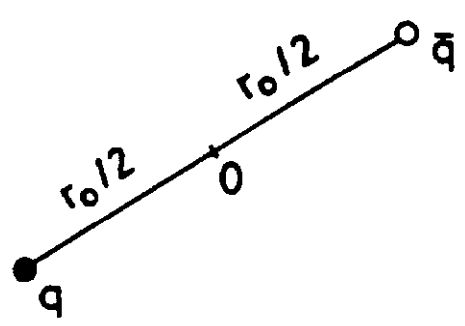


Fig. 17

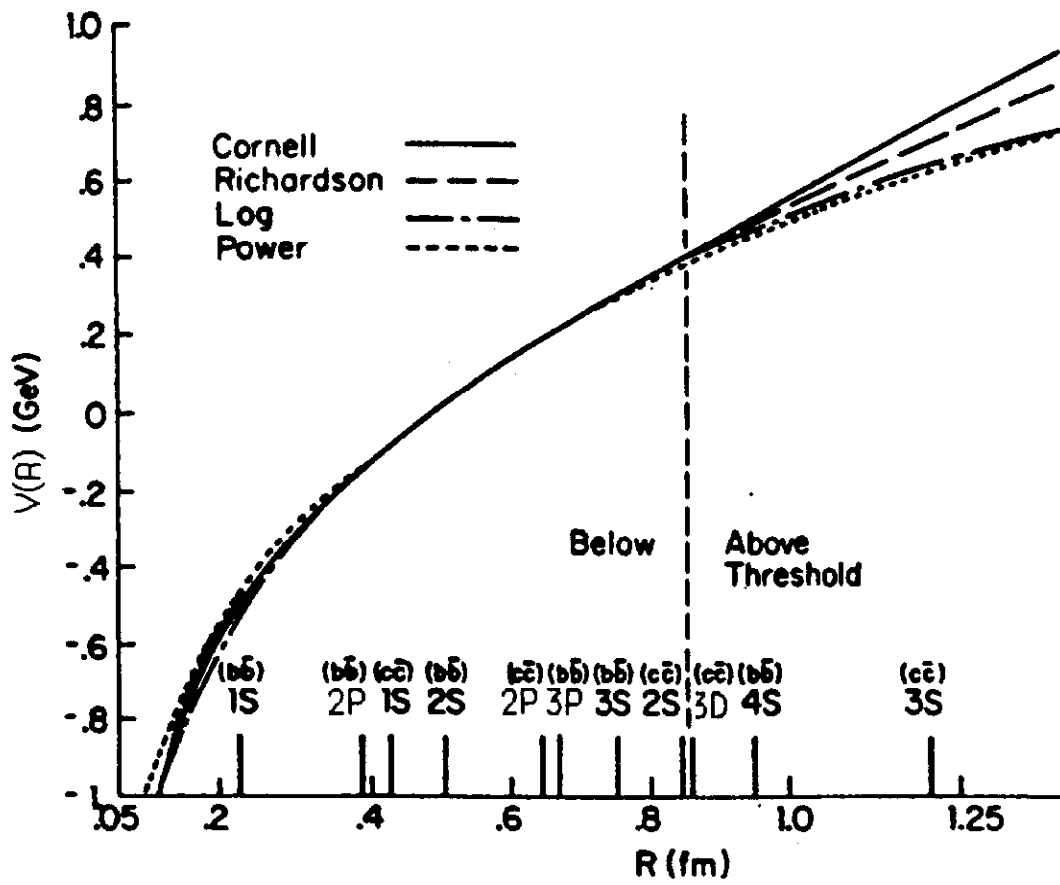


Fig. 18

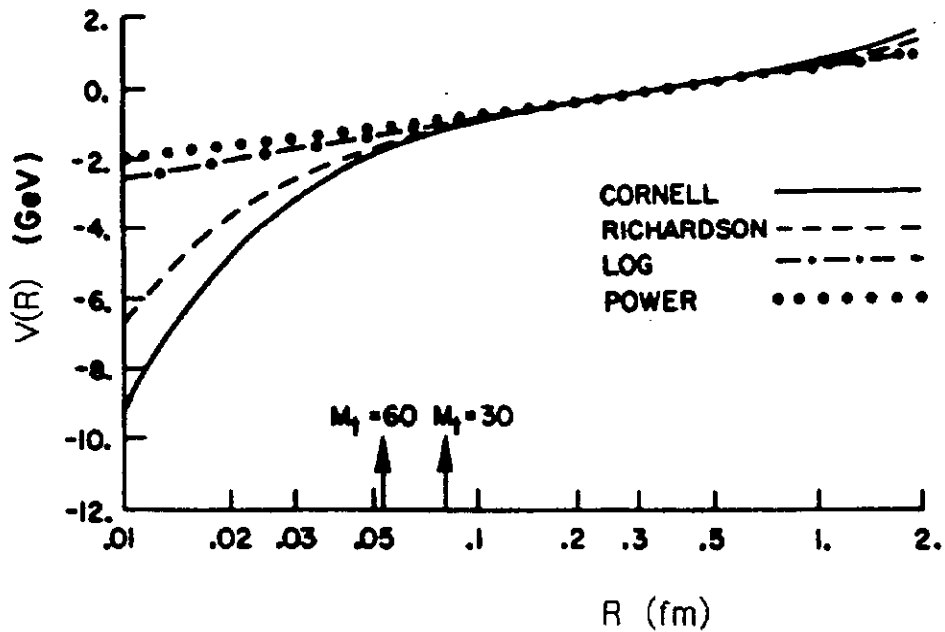


Fig. 19

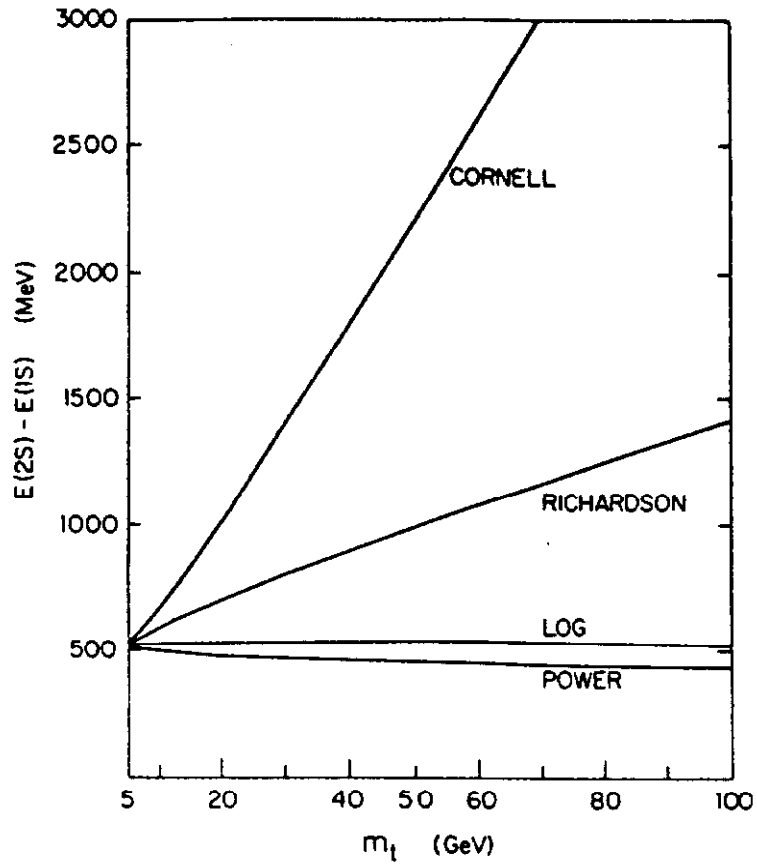


Fig. 20

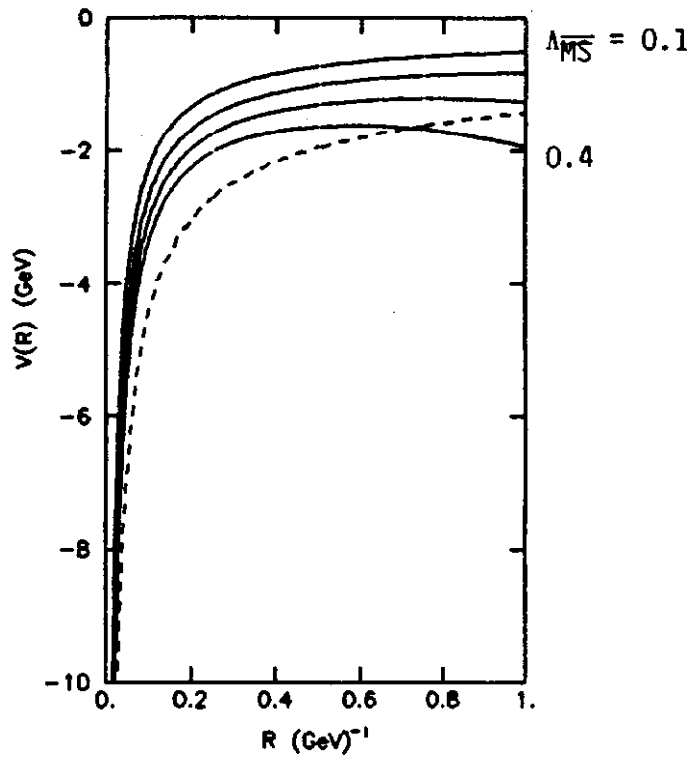


Fig. 21

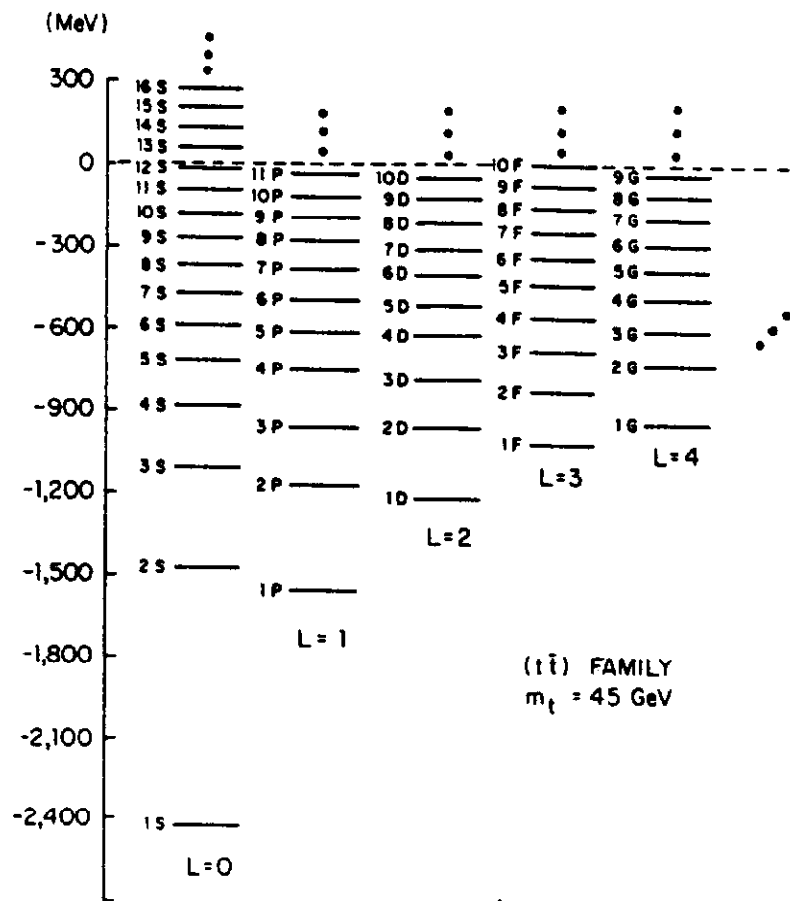


Fig. 22

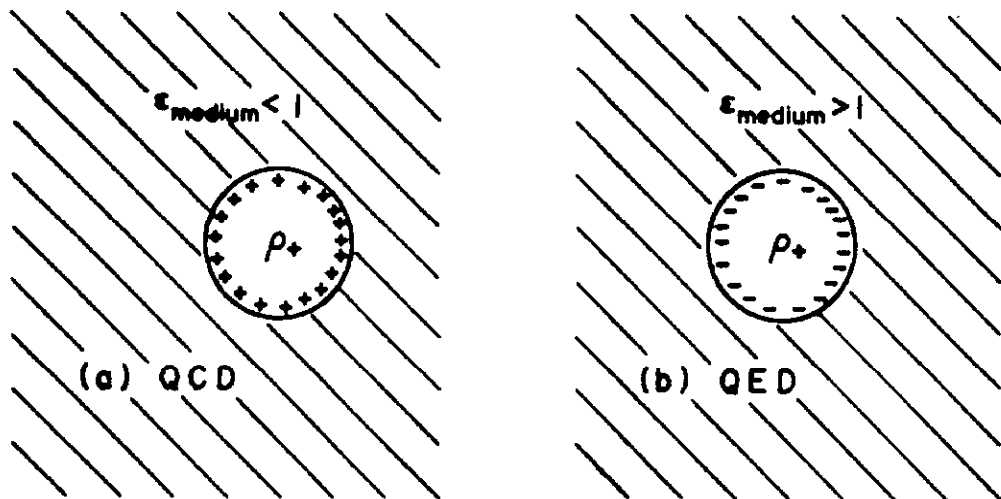


Fig. 23

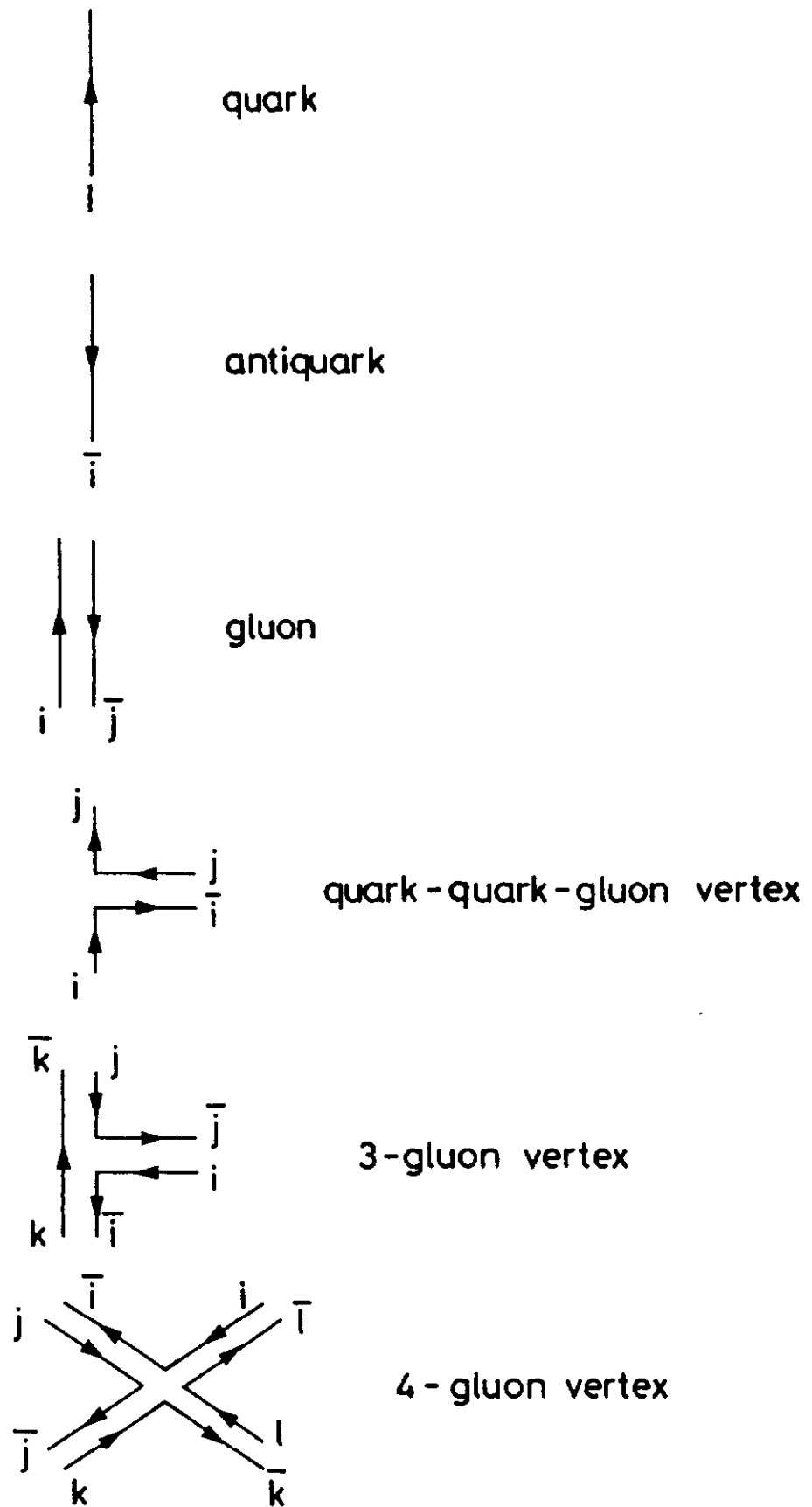


Fig. 24

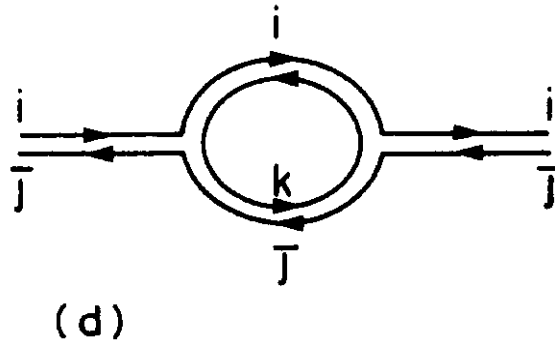
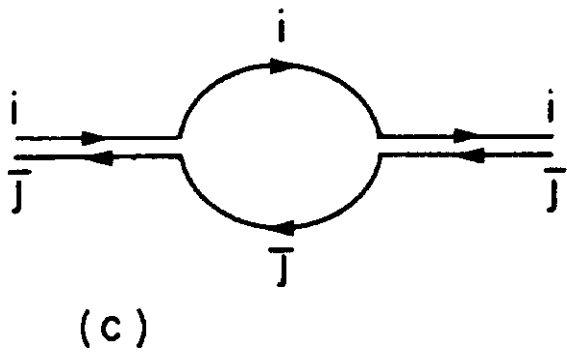
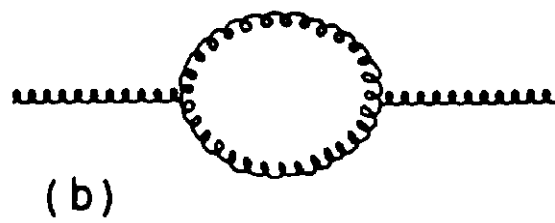
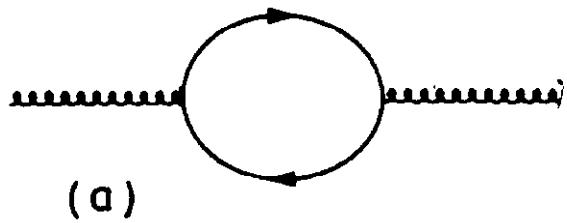


Fig. 25

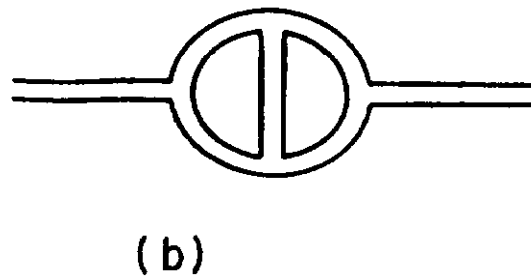
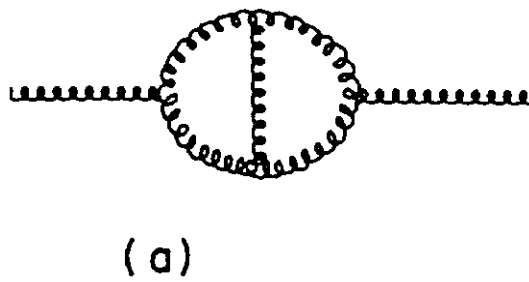


Fig. 26

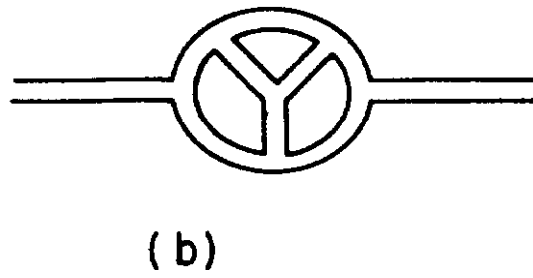
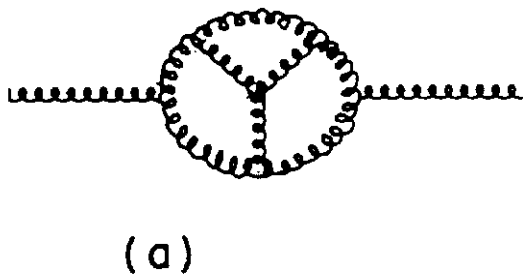
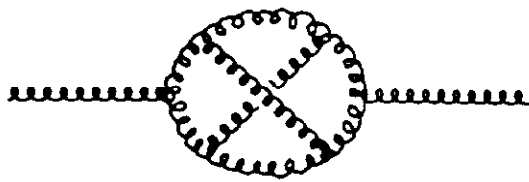
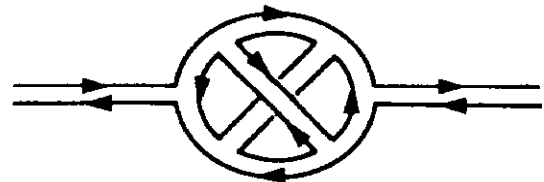


Fig. 27

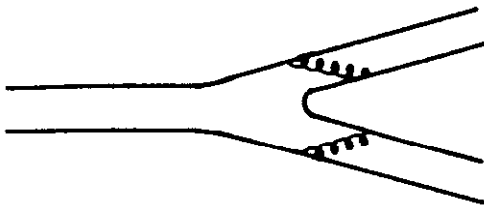


(a)

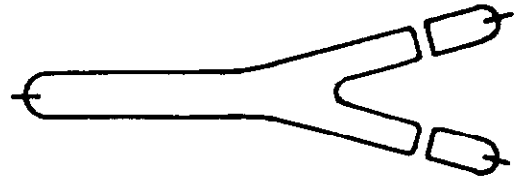


(b)

Fig. 28



(a)



(b)

Fig. 29



=

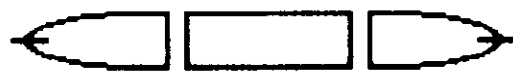
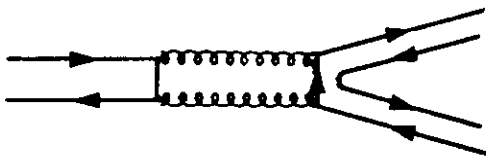
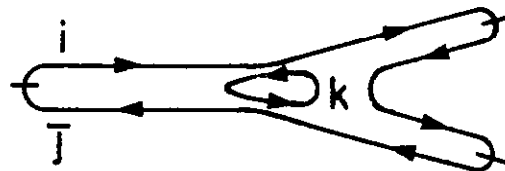


Fig. 30



(a)



(b)

Fig. 31

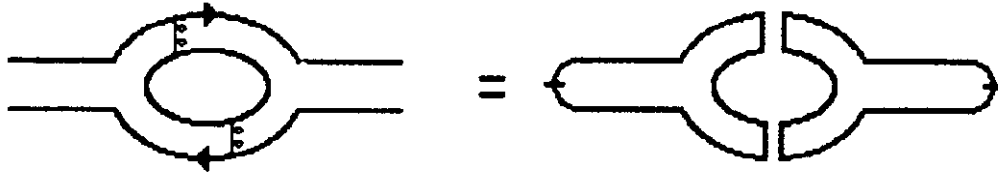


Fig. 32

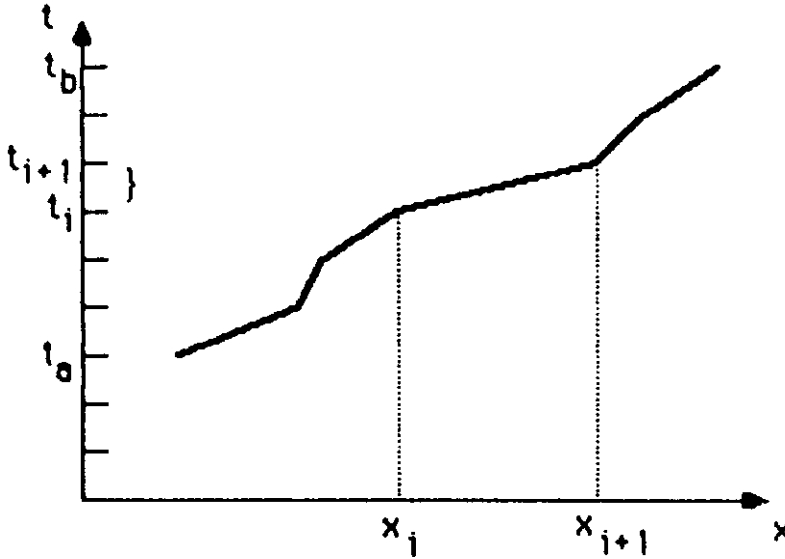


Fig. 33

STATISTICAL MECHANICS

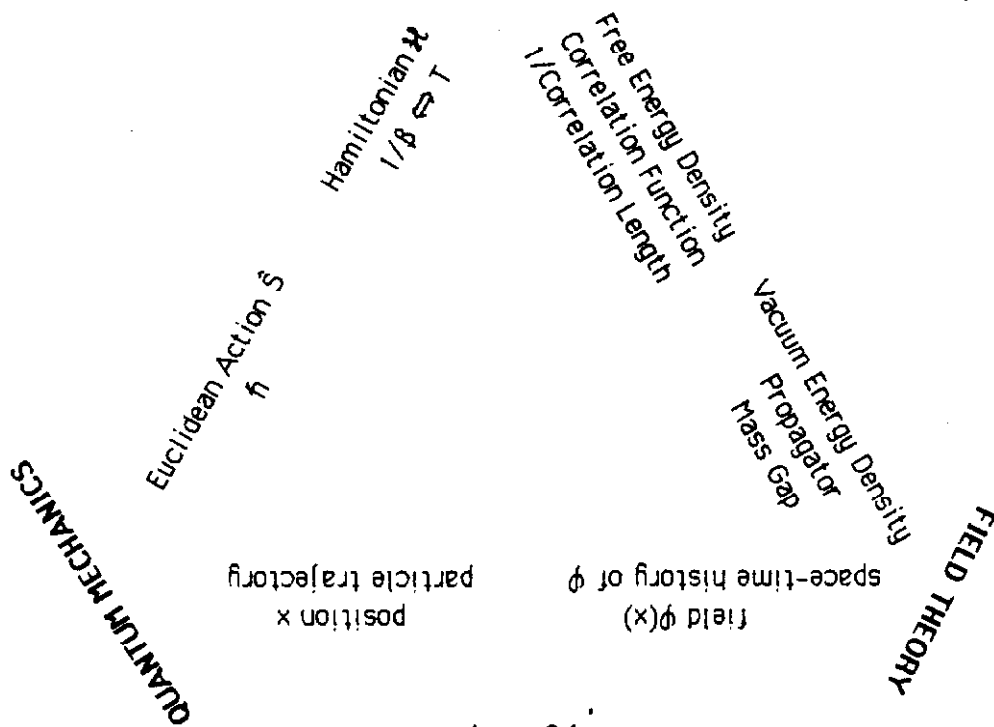


Fig. 34

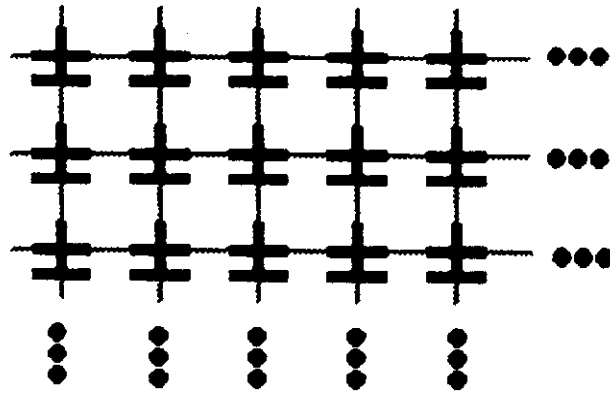


Fig. 35

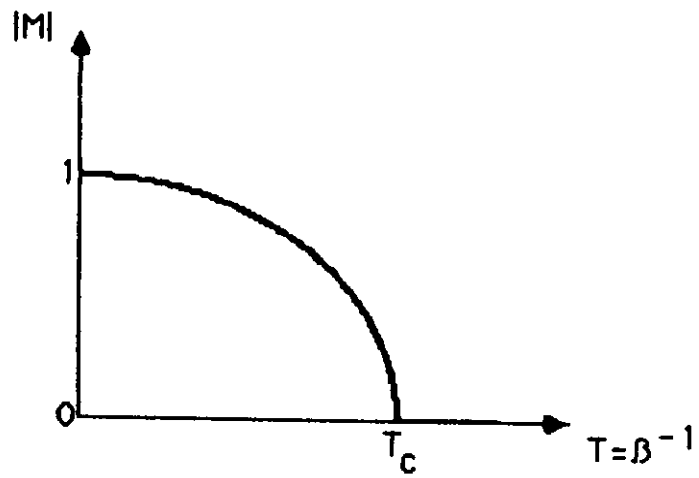


Fig. 36

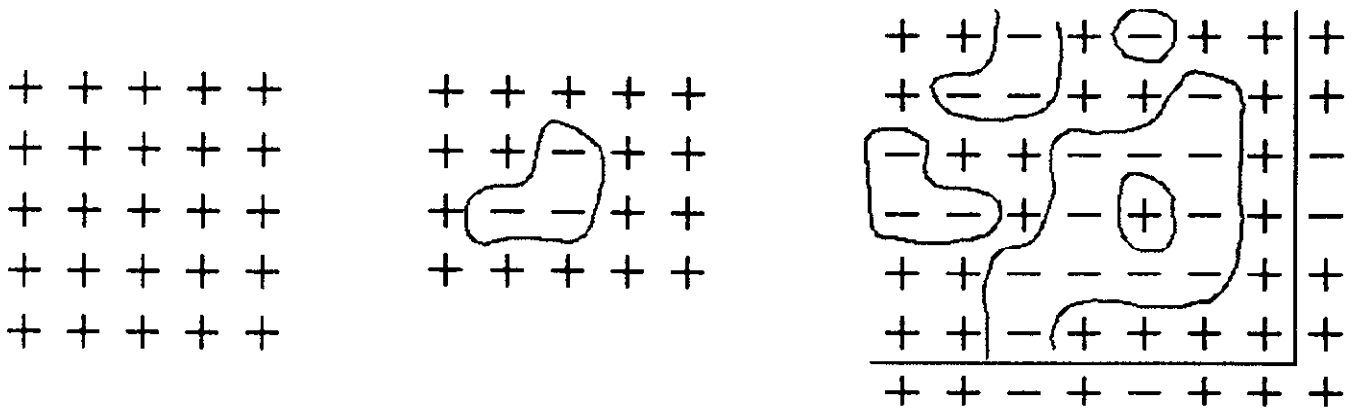


Fig. 37

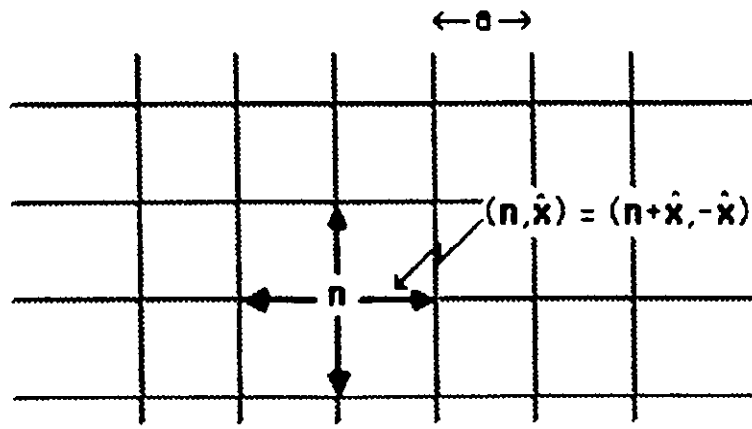


Fig. 38

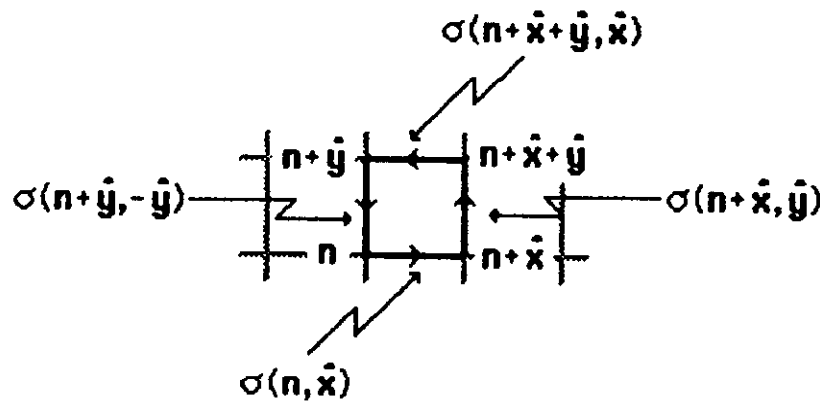


Fig. 39



Fig. 40

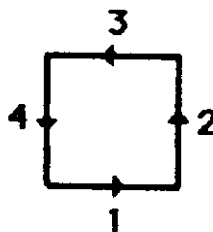


Fig. 41

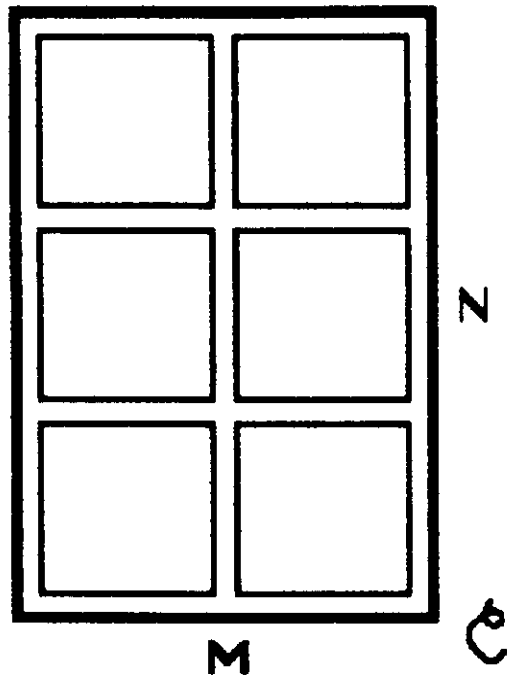


Fig. 42

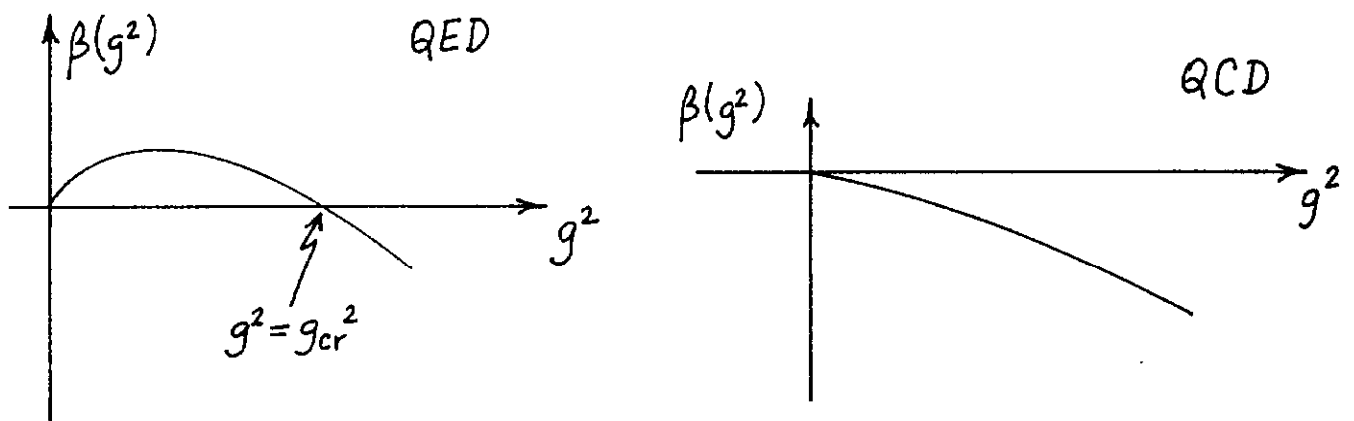


Fig. 43

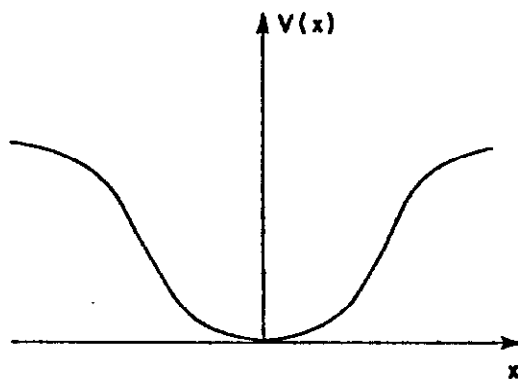


Fig. 44

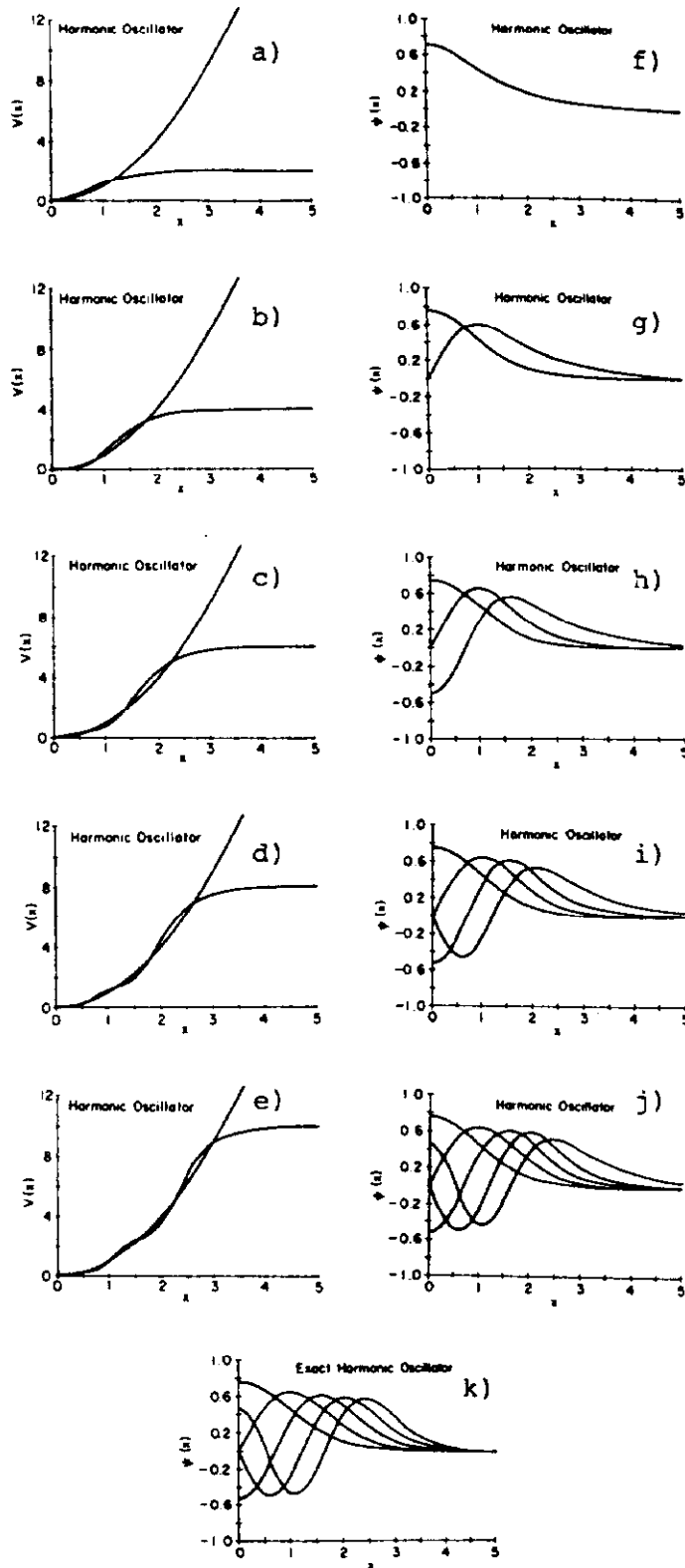


Fig. 45

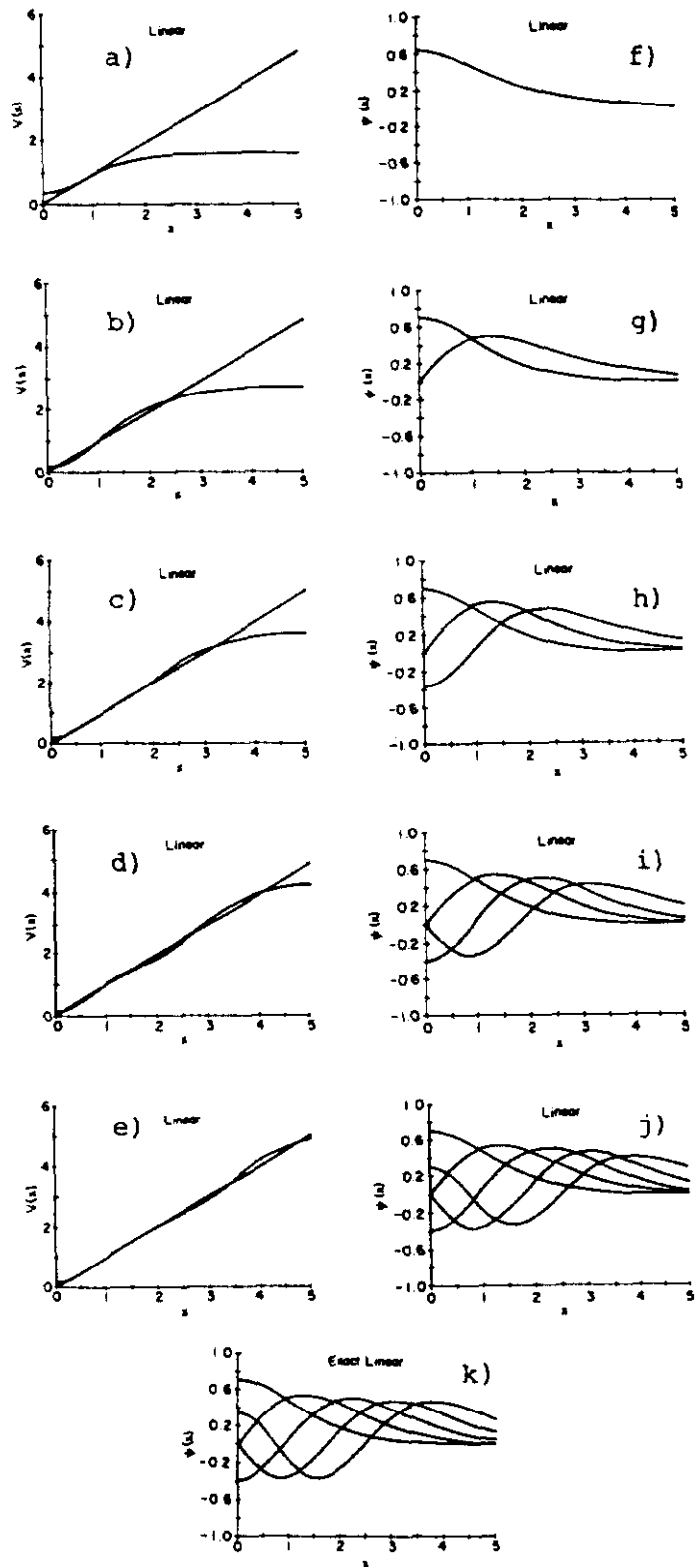


Fig. 46

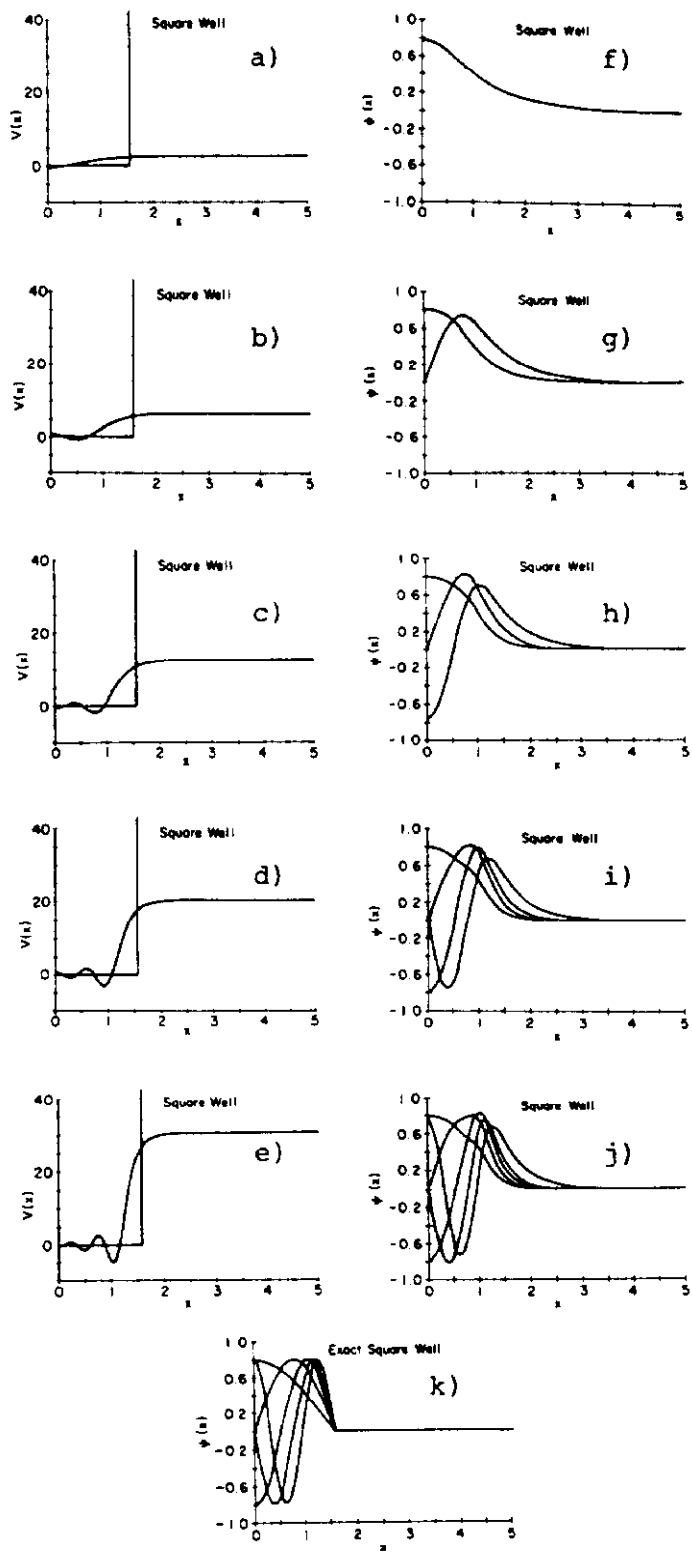


Fig. 47

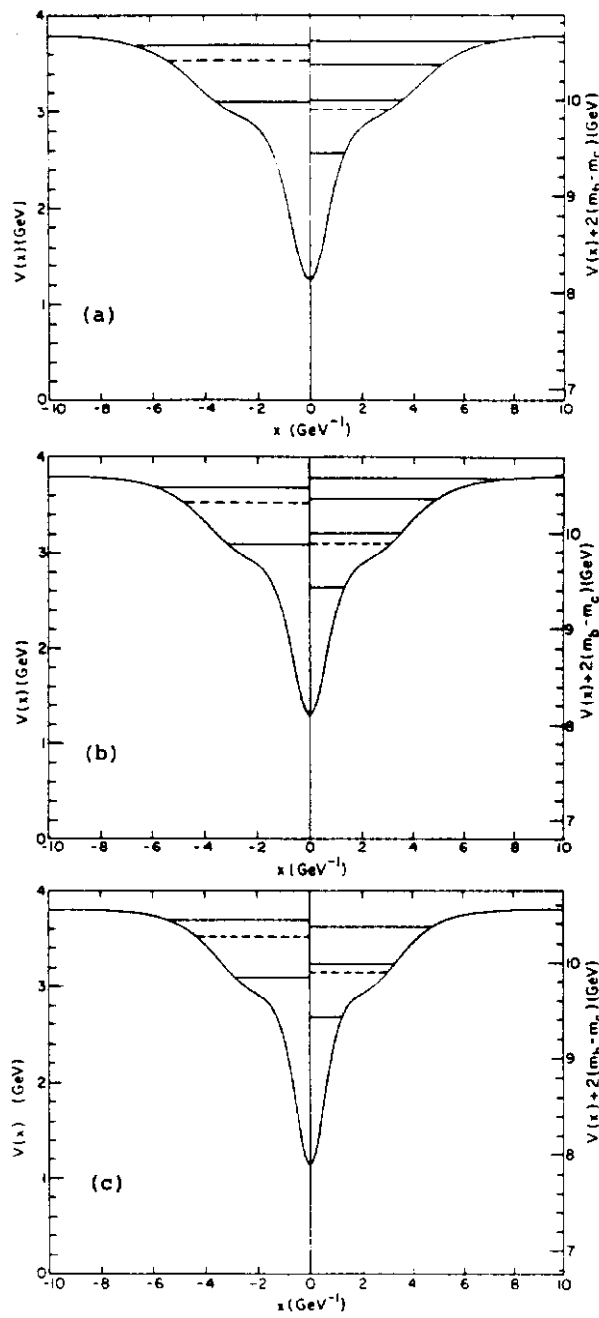


Fig. 48

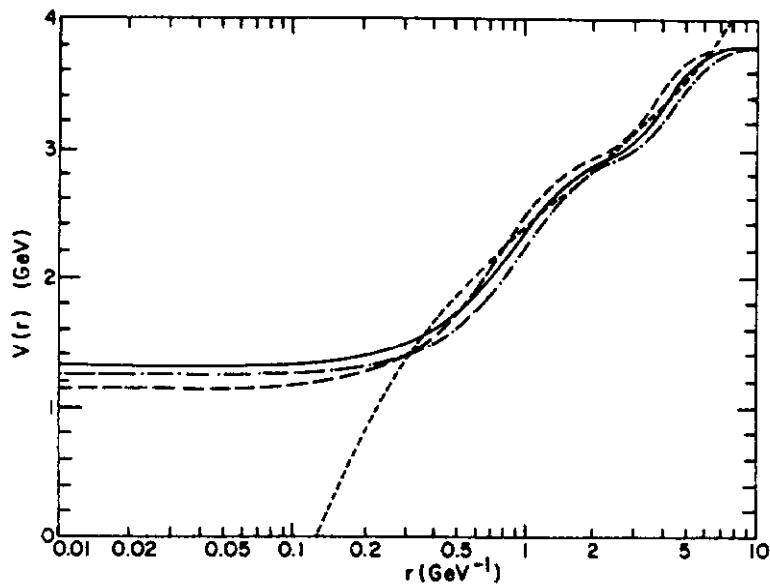


Fig. 49

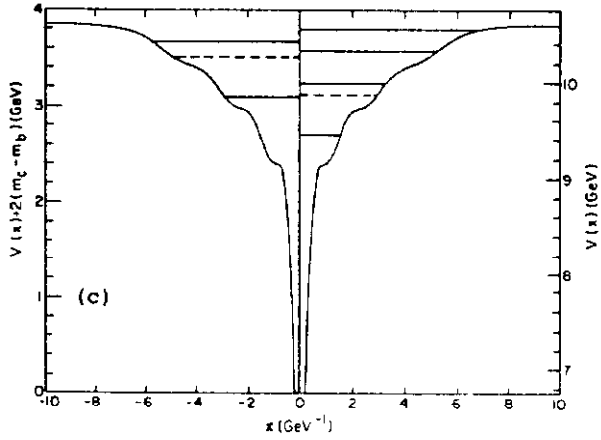
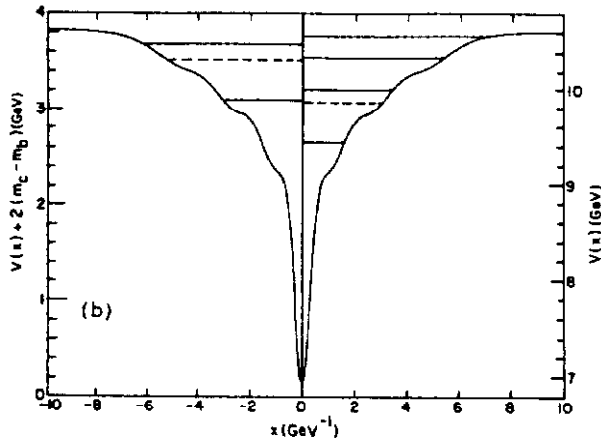
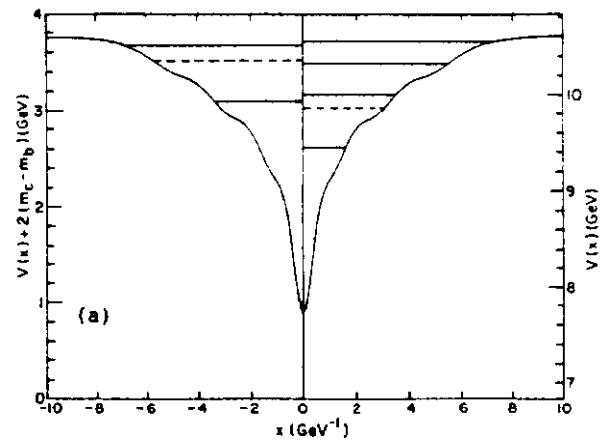


Fig. 50

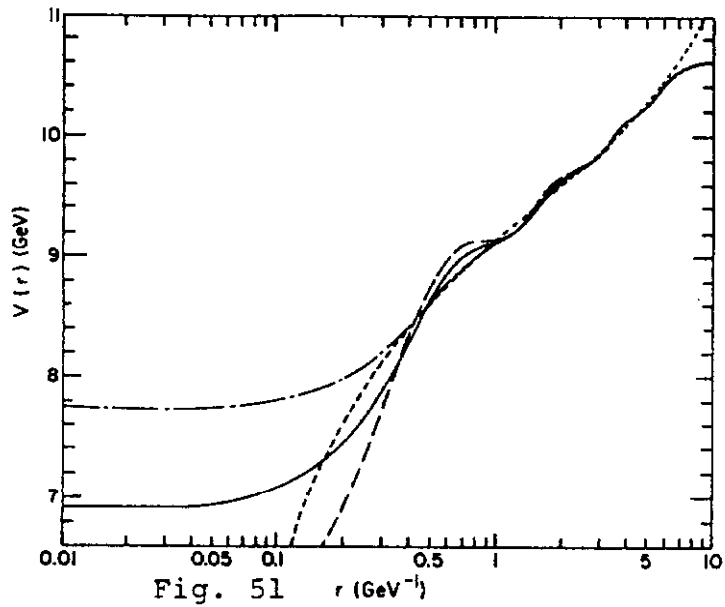


Fig. 51

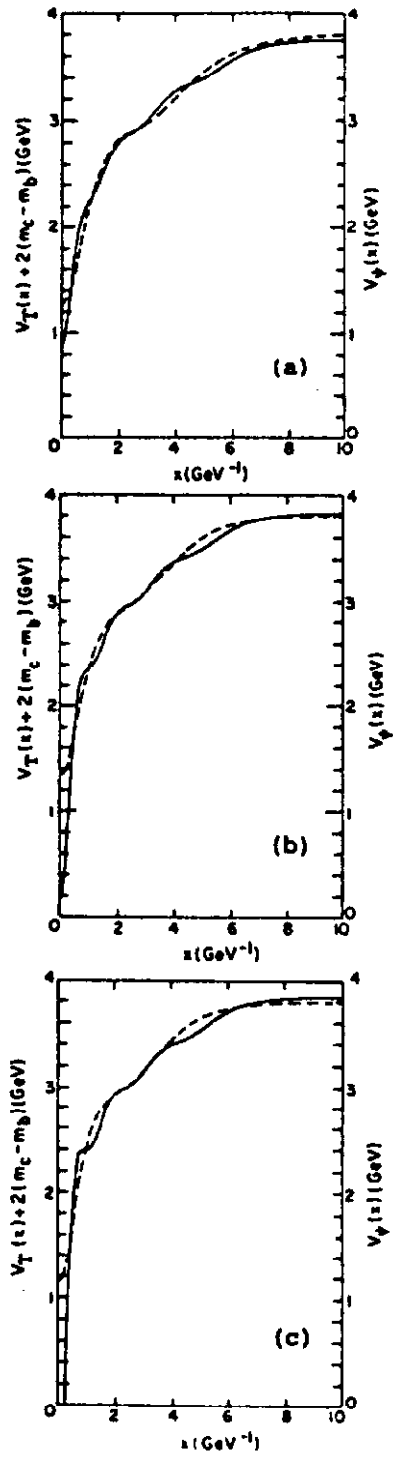


Fig. 52

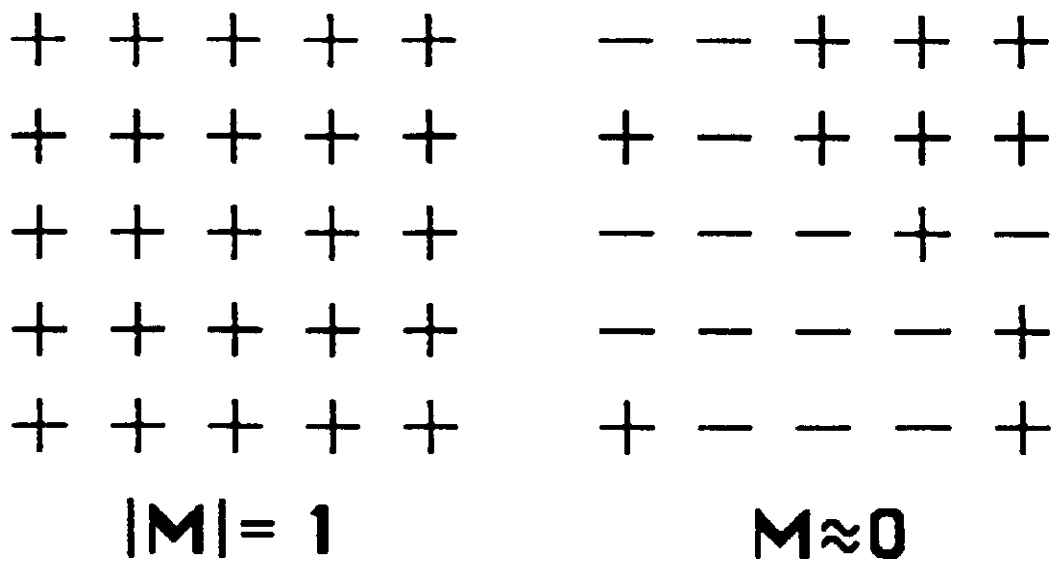


Fig. 53

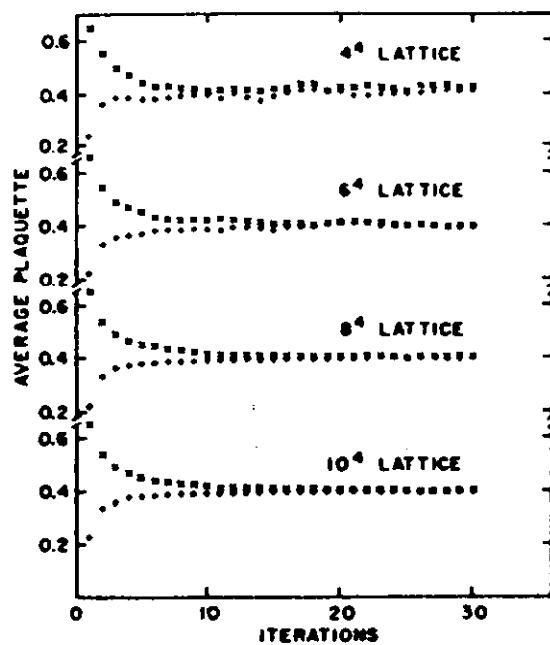


Fig. 54

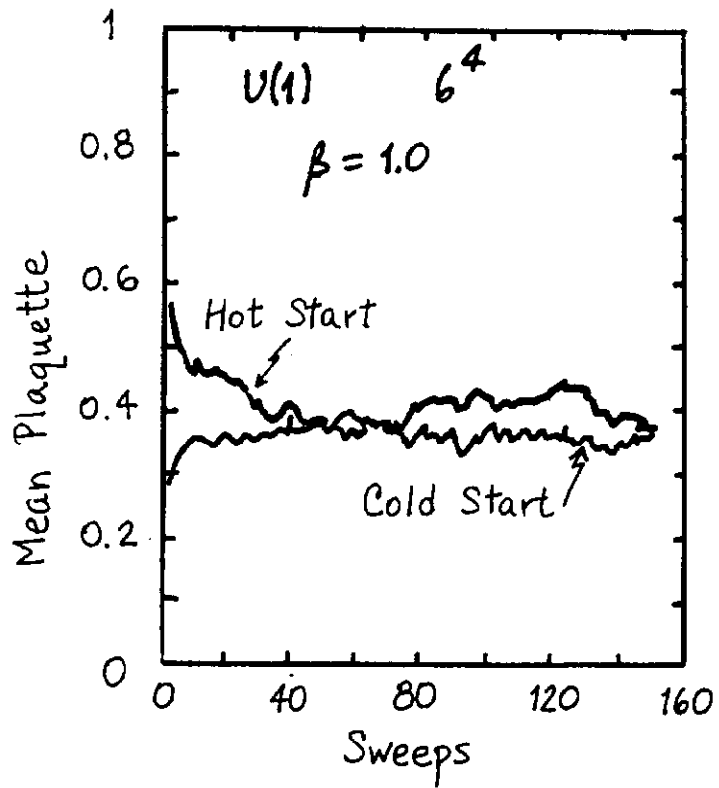


Fig. 55

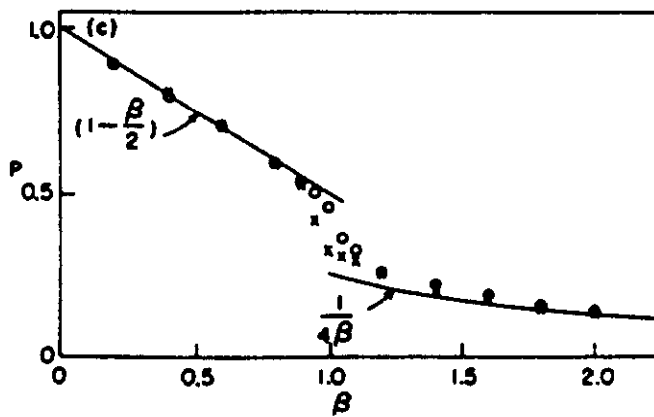


Fig. 56

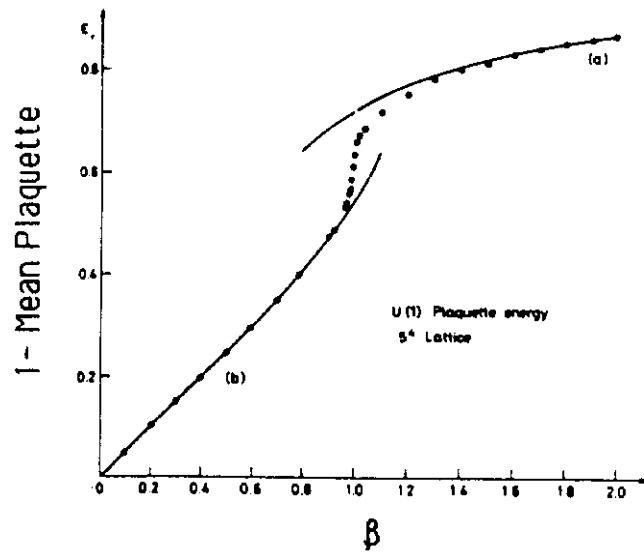


Fig. 57

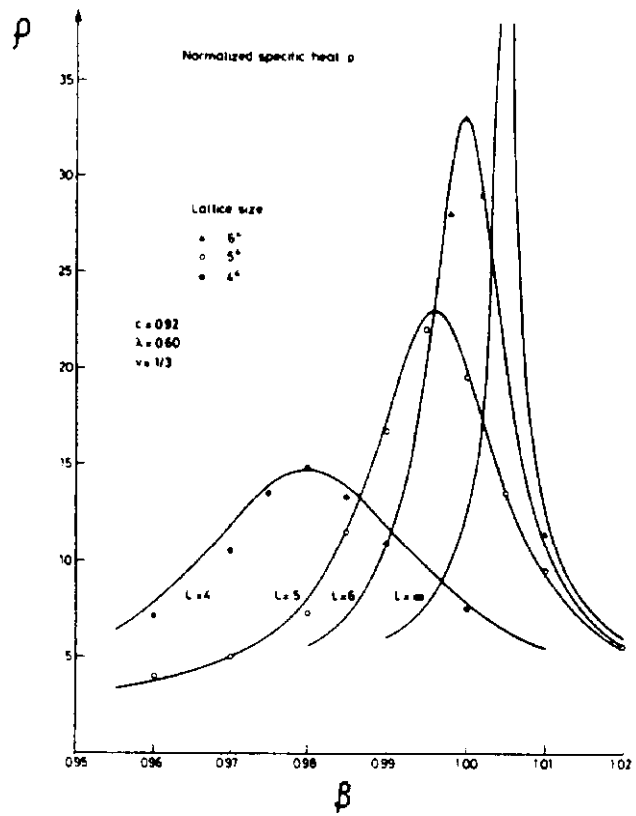


Fig. 58

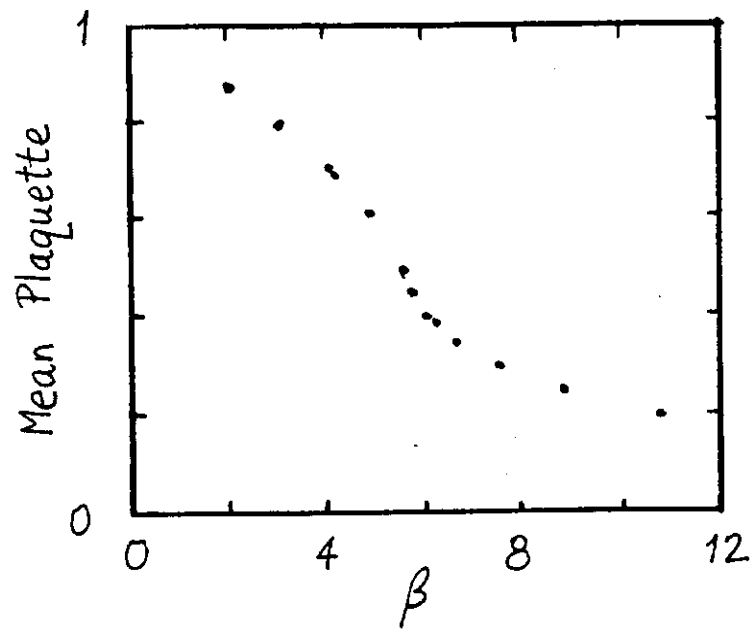


Fig. 59

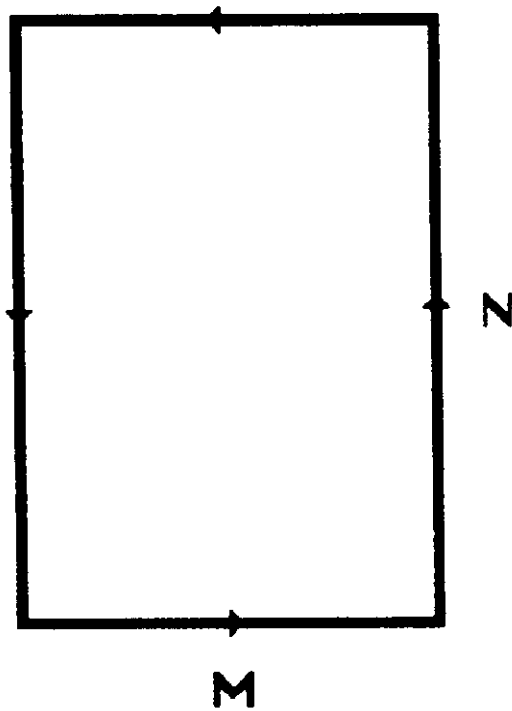


Fig. 60

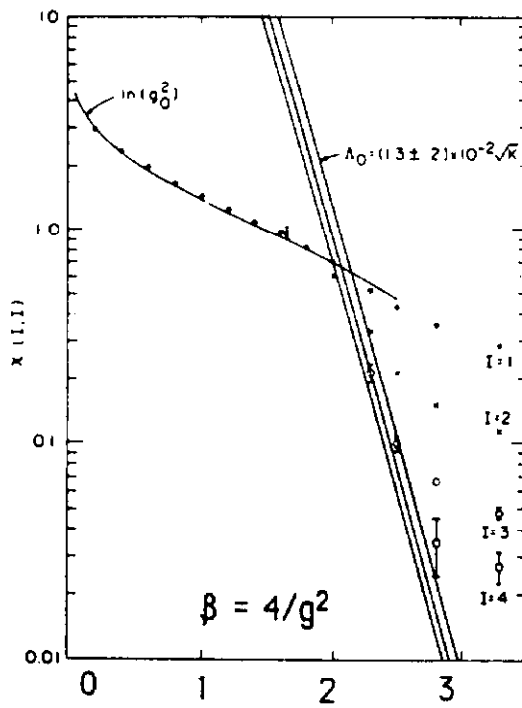


Fig. 61

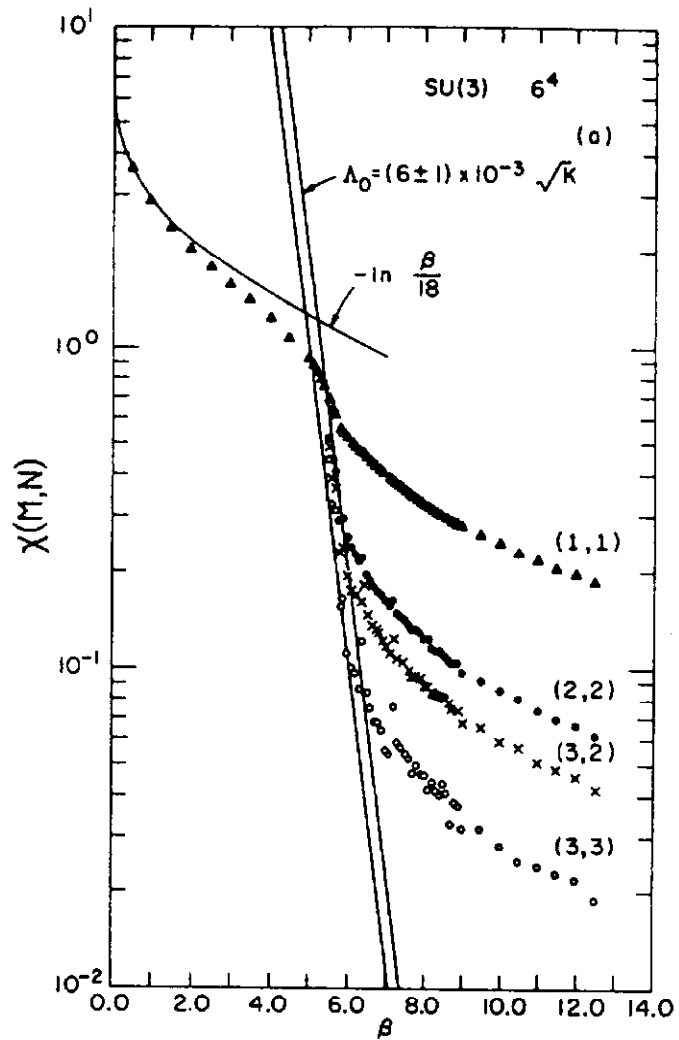


Fig. 62

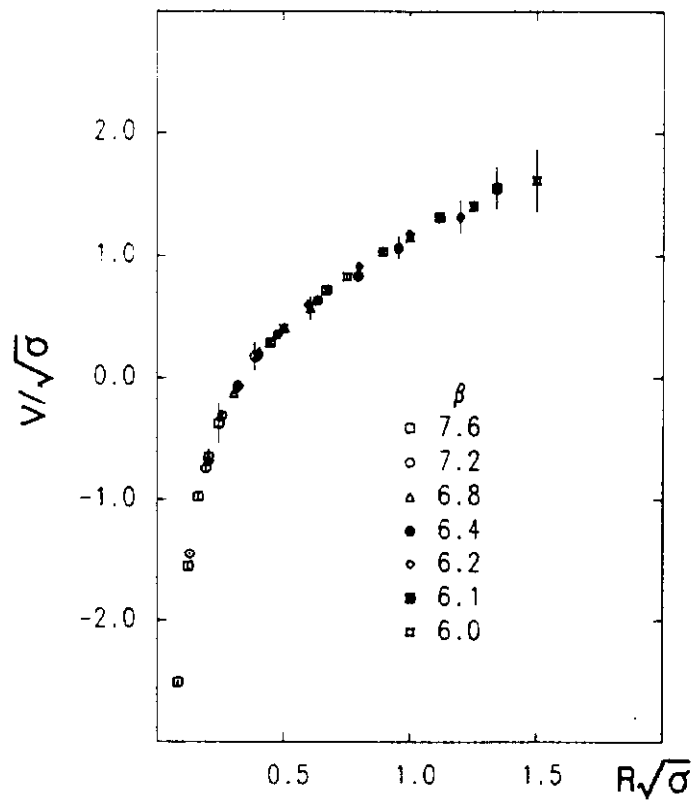


Fig. 63

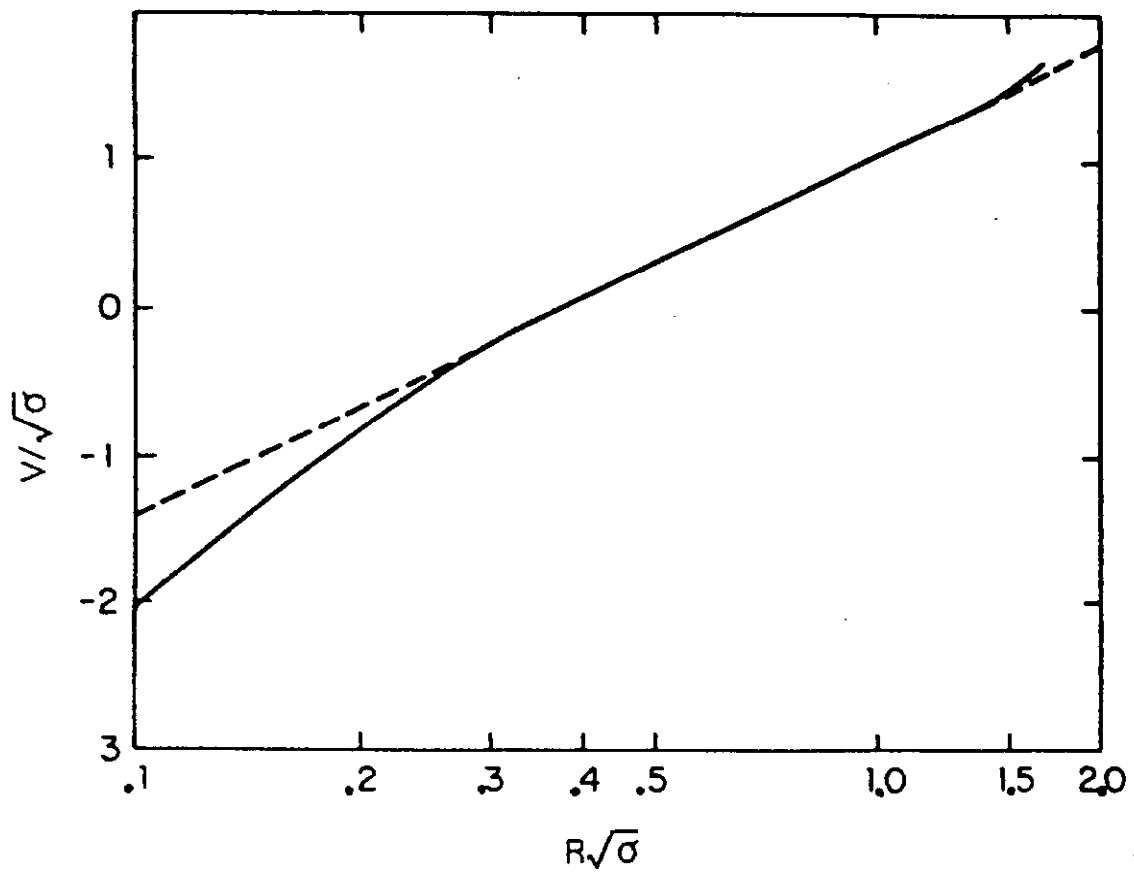


Fig. 64